

**ROLE OF ERBB4 SPLICING IN  
PARVALBUMIN INTERNEURON MATURATION AND SCHIZOPHRENIA**

by

**Daniel Wonjae Chung**

BA, The Johns Hopkins University, 2008

MS, The Johns Hopkins University, 2008

Submitted to the Graduate Faculty of  
the Kenneth P. Dietrich School of Arts and Sciences

in partial fulfillment

of the requirements for the degree of

Doctor of Philosophy

University of Pittsburgh

2016

UNIVERSITY OF PITTSBURGH  
DIETRICH SCHOOL OF ARTS AND SCIENCES

This dissertation was presented

by

Daniel Wonjae Chung

It was defended on

July 12, 2016

and approved by

Lin Mei, PhD, Department of Neuroscience and Regenerative Medicine,

Augusta University, Georgia

Kenneth N. Fish, PhD, Department of Psychiatry

Colleen A. McClung, PhD, Department of Psychiatry

Stephen D. Meriney, PhD, Department of Neuroscience

David W. Volk, Department of Psychiatry

Zachary P. Wills, Department of Neurobiology

Dissertation Advisor: David A. Lewis, MD, Department of Psychiatry

Copyright © by Daniel Wonjae Chung

2016

**ROLE OF ERBB4 SPLICING IN  
PARVALBUMIN INTERNEURON MATURATION AND SCHIZOPHRENIA**

Daniel Wonjae Chung, PhD

University of Pittsburgh, 2016

Cognitive dysfunction is a core and clinically-critical feature of schizophrenia. Certain cognitive deficits, such as impaired working memory, appear to emerge from altered gamma oscillations in the dorsolateral prefrontal cortex (DLPFC). Cortical gamma oscillations require the activity of parvalbumin (PV) interneurons and reduced PV interneuron activity in schizophrenia has been proposed to be due to deficient excitatory drive to these neurons. Synaptic pruning coincides with the period in which individuals with schizophrenia typically present their first clinical symptoms and thus an excessive pruning of excitatory inputs to PV interneurons in the DLPFC during development could provide the neural substrate for altered prefrontal gamma oscillations and working memory dysfunction in schizophrenia. However, evidence for pruning or pathogenic loss of excitatory inputs to PV interneurons in development and schizophrenia, respectively, and molecular mechanisms underlying these processes have not been identified. The formation of excitatory synapses on PV interneurons is mediated by ErbB4 signaling pathway. ErbB4 transcript is alternatively spliced and each splice variant is associated with different functional effects. In schizophrenia, the total ErbB4 expression is unaltered, but alternative splicing of ErbB4 is dysregulated, suggesting that ErbB4 splicing shifts may provide molecular mechanisms for modulating the excitatory synapse number on PV interneurons. Using a top-down translational approach, I first characterized the association between dysregulated ErbB4 splicing shifts and fewer excitatory inputs to PV interneurons in a human cohort of comparison subjects and schizophrenia subjects. Then I assessed the developmental context of

this relationship in a cohort of non-human primates with different ages. Finally, I investigated the cause-and-effect relationship between ErbB4 splicing shifts and excitatory synapse number on PV interneurons using rat primary neuronal culture. Data from these different experimental systems converge onto the hypothesis that developmental shifts in ErbB4 splicing induce pruning of excitatory synapses on PV interneurons and deficits in this process result in a loss of excitatory inputs to PV interneurons in schizophrenia. Therefore, work from this dissertation reinforces the view that schizophrenia is a neurodevelopmental disorder with disturbances in the maturation of prefrontal cortical circuitry.

## TABLE OF CONTENTS

<b>TABLE OF CONTENTS .....</b>	<b>VI</b>
<b>LIST OF TABLES .....</b>	<b>IX</b>
<b>LIST OF FIGURES .....</b>	<b>X</b>
<b>PREFACE.....</b>	<b>XIII</b>
<b>1.0 GENERAL INTRODUCTION.....</b>	<b>1</b>
<b>1.1 COGNITIVE IMPAIRMENT AND ALTERED PREFRONTAL GAMMA OSCILLATIONS IN SCHIZOPHRENIA .....</b>	<b>2</b>
<b>1.2 POTENTIAL COMPONENTS OF CORTICAL CIRCUITRY SUBSERVING ALTERED PREFRONTAL GAMMA OSCILLATIONS IN SCHIZOPHRENIA .....</b>	<b>3</b>
<b>1.3 PROPOSED ROLE OF ERBB4 SPLICING IN PARVALBUMIN INTERNEURON MATURATION AND SCHIZOPHRENIA .....</b>	<b>8</b>
<b>2.0 DYSREGULATED ERBB4 SPLICING IN SCHIZOPHRENIA: SELECTIVE EFFECTS ON PARVALBUMIN EXPRESSION.....</b>	<b>11</b>
<b>2.1 INTRODUCTION .....</b>	<b>11</b>
<b>2.2 MATERIALS AND METHODS .....</b>	<b>13</b>
<b>2.3 RESULTS.....</b>	<b>19</b>
<b>2.4 DISCUSSION.....</b>	<b>27</b>

<b>3.0</b>	<b>PATHOLOGICAL BASIS FOR DEFICIENT EXCITATORY DRIVE TO CORTICAL PARVALBUMIN INTERNEURONS IN SCHIZOPHRENIA.....</b>	<b>32</b>
3.1	INTRODUCTION .....	32
3.2	MATERIALS AND METHODS.....	34
3.3	RESULTS.....	39
3.4	DISCUSSION.....	48
<b>4.0</b>	<b>DEVELOPMENTAL PRUNING OF EXCITATORY INPUTS TO PARVALBUMIN INTERNEURONS IN MONKEY PREFRONTAL CORTEX: CONTRIBUTION OF ERBB4 SPLICING .....</b>	<b>52</b>
4.1	INTRODUCTION .....	52
4.2	MATERIALS AND METHODS.....	54
4.3	RESULTS.....	61
4.4	DISCUSSION.....	71
<b>5.0</b>	<b>GENERAL DISCUSSION .....</b>	<b>76</b>
5.1	SUMMARY OF FINDINGS.....	76
5.2	IMPLICATIONS IN CORTICAL CIRCUITRY MATURATION AND SCHIZOPHRENIA .....	80
5.3	IMPLICATION IN WORKING MEMORY MATURATION AND SCHIZOPHRENIA .....	93
5.4	CONCLUDING REMARKS: FUTURE STUDIES .....	97
APPENDIX A .....		101
APPENDIX B .....		106
APPENDIX C.....		116

<b>APPENDIX D .....</b>	<b>123</b>
<b>BIBLIOGRAPHY .....</b>	<b>126</b>

## LIST OF TABLES

Table 1. Summary of demographic and postmortem characteristics of human subjects used in qPCR assays. ....	15
Table 2. Summary of demographic and postmortem characteristics of human subjects used in immunohistochemical assay . ....	35
Table 3. Demographic, postmortem, and clinical characteristics of human subjects used in this dissertation . ....	101
Table 4. Oligonucleotide sequences of forward and reverse primers for ErbB4 splicing variants, pan-ErbB4 and MIAT. ....	109
Table 5. Summary statistics comparing the levels of transcripts between subject groups in total gray matter, layer 2 or 4 by paired ANCOVA or paired repeated measures models. ....	110
Table 6. Relationship between the ratios of ErbB4 splicing variants and the levels of CR or PV mRNA and in layer 2 or 4, respectively. ....	111
Table 7. Summary statistics displaying the main effect of genotypes and interactions between genotypes and diagnosis on the ratios of JM-a/JM-b variants or CYT-1/CYT-2 variants. ....	111

## LIST OF FIGURES

Figure 1. Proposed role of ErbB4 splicing in parvalbumin interneuron maturation and schizophrenia. ....	9
Figure 2. mRNA levels for pan-ErbB4 and normalized ErbB4 splicing variants in DLPFC area 9 total gray matter for each matched pair of healthy comparison and schizophrenia subjects.....	20
Figure 3. Layer-specific quantification of PV and CR mRNA levels in DLPFC area 9 for each matched pair of healthy comparison and schizophrenia subjects. ....	22
Figure 4. Layer-specific quantification of mRNA levels for pan-ErbB4 and normalized ErbB4 splicing variants .....	24
Figure 5. Quantification of MIAT levels in DLPFC area 9 total gray matter for 62 subject pairs and in Vicia villosa agglutinin (VVA)-positive cells for 14 subject pairs.....	26
Figure 6. Levels of PV immunoreactivity are significantly lower in PV interneurons in schizophrenia. ....	41
Figure 7. Density of excitatory synaptic inputs to PV interneurons is significantly lower in schizophrenia .....	43
Figure 8. Density of excitatory synaptic inputs to CR interneurons is modestly higher in schizophrenia .....	45

Figure 9. Lower density of excitatory synaptic inputs to PV interneurons is associated with lower PV and GAD67 expression in human DLPFC .....	47
Figure 10. Sampling of excitatory synapses on PV interneurons in monkey DLPFC layer 4.....	60
Figure 11. Developmental pruning of excitatory synapses on PV interneurons through adolescence in layer 4 of monkey DLPFC .....	63
Figure 12. Lower density of excitatory synapses on PV interneurons and higher synaptic levels of VGlut1 and PSD95 proteins predict higher PV levels across all animals .....	65
Figure 13. Developmental shifts in alternative splicing of ErbB4 transcripts through adolescence in layer 4 of monkey DLPFC.....	68
Figure 14. Differential regulation of excitatory synapse number on PV interneurons by ErbB4 splice variants in rat primary neuronal culture .....	70
Figure 15. Proposed role of ErbB4 splicing shifts in regulating the number of excitatory synaptic inputs to PV interneurons in development and schizophrenia.....	79
Figure 16. Developmental arrest model for activity-dependent regulation of ErbB4 splicing shifts .....	82
Figure 17. Proposed E/I balance adjustment by activity-dependent synaptic pruning in response to deficits in either pyramidal (top) or PV neurons (bottom) in schizophrenia .....	90
Figure 18. Proposed role of ErbB4 splicing shifts and pruning of excitatory inputs to PV interneurons in working memory maturation and schizophrenia .....	96
Figure 19. Specificity of qPCR primers for calretinin, parvalbumin, ErbB4 splice variants and pan-ErbB4.....	112
Figure 20. qPCR amplicon products blasted to specific ErbB4 splice variants.....	113

Figure 21. No effect of co-morbid factors on the normalized ErbB4 splice variant levels in subjects with schizophrenia. .... 114

Figure 22. Representative raw, deconvolved and masked images of PV+ cell bodies, CR+ cell bodies, VGlut1+ puncta, PSD95+ puncta and lipofuscin in human DLPFC..... 119

Figure 23. Levels of VGlut1 or PSD95 immunoreactivity within VGlut1+ puncta or PSD95+ puncta, respectively, onto PV interneurons are unaltered in schizophrenia subjects. .... 120

Figure 24. No effect of co-morbid factors on the mean density of VGlut1+/PSD95+ puncta onto PV+ cell bodies in subjects with schizophrenia..... 121

Figure 25. Density of excitatory synaptic inputs to PV interneurons is not altered in monkeys treated with psychotropic medications..... 122

## PREFACE

*“But small is the gate and narrow the road that leads to life, and only a few find it.”*

**Matthew 7:14**

I would like to thank my family for their love, support and sacrifice, which have carried me through all those years in college, medical school and PhD training. I would like to thank my mentor Dr. David Lewis for not only teaching me about science and research but also making an example of how one should live his life and treat other people. Moreover, I would like to thank Dr. David Volk, Dr. Ken Fish, Dr. Zak Wills, Dr. Gil Hoftman, Dr. Dibs Datta, Sam Dienel and Mark Zaki for their mentorship, friendship and collegiality. Finally, I would like to thank God for providing me with a mission that constantly drives my passion for research. Although the path I am about to enter is small and narrow, with the support of people around me and under the grace and providence of God, I seek to firmly walk down this path and hope to contribute to improving the lives of those affected with psychiatric illnesses.

## **1.0 GENERAL INTRODUCTION**

Schizophrenia is a debilitating neuropsychiatric disorder that affects 0.5-1% of the world's population (Lewis and Lieberman, 2000). Most affected individuals experience a lifetime of disability while 10% of patients eventually commit suicide (Lewis and Sweet, 2009). Thus, the average life expectancy of patients with schizophrenia is reduced by ~25 years (Saha et al., 2007) and as a result, schizophrenia is a leading cause of years of life lost to disability and premature mortality. Consequently, schizophrenia afflicts emotional burdens to families of those affected and incurs tremendous economic costs for society (Lopez and Disease Control Priorities Project., 2006).

Etiology of schizophrenia is thought to require a complex and variable combination of genetic susceptibility and environmental risk factors that alter brain circuits which clinically manifest as a collection of symptoms and signs (Insel, 2010). Dysfunction of prefrontal cortical circuits is proposed to provide a key neural substrate for the pathophysiology underlying core clinical features of schizophrenia (Lewis et al., 2005). Clinical symptoms of schizophrenia usually appear in adolescence, during which the prefrontal cortical circuitry undergoes a process of massive refinement and maturation (Huttenlocher, 1979; Bourgeois et al., 1994; Rakic et al., 1994). These observations led to a hypothesis that disturbances in the normal maturation process of prefrontal circuitry give rise to the core pathophysiology of schizophrenia (Weinberger, 1987; Lewis, 1997). In order to investigate such a hypothesis, it is crucial to identify components of

neural circuits that are affected in schizophrenia and characterize the normal developmental trajectory of those components. In the following sections, I will 1) review the core clinical feature and the associated prefrontal pathophysiology of schizophrenia, 2) introduce synaptic, molecular and transcriptional components of prefrontal cortical circuitry that might be disrupted in the illness, and 3) propose a model and testable hypotheses that could interlink the roles of these components in prefrontal cortical maturation and schizophrenia.

## **1.1 COGNITIVE IMPAIRMENT AND ALTERED PREFRONTAL GAMMA OSCILLATIONS IN SCHIZOPHRENIA**

The core and clinically critical feature of schizophrenia constitutes cognitive impairments (Kahn and Keefe, 2013). First, poor cognitive performance, as measured by low IQ score or low scholastic achievement, is a robust risk factor for developing schizophrenia (MacCabe et al., 2008; Khandaker et al., 2011). Second, decline in cognitive function begins in early puberty, years prior to the onset of psychosis (van Oel et al., 2002). Third, this decline does not necessarily stop once psychosis develops, but may gradually worsen over the disease progress (Hedman et al., 2013). Fourth, the time course of cognitive decline differentiates schizophrenia from bipolar disorder although both disorders are associated with psychotic symptoms (Reichenberg et al., 2002). Finally, cognitive impairment is the best predictor of long-term functional outcome for patients with schizophrenia (Bowie et al., 2006; Mohamed et al., 2008). Although such evidence supports the hypothesis that schizophrenia is a disorder of cognition, current pharmacological agents do not target etiopathogenic elements underlying cognitive dysfunction.

Certain cognitive features, such as working memory, that are affected in schizophrenia are thought to depend on the precisely timed transmission of information in cortical regions via synchronous oscillations at gamma band frequency (Uhlhaas and Singer, 2010; Senkowski and Gallinat, 2015). Numerous electroencephalography and magnetoencephalography studies have shown that the power of prefrontal gamma oscillations is reduced in patients with schizophrenia during cognitive tasks such as delayed discrimination task (Cho et al., 2006), Sternberg task (Chen et al., 2014) or oddball paradigms (Gallinat et al., 2004; Fujimoto et al., 2012). *Thus, identifying pathogenic components of prefrontal cortical circuits underlying altered prefrontal gamma oscillations in schizophrenia is critical for the development of new therapeutic interventions for this illness.*

## **1.2 POTENTIAL COMPONENTS OF CORTICAL CIRCUITRY SUBSERVING ALTERED PREFRONTAL GAMMA OSCILLATIONS IN SCHIZOPHRENIA**

### **1.2.1 Synaptic component: role of excitatory synaptic inputs to parvalbumin interneurons in generation of gamma oscillations**

The prefrontal neural network that generates gamma oscillations is proposed to involve pyramidal neurons and local GABAergic interneurons (Whittington et al., 2000). In this model, excitation from DLPFC pyramidal neurons recruits local interneurons, which in turn provide feedback inhibitory inputs to populations of asynchronously firing pyramidal neurons. Following the synaptic decay of the inhibitory transmission, the postsynaptic pyramidal cells subsequently fire in synchrony. A subset of interneurons that express the calcium binding protein parvalbumin

(PV) intrinsically provides inhibitory inputs at gamma frequency, generating a synchronous gamma oscillation in the pyramidal neuron network (Gonzalez-Burgos et al., 2015a). Thus, recruitment of PV interneurons by excitation from pyramidal neurons is critical in generating prefrontal gamma oscillations.

A number of studies suggest that altered prefrontal gamma oscillations in schizophrenia may be due to deficits in excitatory synaptic inputs to PV interneurons. For example, abnormal gamma oscillations are observed in mouse models in which 1) glutamatergic receptor subunits, such as GluN1 or GluR1, are selectively knocked out in PV interneurons (Fuchs et al., 2007; Belforte et al., 2010), 2) signaling pathways that are involved in the formation of excitatory synapses on PV interneurons are disrupted (Del Pino et al., 2013; Pelkey et al., 2015) or 3) excitation of PV interneurons is optogenetically inhibited (Sohal et al., 2009). Consistent with these data, postmortem studies have repeatedly shown lower expression levels of activity-dependent gene products (e.g., PV and the GABA-synthesizing enzyme glutamic acid decarboxylase 67, GAD67) in the DLPFC of schizophrenia, which are thought to reflect deficient excitatory drive to a subset of PV interneurons and not a loss of PV interneurons (Akbarian et al., 1995; Woo et al., 1997; Hashimoto et al., 2003; Enwright et al., 2016). These deficits do not seem to be caused by a global reduction in excitatory drive to all GABAergic interneurons, as calretinin-containing (CR) interneurons, the most abundant interneuron subtype in the primate DLPFC (Conde et al., 1994), are unaffected in schizophrenia (Hashimoto et al., 2003; Fung et al., 2010). *However, a pathological basis for deficient excitatory synaptic inputs to PV interneurons, such as fewer excitatory synapses on these neurons, has not been identified in the DLPFC of people with schizophrenia.*

### **1.2.2 Molecular component: role of ErbB4 signaling in formation of excitatory synapses on parvalbumin interneurons**

Formation and elimination of excitatory synapses on PV interneurons in the DLPFC could be, at least partly, modulated by ErbB4 signaling pathway. ErbB4 is a member of the ErbB transmembrane receptor tyrosine kinase family (Bublil and Yarden, 2007). Each ErbB protein has an extracellular region containing two extracellular cysteine-rich domains, a transmembrane domain, a short intracellular juxtamembrane region, a tyrosine kinase domain and a carboxyl-terminal tail. In response to binding of its ligand neuregulins, ErbB proteins become dimerized to form homo- or heterodimers (Britsch, 2007). Among ErbB proteins, ErbB4 is the only autonomous NRG1-specific ErbB protein that can both interact with the ligand and become activated without forming heterodimers with other ErbB proteins.

Activation of ErbB4 participates in various processes of neurodevelopment, including neuronal migration, axonal guidance, myelination, oligodendrocyte development, neuromuscular formation and synaptic plasticity (Mei and Xiong, 2008). More recently, ErbB4 has been shown to localize primarily in the cell bodies and the proximal dendrites of PV interneurons as well as CR interneurons (Vullhorst et al., 2009; Neddens et al., 2011) and participates in the development of GABAergic circuitry (Fazzari et al., 2010; Rico and Marin, 2011; Mei and Nave, 2014). Importantly, the activation of ErbB4 signaling regulates the formation of excitatory synapses on PV interneurons, primarily by directly interacting with and stabilizing PSD95 at the synapse via its kinase motif and PDZ-binding motif (Huang et al., 2000; Ting et al., 2011; Del Pino et al., 2013; Seshadri et al., 2015). Therefore, a potential loss of excitatory synapses on PV interneurons in schizophrenia could be a result of abnormal ErbB4 signaling in these neurons.

*However, evidence for disrupted ErbB4 signaling in PV interneurons has not been identified in the DLPFC of people with schizophrenia.*

### **1.2.3 Transcriptional component: role of alternative splicing in ErbB4 signaling**

Functional consequence of ErbB4 signaling can be modulated by alternative splicing. Alternative splicing of ErbB4 pre-mRNA results in four ErbB4 variants, each with different downstream signaling pathway (Veikkolainen et al., 2011). Splicing at the Juxtamembrane (JM) locus produces the minor JM-a and major JM-b variants based on the inclusion of exon 16 or exon 15b, respectively (Tan et al., 2010). Unlike the JM-b isoform, the inclusion of exon 16 renders the JM-a isoform susceptible to proteolytic cleavage at the JM domain (Rio et al., 2000; Ni et al., 2001; Lee et al., 2002), generating soluble extracellular and intracellular truncated peptides, which could interfere with normal ErbB4 signaling. Furthermore, splicing at the Cytoplasmic (CYT) locus produces the minor CYT-1 and major CYT-2 variants based on the inclusion or exclusion of exon 26, respectively. Unlike the CYT-2 variant, the CYT-1 variant contains a binding site for Nedd4, an E3 ubiquitin ligase (Zeng et al., 2009). Binding of Nedd4 to CYT-1 results in an increased ubiquitination and a subsequent degradation of ErbB4, which could result in a loss of normal ErbB4 signaling. *These findings suggest that a shift in alternative splicing from ErbB4 JM-b/CYT-2 to JM-a/CYT-1 variants could result in a loss of ErbB4 signaling.*

Consistent with the idea that ErbB4 signaling is disrupted in the illness, levels of ErbB4 JM-a/CYT-1 variants are higher in the total gray matter DLPFC of schizophrenia (Silberberg et al., 2006; Law et al., 2007; Joshi et al., 2014). Moreover, the elevated ErbB4 splicing variants have been associated with the intronic SNPs at the ErbB4 locus that are linked to schizophrenia

(Law et al., 2007; Law et al., 2012). Finally, levels of myocardial infarction associated transcript (MIAT), a non-coding RNA that regulates the splicing of ErbB4 transcripts, are altered in schizophrenia (Barry et al., 2014). In concert, these findings suggest that a potential disruption in ErbB4 signaling in PV interneurons of schizophrenia could be due to an abnormal splicing of ErbB4 transcripts. *However, evidence for dysregulated ErbB4 splicing in PV interneurons and its functional consequences has not been identified in the DLPFC of people with schizophrenia.*

#### **1.2.4 Potential role of these components in prefrontal cortical maturation**

In humans and non-human primates, working memory performance and the associated DLPFC activity continue to improve through adolescence (Alexander, 1982; Goldman-Rakic, 1987; Luna et al., 2010). During this period, excitatory synapses in the DLPFC undergo pruning (Huttenlocher, 1979; Bourgeois et al., 1994; Anderson et al., 1995; Petanjek et al., 2011), a maturation process that is thought to refine and strengthen functionally relevant synapses while eliminating weak or imprecise connections (Lichtman and Colman, 2000; Holtmaat and Svoboda, 2009). During gamma oscillations, PV interneurons require efficient detection of excitatory inputs with high precision and low variability, mainly due to the narrow time window of PV interneuron recruitment by pyramidal neurons (Jonas et al., 2004; Hu et al., 2014). Therefore, elimination of weak and imprecise excitatory synapses on PV interneurons could play a crucial role in the improvement of PV interneuron recruitment during gamma oscillations and consequently the maturation of working memory function through adolescence. Moreover, based on the idea that formation and elimination of excitatory synapses on PV interneurons may be modulated by ErbB4 signaling, a developmental shift in alternative splicing of ErbB4 transcripts

in PV interneurons could provide a molecular switch that regulates the pruning of excitatory synapses on these neurons.

### **1.3 PROPOSED ROLE OF ERBB4 SPLICING IN PARVALBUMIN INTERNEURON MATURATION AND SCHIZOPHRENIA**

Based on these previous observations and ideas, I propose the following model that could interlink the role of ErbB4 splicing, ErbB4 signaling and excitatory synaptic input to PV interneurons in parvalbumin interneuron maturation and schizophrenia (**Figure 1**). In this model, alternative splicing of ErbB4 is developmentally shifted from the JM-b/CYT-2 to JM-a/CYT-1 variants in PV interneurons through adolescence. This splicing shift results in a mild loss of ErbB4 signaling, which in turn induces an elimination of some of the excitatory synapses on PV interneurons. In schizophrenia, ErbB4 splicing shift is dysregulated and results in abnormally high levels of JM-a/CYT-1 variant and low levels of JM-b/CYT-2 variant. This abnormal splicing shift induces a pathogenic loss of ErbB4 signaling, which in turn induces an excessive loss of excitatory synapses on PV interneurons in schizophrenia.

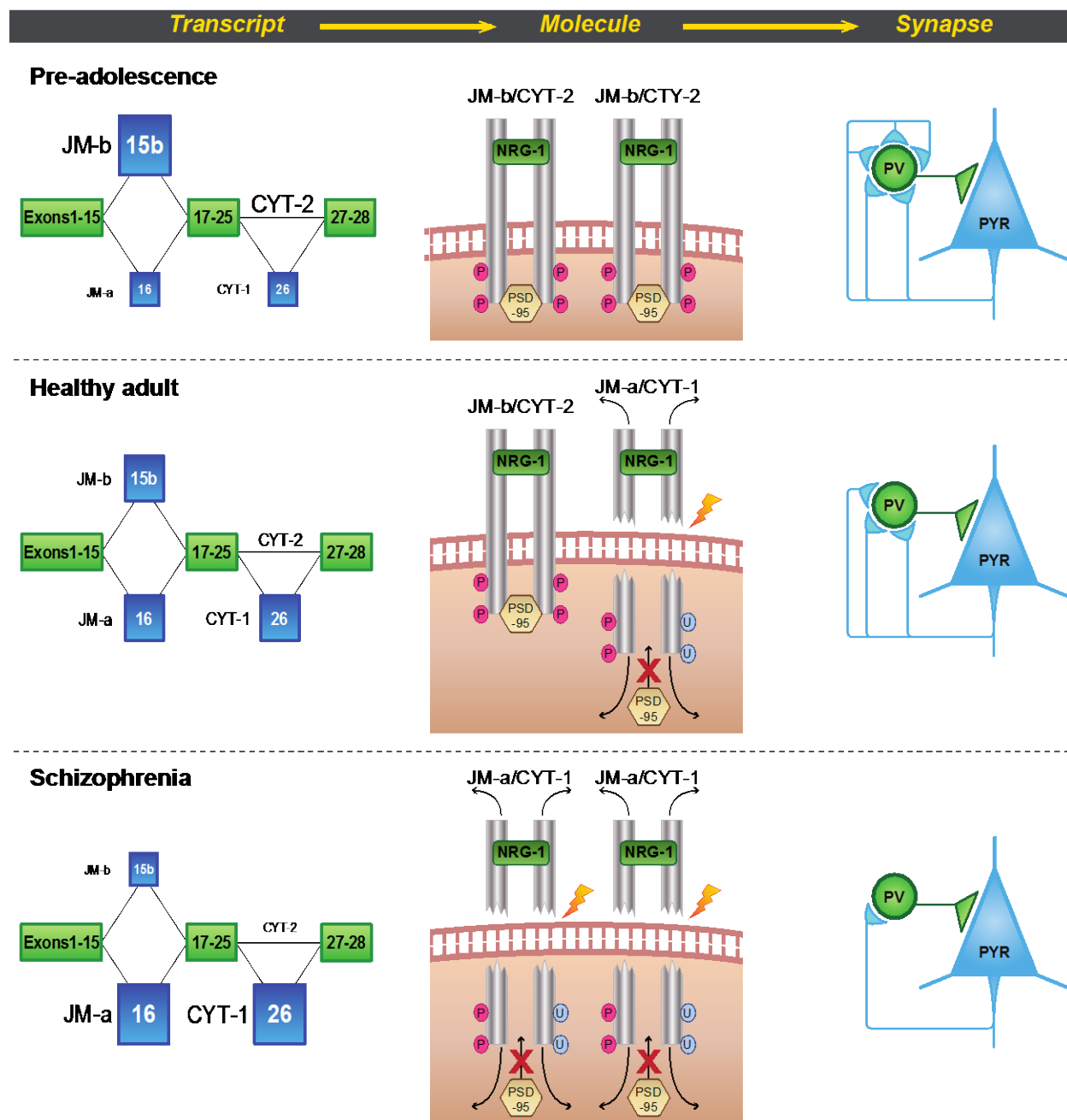


**Figure 1. Proposed role of ErbB4 splicing in parvalbumin interneuron maturation and schizophrenia.**

Developmentally shifts in ErbB4 splicing from the JM-b/CYT-2 to JM-a/CYT-1 variants in PV interneurons through adolescence results in a mild loss of ErbB4 signaling, which in turn induces an elimination of some of the excitatory synapses on PV interneurons. In schizophrenia, ErbB4 splicing shift is dysregulated and results in abnormally high levels of JM-a/CYT-1 variant and low levels of JM-b/CYT-2 variant. This abnormal splicing shift induces a pathogenic loss of ErbB4 signaling, which in turn induces an excessive loss of excitatory synapses on PV interneurons in schizophrenia.

In order to investigate the validity of this model, I have constructed three sets of specific hypotheses; subsequent chapters of this dissertation are dedicated to testing each of these hypotheses sets. In the first set of hypotheses (**Chapter 2**), I hypothesize that 1) in the DLPFC of schizophrenia, the levels of ErbB4 splicing variants are altered in PV but not in CR interneurons; 2) dysregulated ErbB4 splicing in schizophrenia is associated with lower PV mRNA levels; and 3) altered levels of MIAT and/or the schizophrenia-associated intronic SNPs at the ErbB4 locus predict dysregulated ErbB4 splicing in schizophrenia. In the second set of hypotheses (**Chapter 3**), I hypothesize that 1) in the DLPFC of schizophrenia, lower PV levels reflect altered PV expression per neuron and not a loss of PV interneurons; 2) PV interneurons, but not CR interneurons, receive fewer excitatory synaptic inputs in schizophrenia; and 3) fewer excitatory synapses on PV interneurons are associated with dysregulated splicing of ErbB4 transcripts in schizophrenia. Finally, in the last set of hypotheses (**Chapter 4**), I hypothesize that 1) excitatory synapses on PV interneurons in monkey DLPFC undergo pruning during adolescence, 2) this developmental pruning is associated with shifts in alternative splicing of ErbB4 in PV interneurons, and 3) experimental manipulations of ErbB4 splice variants produce the predicted changes in excitatory inputs to PV interneurons. By testing these sets of hypotheses, the goal of this dissertation is to identify novel pathogenic elements in the prefrontal cortical circuitry associated with schizophrenia and characterize the role of these elements in the maturation of prefrontal cortical circuitry in order to further expand the understanding of pathogenic mechanisms subserving developmental disturbances in neural circuits affected in schizophrenia.

## **2.0 DYSREGULATED ERBB4 SPLICING IN SCHIZOPHRENIA: SELECTIVE EFFECTS ON PARVALBUMIN EXPRESSION**

Adapted from Chung DW, *et al.* (2016) Dysregulated ErbB4 Splicing in Schizophrenia: Selective Effects on Parvalbumin Expression. *Am J Psychiatry* 173(1):60-68.

### **2.1 INTRODUCTION**

Neuregulin-1 and its receptor ErbB4 have been implicated in the pathogenesis of schizophrenia, and this association appears to involve dysregulated splicing of ErbB4 transcripts (Rico and Marin, 2011; Mei and Nave, 2014). For example, transcript levels of some ErbB4 splicing variants are higher in the dorsolateral prefrontal cortex (DLPFC) of schizophrenia subjects (Silberberg et al., 2006; Law et al., 2007; Joshi et al., 2014), whereas total ErbB4 mRNA levels are unaltered (Silberberg et al., 2006; Law et al., 2007). Furthermore, the elevated ErbB4 splicing variants are associated with the intronic SNPs at the ErbB4 locus that are linked to schizophrenia (Law et al., 2007; Law et al., 2012). Finally, levels of myocardial infarction associated transcript (MIAT), a non-coding RNA that regulates the splicing of ErbB4 transcripts, are altered in schizophrenia (Barry et al., 2014). In concert, these findings support a role for dysregulated ErbB4 splicing in the pathogenesis of schizophrenia.

Alternative splicing of ErbB4 pre-mRNA results in four ErbB4 variants, each with different functional effects (Veikkolainen et al., 2011). Splicing at the Juxtamembrane (JM) locus produces the minor JM-a and major JM-b variants based on the inclusion of exon 16 or exon 15b, respectively (Tan et al., 2010). The inclusion of exon 16 renders the JM-a isoform susceptible to proteolytic cleavage at the juxtamembrane domain (Rio et al., 2000; Ni et al., 2001; Lee et al., 2002). Splicing at the Cytoplasmic (CYT) locus produces the minor CYT-1 and major CYT-2 variants based on the inclusion or exclusion of exon 26, respectively. Both the CYT-1 and CYT-2 isoforms couple to the MAPK signaling pathway, whereas only the CYT-1 isoform activates the phosphoinositide 3-kinase (PI3-K)-Akt pathway (Junttila et al., 2000). Thus, although alternative splicing clearly influences ErbB4 signaling, the consequences of dysregulated ErbB4 splicing on DLPFC function in schizophrenia are unknown.

In mouse prefrontal cortex, ErbB4 is preferentially expressed in parvalbumin (PV)-positive interneurons (Fazzari et al., 2010) where it regulates the formation of excitatory inputs to, and hence the activity of, these cells (Ting et al., 2011; Del Pino et al., 2013). The activity of cortical PV interneurons is thought to be reduced in schizophrenia since the expression of two activity-dependent transcripts (Kinney et al., 2006; Belforte et al., 2010; Lau and Murthy, 2012), PV and glutamic acid decarboxylase (GAD67), are lower in PV interneurons in schizophrenia subjects (Hashimoto et al., 2003; Mellios et al., 2009; Fung et al., 2010; Volk et al., 2012b). Consistent with these findings, protein levels of PV and GAD67 are also lower in PV axon terminals in schizophrenia (Curley et al., 2011; Glausier et al., 2014). The idea that these alterations in PV neurons could be attributed to disturbed ErbB4 signaling is supported by findings that deletion of ErbB4 in PV interneurons in mice results in lower PV interneuron activity accompanied by lower PV and GAD67 levels (Del Pino et al., 2013).

Similar to mouse prefrontal cortex, ErbB4 is expressed in virtually all PV interneurons in primate DLPFC (Neddens et al., 2011). PV interneurons are heavily enriched in DLPFC layer 4 and lower PV mRNA levels are restricted to DLPFC layers 3-4 in schizophrenia subjects (Hashimoto et al., 2003). ErbB4 is also expressed in all calretinin (CR)-positive interneurons, which are preferentially localized to primate DLPFC layer 2. Interestingly, CR mRNA levels are not altered in schizophrenia (Beasley et al., 2002; Hashimoto et al., 2003), suggesting that CR interneurons are relatively intact in the disease.

Therefore, in this study, we sought to determine whether dysregulated ErbB4 splicing is associated selectively with PV interneurons, and not with CR interneurons, in schizophrenia. First, we hypothesized that in schizophrenia the levels of ErbB4 splicing variants are altered in DLPFC layer 4, where PV interneurons are heavily enriched, and not in DLPFC layer 2, where CR interneurons are highly localized. Second, we hypothesized that dysregulated ErbB4 splicing in schizophrenia is associated with lower PV mRNA levels in DLPFC layer 4. Finally, we hypothesized that the altered levels of MIAT and/or the schizophrenia-associated intronic SNPs at the ErbB4 locus contribute to dysregulated ErbB4 splicing in schizophrenia

## **2.2 MATERIALS AND METHODS**

### **2.2.1 Human subjects**

Brain specimens were obtained during routine autopsies conducted at the Allegheny County Office of the Medical Examiner (Pittsburgh, PA) after consent was obtained from next-of-kin. Consensus DSM-IV diagnoses for each subject were made by an independent team of

clinicians using structured interviews with family members and review of medical records (Volk et al., 2012b). The absence of a psychiatric diagnosis was confirmed in healthy comparison subjects using the same approach.

To control for experimental variance and reduce biological variance, each subject with schizophrenia or schizoaffective disorder was matched with one healthy comparison subject for sex and as closely as possible for age. For the initial analysis of ErbB4 variant expression in gray matter, 62 pairs of subjects were used. For the layer-specific analysis of ErbB4 variant expression, a subset of these pairs (n=39) were used due to limitations in the availability of tissue sections for laser-microdissection (**Appendix A; Table 3**). The mean age, postmortem interval (PMI), RNA integrity number (RIN; Agilent Bioanalyzer, Agilent Technologies, Santa Clara, California), and tissue storage time did not differ between subject groups for either the 62 or 39 subject pairs (**Table 1**). Although brain pH significantly differed between subject groups ( $t_{61}=2.68$ ,  $p=0.009$  for 62 pairs;  $t_{38}=3.12$ ,  $p=0.003$  for 39 pairs), the mean differences were very small (0.1 pH unit). Each subject had a RIN value  $\geq 7.0$ , indicating an excellent quality of total RNA.

**Table 1. Summary of demographic and postmortem characteristics of human subjects used in qPCR assays.**

Characteristic	Total gray matter qPCR (N=62)				Layer-specific qPCR (N=39)			
	Comparison		Schizophrenia		Comparison		Schizophrenia	
	N	%	N	%	N	%	N	%
Male	47	76	47	76	30	77	30	77
White	52	84	52	84	34	87	34	87
Black	10	16	10	16	5	13	5	13
	Mean	SD	Mean	SD	Mean	SD	Mean	SD
Age (years)	48.7	13.8	47.7	12.7	49.2	12.9	47.5	12.0
Postmortem interval (hours)	18.8	5.5	19.2	8.5	19.2	5.6	20.1	8.0
Brain pH	6.7	0.2	6.6	0.3	6.7	0.2	6.5	0.2
RNA integrity number	8.2	0.6	8.1	0.6	7.9	0.5	7.9	0.5
Storage time (months)	130.8	59.6	127.0	64.1	92.4	36.0	83.9	33.8

### 2.2.2 Total and layer-specific RNA extraction

Tissue was collected from DLPFC area 9 and total RNA samples were prepared as described previously (Volk et al., 2012b). Fresh-frozen sections (12 $\mu$ m) from DLPFC area 9 were mounted on microdissection slides (Leica Microsystems, Bannockburn, Illinois), fixed in ethanol/sodium acetate, stained in 0.5% thionin, and dehydrated with ethanol as previously described (Arion et al., 2015). The boundaries of layers 2 and 4 were determined based on the size and packing density of stained cells. A Leica microdissection system (LMD 6500, Leica Microsystems) was used to collect  $\sim 3 \times 10^6 \mu\text{m}^2$  of tissue from each of layers 2 and 4 per subject from the same section. The collected tissue was lysed by vortexing for 30 seconds in 200 $\mu$ l of RLTplus buffer (Qiagen, Valencia, California). RNA was extracted using the RNeasy Plus Micro Kit (Qiagen) and complementary DNA (cDNA) was synthesized using the qScript cDNA SuperMix (Quanta Bioscience, Gaithersburg, Maryland) as previously described (Arion et al., 2015).

### 2.2.3 Quantitative PCR

Primer sets were designed to quantify transcripts levels for parvalbumin, calretinin, four splicing variants of ErbB4 mRNA (JM-a, JM-b, CYT-1, CYT-2), pan-ErbB4 and MIAT (**Appendix B; Table 4**). All primer pairs showed amplification efficiency >98% in standard curve analyses and specific single products in dissociation curve analyses. The qPCR amplicons for each ErbB4 splicing variant yielded a single band of the predicted size on a gel (**Appendix B; Figure 19**) and were confirmed to span the alternative exons of ErbB4 transcripts (**Appendix B;**

**Figure 20).** The qPCR reactions were carried out in quadruplicate using an ABI StepOnePlus Real-Time PCR System (Applied Biosystem, Foster City, California). Beta-actin, glyceraldehyde 3-phosphate dehydrogenase and cyclophilin A were used as reference genes to normalize the expression levels of transcripts, as these three house-keeping genes have stable levels of expression across both subject groups (Hashimoto et al., 2008a; Volk et al., 2014). The delta cycle thresholds (dCTs) were calculated for each sample using the geometric mean of the three endogenous reference genes as the normalizing factor. The expression level for each transcript was then calculated as the expression ratio value (expression ratio =  $2^{-dCTs}$ ).

#### **2.2.4 Microarray analysis**

Microarray analysis of MIAT expression in *Vicia villosa* agglutinin (VVA)-positive PV interneurons was performed as previously described (see **Appendix B; Supplementary Methods**) (Georgiev et al., 2014).

#### **2.2.5 Genotype analysis**

DNA samples from the 62 subject pairs were genotyped as part of the CommonMind Consortium (<http://commonmind.org/WP/>) (see **Appendix B; Supplementary Methods**).

#### **2.2.6 Statistical analysis**

Two analyses of covariance (ANCOVA) models (paired and unpaired) were used to compare transcript levels in DLPFC gray matter, layer 2 or layer 4 between subject groups. The

paired ANCOVA model included mRNA level as the dependent variable; diagnosis as the main effect; subject pair as a blocking factor; and brain pH, RIN, PMI, and tissue storage time as covariates. This paired model accounts both for our attempts to balance diagnostic groups for sex and age and for the parallel tissue processing of both subjects in a pair, but is not a true statistical paired design. Therefore, we also used an unpaired ANCOVA model that included mRNA level as the dependent variable; diagnosis as the main effect; and sex, age, brain pH, RIN, PMI and storage time as covariates. Non-significant covariates were not included in the final analyses. Repeated measures models were also used to compare the levels of CR, PV, pan-ErbB4 and ErbB4 splicing variant mRNAs in layers 2 and 4 between subject groups (see **Appendix B; Supplementary Methods**).

The paired and unpaired analyses from the ANCOVA and the repeated measures model produced comparable levels of statistical significance for the main effect of diagnosis on all transcript levels, except for JM-b levels in layer 2. The results from the paired ANCOVA analyses are reported in the main text and summarized in **Appendix B, Table 5**. For the repeated measures models only the main effect of layers on PV or CR mRNA levels within subjects are reported in the main text with the remaining outcomes summarized in **Appendix B, Table 5**. The potential influence of co-morbid factors on the layer-specific levels of ErbB4 splicing variants in schizophrenia subjects were assessed as previously described (Volk et al., 2012b) (see **Appendix B; Supplementary Methods**). Pearson's correlation analyses were performed to assess the layer-specific association among the ErbB4 splicing variants and PV or CR levels (see **Appendix B; Supplementary Methods**). In the microarray analysis, normalized and log<sub>2</sub>-transformed signals of MIAT were compared between subject groups using paired t test as previously described (Georgiev et al., 2014). In the genotype analyses, analyses of variance

models were used to test the main effect of genotypes on the ratios of JM-a/JM-b variants and CYT-1/CYT-2 variants in total gray matter of 62 subject pairs or layer 4 of 39 subject pairs.

## 2.3 RESULTS

### 2.3.1 ErbB4 splicing is dysregulated in DLPFC of subjects with schizophrenia

In DLPFC gray matter homogenates from the 62 pairs of schizophrenia and healthy comparison subjects, mean pan-ErbB4 mRNA levels did not differ between subject groups (**Figure 2A**). Consequently, we normalized the levels of ErbB4 splicing variants to the pan-ErbB4 levels within each subject to reduce the variability in ErbB4 splicing variant levels attributable to between-subject differences in total ErbB4 expression. Mean normalized JM-a mRNA levels were significantly ( $F_{1,61}=7.49$ ;  $p=0.008$ ) 10.9% higher and mean normalized JM-b mRNA levels were significantly ( $F_{1,61}=17.1$ ;  $p<0.001$ ) 11.5% lower in schizophrenia subjects relative to healthy comparison subjects (**Figure 2B**). Although mean normalized CYT-1 mRNA levels did not differ between subject groups, mean normalized CYT-2 mRNA levels were significantly ( $F_{1,60}=12.3$ ;  $p<0.001$ ) 10.0% lower in schizophrenia subjects (**Figure 2C**). None of the covariates were significant in any of these analyses except for an effect of RIN on CYT-2 mRNA levels ( $F_{1,60}=5.02$ ,  $p=0.029$ ).

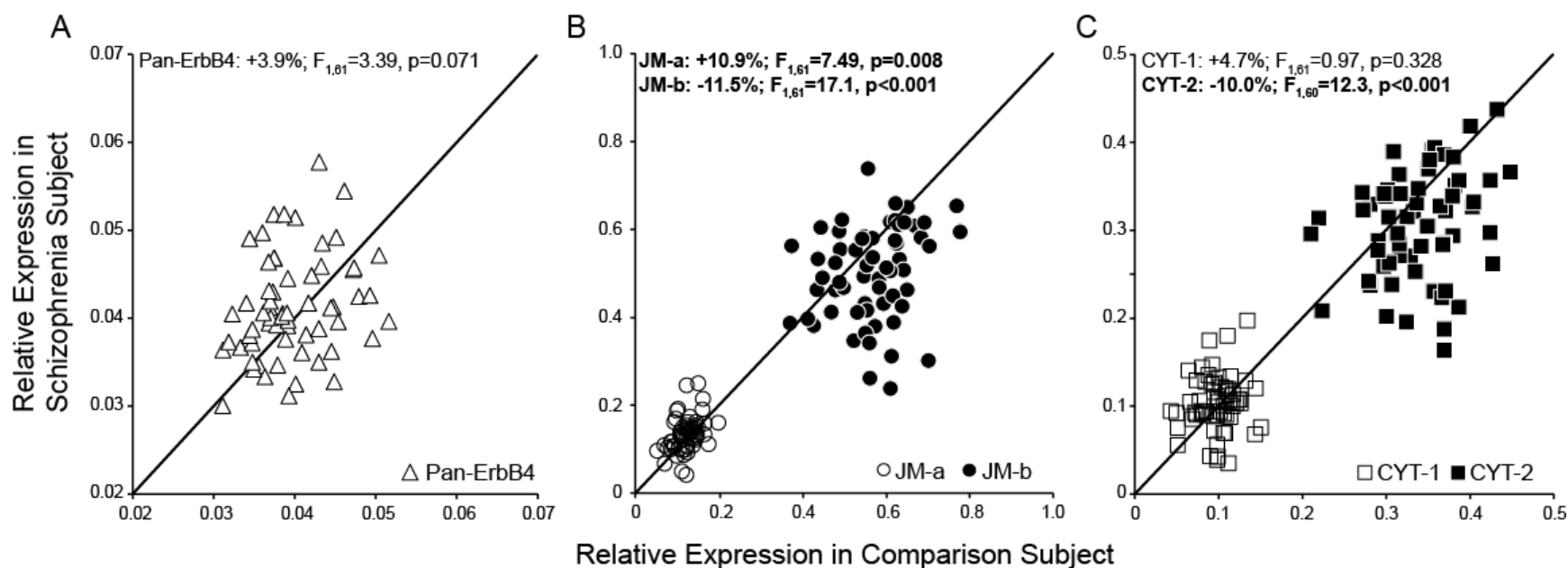


**Figure 2. mRNA levels for pan-ErbB4 and normalized ErbB4 splicing variants in DLPFC area 9 total gray matter for each matched pair of healthy comparison and schizophrenia subjects.**

Markers to the right or left of the diagonal unity line indicate lower or higher mRNA levels in schizophrenia subjects, respectively. (A) Mean ( $\pm$ SD) mRNA levels for pan-ErbB4 mRNA levels did not differ between schizophrenia ( $0.041\pm 0.006$ ) and comparison subjects ( $0.040\pm 0.005$ ). (B) Mean mRNA levels were statistically significantly higher for JM-a and lower for JM-b in schizophrenia (JM-a:  $0.133\pm 0.04$ , JM-b:  $0.500\pm 0.12$ ) relative to comparison subjects (JM-a:  $0.120\pm 0.03$ , JM-b:  $0.565\pm 0.09$ ). (C) CYT-1 mRNA levels did not differ whereas CYT-2 mRNA levels were lower in schizophrenia (CYT-1:  $0.103\pm 0.03$ , CYT-2:  $0.304\pm 0.06$ ) relative to comparison subjects (CYT-1:  $0.098\pm 0.02$ , CYT-2:  $0.338\pm 0.05$ ).

### **2.3.2 Micro-dissection of layer 2 or 4 yields samples enriched in CR or PV interneurons, respectively**

Next, we quantified CR and PV mRNA levels in micro-dissected samples of cortical layers 2 and 4 from the 39 matched pairs of schizophrenia and comparison subjects (**Figure 3A, B**). Relative to layer 4, CR mRNA levels in layer 2 were significantly 9.4 and 9.8 fold higher, respectively, in healthy comparison (Repeated Measures:  $F_{1,114}=593$ ;  $p<0.001$ ) and in schizophrenia (Repeated Measures:  $F_{1,114}=517$ ;  $p<0.001$ ) subjects. Relative to layer 2, PV mRNA levels in layer 4 were significantly 13.9 and 10.9 fold higher, respectively, in healthy comparison (Repeated Measures:  $F_{1,114}=590$ ;  $p<0.001$ ) and in schizophrenia (Repeated Measures:  $F_{1,114}=373$ ;  $p<0.001$ ) subjects. These data confirm that layer 2 is largely devoid of PV interneurons and heavily enriched in CR interneurons, whereas the opposite is true for layer 4. Mean CR mRNA levels did not differ in either layer 2 or 4 between subject groups (**Figure 3C, D**). In contrast, mean PV mRNA levels were significantly ( $F_{1,38}=14.6$ ;  $p<0.001$ ) 19.5% lower in layer 4 of schizophrenia subjects but did not differ in layer 2 between subject groups (**Figure 3C, D**). In concert, these findings are consistent with a prior report that in the DLFPC of schizophrenia subjects PV expression is selectively altered in layer 4 but not in layer 2, whereas CR expression is not altered in any layer (Hashimoto et al., 2003).

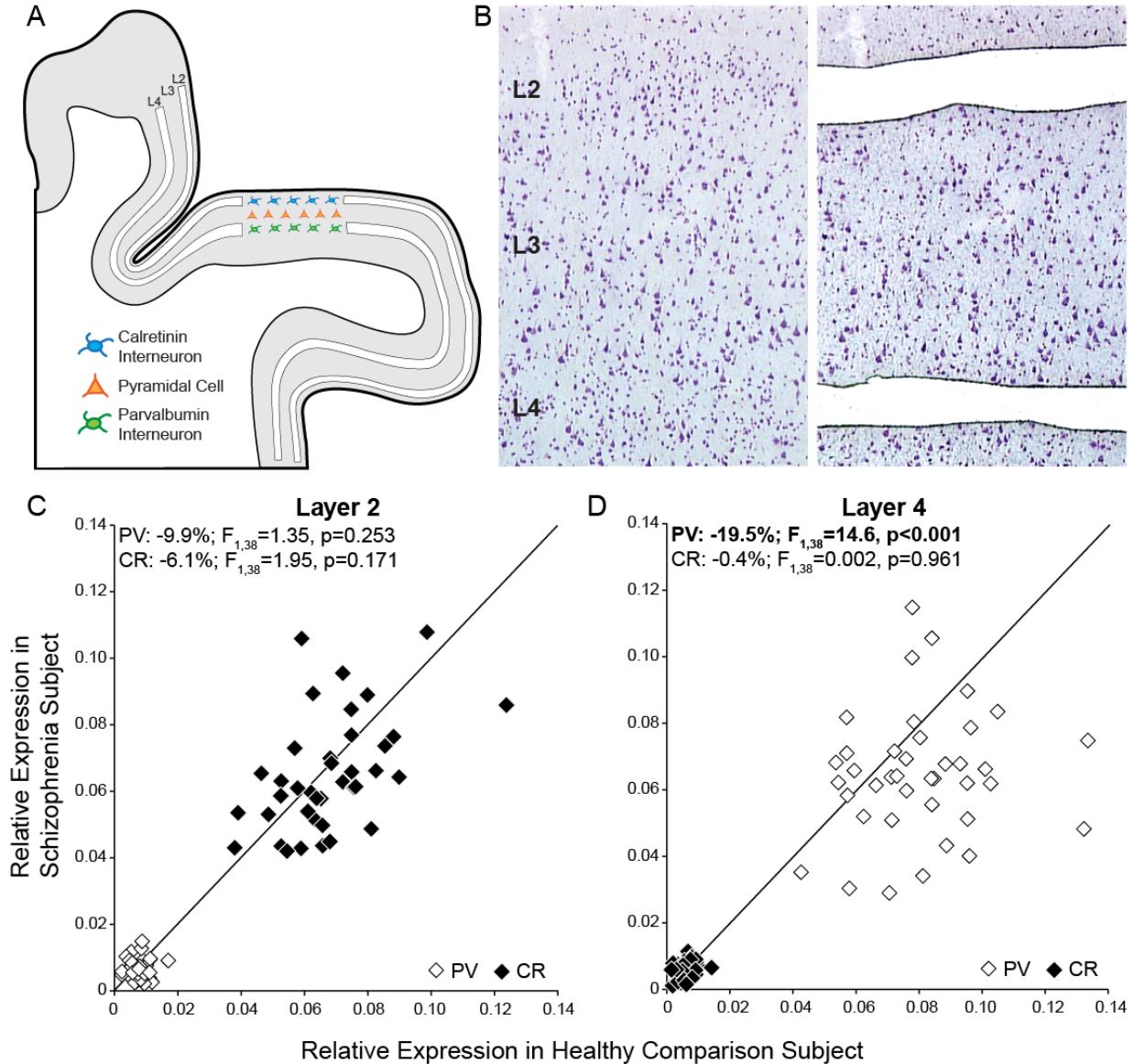


**Figure 3. Layer-specific quantification of PV and CR mRNA levels in DLPFC area 9 for each matched pair of healthy comparison and schizophrenia subjects.**

(A) Based on the size and packing density of Nissl-stained cells, layers 2 and 4 were identified and laser microdissected from the same section. (B) In layer 2, CR mRNA was heavily expressed relative to PV mRNA and CR mRNA levels did not differ between schizophrenia (CR:  $0.065 \pm 0.02$ , PV:  $0.007 \pm 0.003$ ) and comparison subjects (CR:  $0.069 \pm 0.02$ , PV:  $0.007 \pm 0.003$ ). (C) In layer 4, PV mRNA was heavily expressed relative to CR mRNA and PV mRNA levels were significantly lower in schizophrenia (CR:  $0.006 \pm 0.002$ , PV:  $0.065 \pm 0.02$ ) relative to comparison subjects (CR:  $0.006 \pm 0.003$ , PV:  $0.080 \pm 0.02$ ).

### **2.3.3 Abnormal shifts in ErbB4 splicing from major to minor variants occur selectively in DLPFC layer 4 of schizophrenia subjects**

Mean pan-ErbB4 mRNA levels did not differ in either layer 2 or layer 4 between subject groups (**Figure 4A, D**). Mean normalized JM-a mRNA levels were significantly ( $F_{1,38}=4.62$ ,  $p=0.038$ ) 22.1% higher, whereas mean normalized JM-b mRNA levels were significantly ( $F_{1,38}=15.1$ ,  $p<0.001$ ) 17.0% lower in layer 4 of schizophrenia subjects (**Figure 4E**). Neither transcript level was significantly different between subject groups in layer 2 (**Figure 4B**). Mean normalized CYT-1 mRNA levels were significantly ( $F_{1,38}=7.07$ ,  $p=0.011$ ) 19.3% higher, whereas mean normalized CYT-2 mRNA levels were nearly significantly ( $F_{1,38}=3.98$ ,  $p=0.053$ ) 10.2% lower in layer 4 of schizophrenia subjects (**Figure 4F**). Neither transcript level was significantly different between subject groups in layer 2 (**Figure 4C**). None of the covariates were significant in any of these analyses except for an effect of brain pH on JM-b mRNA levels in layer 2 ( $F_{1,37}=8.34$ ,  $p=0.006$ ). In addition, mean normalized levels of JM-a, JM-b, CYT-1 and CYT-2 mRNAs in layer 4 of schizophrenia subjects did not differ significantly as a function of sex, diagnosis of schizoaffective disorder, history of substance dependence or abuse, nicotine use at the time of death, use of antipsychotics, antidepressants, or benzodiazepines and/or sodium valproate at the time of death, or death by suicide (**Appendix B; Figure 21**).

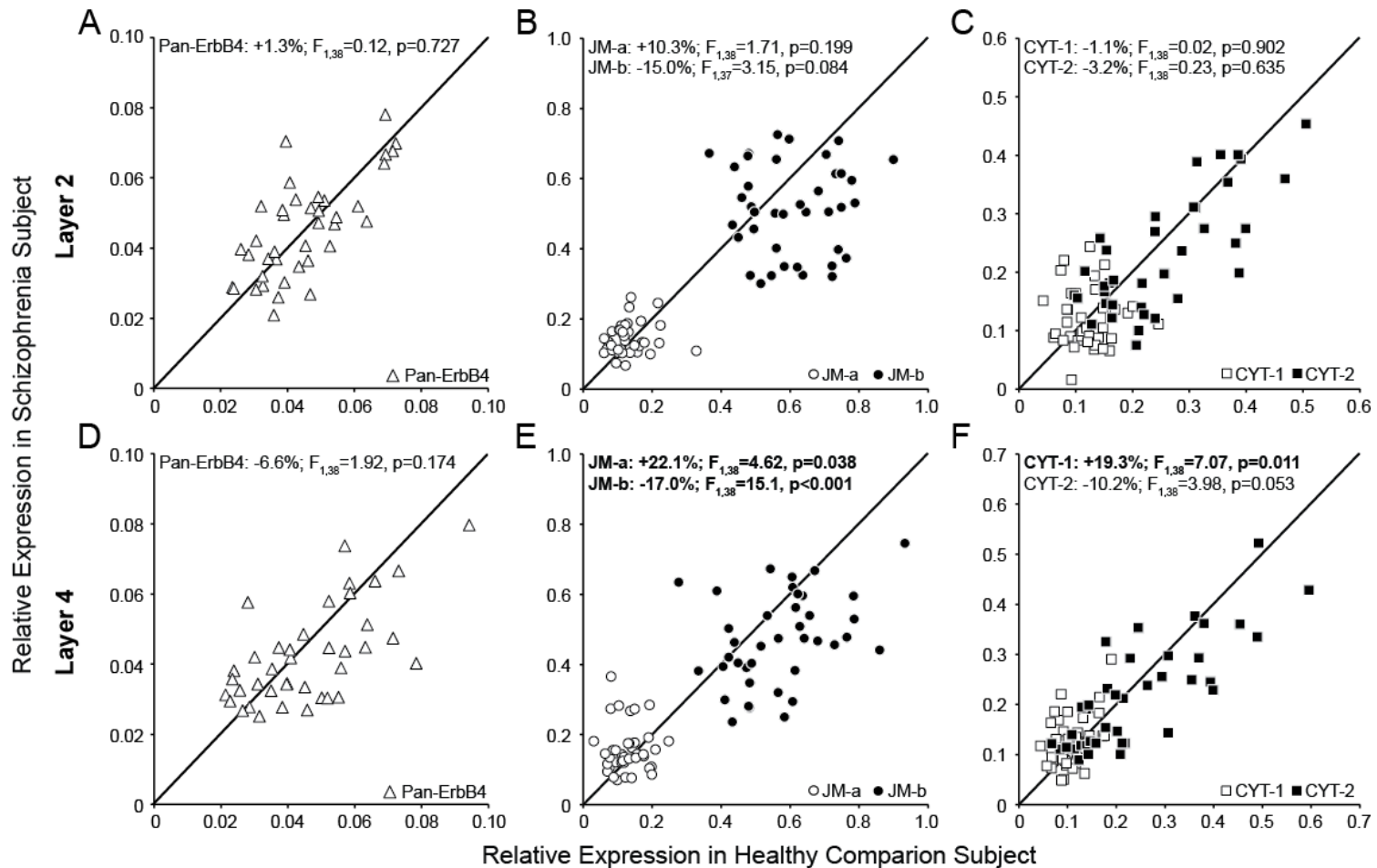


**Figure 4. Layer-specific quantification of mRNA levels for pan-ErbB4 and normalized ErbB4 splicing variants**

(A, D) In layers 2 and 4, mean ( $\pm$ SD) pan-ErbB4 mRNA levels did not differ between schizophrenia (layer 2:  $0.045\pm 0.01$ , layer 4:  $0.042\pm 0.01$ ) and comparison subjects (layer 2:  $0.045\pm 0.01$ , layer 4:  $0.045\pm 0.02$ ). (B, C) In layer 2, JM-b levels were lower whereas CYT-1, CYT-2 and JM-a levels did not differ between schizophrenia (JM-a:  $0.144\pm 0.04$ , JM-b:  $0.515\pm 0.13$ , CYT-1:  $0.119\pm 0.05$ , CYT-2:  $0.240\pm 0.12$ ) and healthy comparison subjects (JM-a:  $0.131\pm 0.05$ , JM-b:  $0.606\pm 0.13$ , CYT-1:  $0.121\pm 0.04$ , CYT-2:  $0.248\pm 0.11$ ). (E, F) In layer 4, CYT-1 and JM-a levels were higher, JM-b levels were lower and CYT-2 levels did not differ in schizophrenia subjects (JM-a:  $0.157\pm 0.07$ , JM-b:  $0.471\pm 0.13$ , CYT-1:  $0.127\pm 0.05$ , CYT-2:  $0.217\pm 0.11$ ) relative to healthy comparison subjects (JM-a:  $0.129\pm 0.05$ , JM-b:  $0.567\pm 0.14$ , CYT-1:  $0.107\pm 0.03$ , CYT-2:  $0.242\pm 0.13$ ).

### **2.3.4 PV mRNA levels are negatively correlated with the ratio of JM-a/JM-b variants in DLPFC layer 4 of schizophrenia subjects**

In layer 2, CR mRNA levels did not correlate with the ratio of either JM-a/JM-b variants or CYT-1/CYT-2 variants in either schizophrenia or healthy comparison subjects. In layer 4, a strong negative correlation was observed between PV mRNA levels and the ratio of JM-a/JM-b variants only in schizophrenia subjects ( $r=-0.50$ ;  $p<0.001$ ). The ratio of CYT-1/CYT-2 variants did not correlate with PV mRNA levels in layer 4 of either subject group (**Appendix B; Table 6**).

### **2.3.5 MIAT levels are increased preferentially in PV interneurons in schizophrenia subjects**

Next we assessed whether abnormal MIAT levels might contribute to dysregulated ErbB4 splicing in schizophrenia. In DLPFC gray matter homogenates from the 62 subject pairs, mean MIAT levels were significantly ( $F_{1,60}=6.79$ ,  $p=0.012$ ) 12.6% higher in schizophrenia subjects relative to healthy comparison subjects (**Figure 5A**). None of the covariates were significant except for an effect of RIN ( $F_{1,60}=4.08$ ,  $p=0.048$ ). In DLPFC gray matter, the levels of MIAT were significantly positively correlated with the ratio of JM-a/JM-b variants ( $r=0.26$ ;  $p=0.004$ ) and the ratio of CYT-1/CYT-2 variants ( $r=0.21$ ;  $p=0.021$ ) and significantly negatively correlated with PV mRNA levels ( $r=-0.20$ ;  $p=0.027$ ) across all subjects. MIAT is expressed not only in layers 2 and 4, but is also found in high levels in layers 3 and 5 (Hawrylycz et al., 2012), suggesting that MIAT may be expressed in both pyramidal cells and interneurons in DLPFC

layer 4. Thus, in order to assess MIAT levels selectively in PV interneurons, we evaluated MIAT levels in laser-microdissected cells labeled with the PV-specific marker *Vicia villosa agglutinin* (VVA) from available microarray data in 14 of our subject pairs (**Appendix A; Table 3**) (Georgiev et al., 2014). Mean MIAT levels were significantly ( $t_{13}=-3.17$ ,  $p=0.007$ ) 50.8% higher in VVA-positive cells in subjects with schizophrenia relative to healthy comparison subjects (**Figure 5B**). In the DLPFC gray matter of these 14 subject pairs, mean MIAT levels did not differ ( $F_{1,13}=0.17$ ,  $p=0.690$ ) between subject groups (**Figure 5A**) suggesting that increased MIAT expression preferentially occurs in PV neurons.

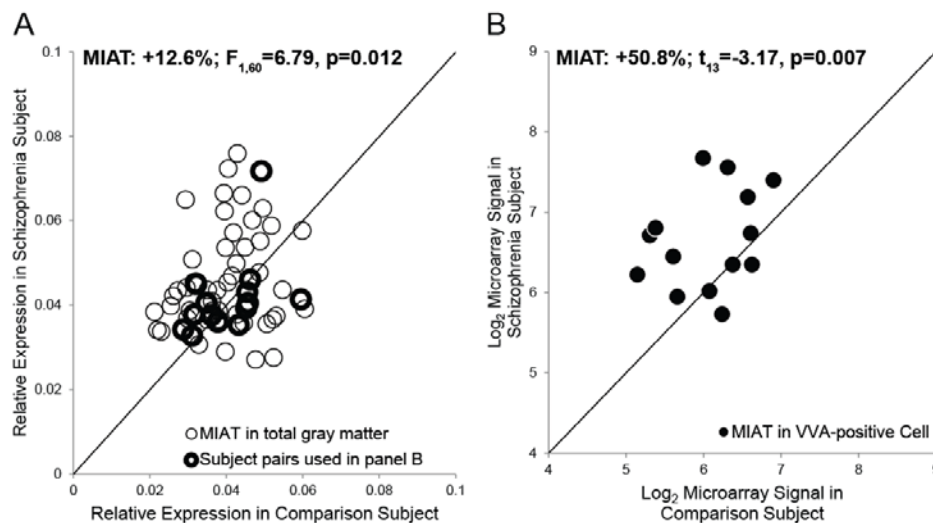


**Figure 5. Quantification of MIAT levels in DLPFC area 9 total gray matter for 62 subject pairs and in *Vicia villosa agglutinin* (VVA)-positive cells for 14 subject pairs.**

(**A, B**) Mean MIAT levels were significantly higher in DLPFC total gray matter and in VVA-positive cells of schizophrenia (total gray matter:  $0.045\pm 0.01$ , VVA ( $\log_2$  value):  $6.059\pm 0.56$ ) relative to healthy comparison subjects (total gray matter:  $0.040\pm 0.01$ , VVA ( $\log_2$  value):  $6.652\pm 0.61$ ).

### **2.3.6 Schizophrenia-associated intronic SNPs at the ErbB4 locus are not associated with the ratios of ErbB4 splicing variants**

Finally, we investigated the effect of schizophrenia-associated intronic SNPs at the ErbB4 locus on the ratios of ErbB4 splicing variants in DLPFC total gray matter of 62 subject pairs or in DLPFC layer 4 of 39 subject pairs. The risk SNP at rs4673620 was previously implicated with higher JM-a mRNA levels, whereas the risk SNPs at rs7598440, rs707284 and rs839523 were associated with higher CYT-1 mRNA levels in schizophrenia subjects (Law et al., 2007). Our SNP analyses did not reveal a main effect of rs4673620 on the ratio of JM-a/JM-b variants in total gray matter or in layer 4 of all subjects. No main effect of rs7598440, rs707284 or rs839523 on the ratio of CYT-1/CYT-2 variants in either total gray matter or in layer 4 was observed in all subjects. Interactions between diagnosis and genotypes were also not detected in either total gray matter or layer 4 of all subjects (**Appendix B; Table 7**).

## **2.4 DISCUSSION**

Dysregulated alternative splicing of ErbB4 mRNAs has been consistently observed in the DLPFC of schizophrenia subjects (Silberberg et al., 2006; Law et al., 2007; Law et al., 2012; Joshi et al., 2014). Higher JM-a variant and unaltered pan-ErbB4 levels in schizophrenia subjects have been replicated in all prior studies and were also confirmed in the present study. In contrast to prior studies, we also detected the expected lower levels of JM-b mRNA in schizophrenia subjects. Reciprocal differences in the levels of JM variants, accompanied by unchanged pan-ErbB4 mRNA levels, argue for an abnormal shift in ErbB4 splicing from JM-b to JM-a variants

in schizophrenia. Three previous reports showed higher CYT-1 variant levels in the DLPFC of schizophrenia subjects (Silberberg et al., 2006; Law et al., 2007; Law et al., 2012), whereas the most recent study found no change (Joshi et al., 2014). We found unaltered CYT-1 variant levels but did detect lower levels of CYT-2 variants in schizophrenia subjects. In concert, these findings suggest that a modest shift in splicing from CYT-2 to CYT-1 variants may occur in some subjects with schizophrenia.

Next, we sought to investigate whether dysregulated ErbB4 splicing is associated selectively with PV interneurons and contributes to lower PV mRNA levels in schizophrenia. The laminar micro-dissection yielded preferential enrichment of CR or PV mRNA in layer 2 or 4, respectively, and comparable levels of pan-ErbB4 in both layers. Because ErbB4 is localized in CR and PV interneurons in the primate DLPFC (Neddens et al., 2011), our results support the idea that the layer-specific quantification of ErbB4 mRNAs allows an indirect measurement of their levels in each of those cell types. Pan-ErbB4 mRNA levels were unaltered in either layer 2 or 4 of schizophrenia subjects, suggesting that transcription of the ErbB4 gene is not affected in either CR or PV interneurons in schizophrenia. We found significantly higher levels of JM-a and CYT-1 variants and significantly lower levels of JM-b variants and nearly significantly lower CYT-2 variant levels in layer 4, but not in layer 2, of schizophrenia subjects. These findings suggest that the dysregulated shift in ErbB4 splicing from major to minor variants occurs selectively in PV interneurons. Finally, the negative correlation between the JM-a/JM-b variants ratio and PV mRNA levels selectively in layer 4 of schizophrenia subjects supports the hypothesis that dysregulated splicing at the JM locus contributes to an activity-dependent down-regulation of PV expression in schizophrenia.

In layer 2 we also detected non-significantly higher JM-a and lower JM-b levels in schizophrenia subjects, indicating a weak shift in splicing from JM-b to JM-a variants. Interestingly, ErbB4 is also present in most of the cholecystokinin-positive (CCK) interneurons as well as in ~ 10 to 30% of calbindin-positive interneurons, which together comprise ~18% of ErbB4-positive cells in the superficial layers (but only ~5 % in the middle layers) of primate DLPFC (Neddens et al., 2011). The majority of calbindin-positive cells also express somatostatin (SST) (Gonzalez-Albo et al., 2001). Therefore, although the majority of ErbB4 transcripts quantified in layer 2 are from CR interneurons, some proportion of these ErbB4 transcripts would likely be from CCK and SST interneurons. Interestingly, both CCK and SST mRNAs levels are lower in the DLPFC of schizophrenia subjects (Hashimoto et al., 2008b), suggesting that the modest shift in splicing at the JM locus in layer 2 of schizophrenia subjects may represent dysregulated ErbB4 splicing in these cell populations.

The non-coding RNA MIAT was recently reported to regulate the alternative splicing of ErbB4 transcripts (Barry et al., 2014). In DLPFC total gray matter homogenates of our 62 subject pairs, MIAT levels were higher in schizophrenia subjects, positively correlated with the ratios of minor to major variants, and negatively correlated with PV mRNA levels across all subjects. These findings implicate higher MIAT levels as a possible mechanism responsible for the abnormal shifts in ErbB4 splicing in PV interneurons in schizophrenia. In support of this idea, MIAT levels were higher in VVA-positive PV interneurons but unaltered in total gray matter homogenates of schizophrenia subjects in the 14 subject pairs used for both the microarray and the qPCR analyses, demonstrating that MIAT levels are higher preferentially in PV interneurons in schizophrenia.

Converging evidence suggests that ErbB4 signaling positively regulates the activity of PV interneurons. ErbB4 signaling increases the formation of excitatory inputs onto PV interneurons by regulating the synaptic accumulation of PSD-95 (Ting et al., 2011; Del Pino et al., 2013) and the AMPA receptor subunit GluA1 (Abe et al., 2011). Moreover, ErbB4 activation inhibits the activity of Kv 1.1 channel in PV interneurons (Li et al., 2012) and decreases postsynaptic inhibitory currents by internalizing GABA(A)  $\alpha$ 1 receptors (Mitchell et al., 2013). Previous literature suggested that higher JM-a levels might lead to the loss of ErbB4 signaling, given the differential downstream consequences of the JM isoforms (Silberberg et al., 2006; Law et al., 2007; Joshi et al., 2014). Our data suggest that the PV-specific dysregulated splicing at the JM locus produces a gain of the JM-a isoform as well as a loss of the JM-b isoform in schizophrenia, which may additively contribute to impaired ErbB4 signaling in PV interneurons.

Our study presents novel evidence for alterations in a molecular cascade that may contribute to PV interneuron dysfunction in schizophrenia. Specifically, higher MIAT levels in PV interneurons may lead to an abnormal shift in ErbB4 splicing from JM-b to JM-a variants, which would result in impaired ErbB4 signaling. Given the role of ErbB4 signaling in the formation of excitatory inputs, the resulting reduction in excitatory drive to PV neurons would lead to a corresponding activity-dependent down-regulation of PV expression in schizophrenia. Lower PV interneuron activity is associated with reduced cortical network activity at gamma-band frequency (Sohal et al., 2009) which is required for normal cognitive functions, such as working memory (Fries, 2009). Indeed, patients with schizophrenia demonstrate lower gamma-band power during working memory tasks (Cho et al., 2006). Thus, our findings suggest that dysregulated ErbB4 splicing may provide, at least in part, a molecular substrate for lower PV

interneuron activity that could contribute to impaired gamma oscillations and cognitive dysfunction in individuals with schizophrenia.

### **3.0 PATHOLOGICAL BASIS FOR DEFICIENT EXCITATORY DRIVE TO CORTICAL PARVALBUMIN INTERNEURONS IN SCHIZOPHRENIA**

Adapted from Chung DW, *et al.* (2016) Pathological basis for deficient excitatory drive to cortical parvalbumin interneurons in schizophrenia. *Am J Psychiatry* in press.

#### **3.1 INTRODUCTION**

Cognitive dysfunction is a core and clinically-critical feature of schizophrenia(Kahn and Keefe, 2013) but responds poorly to available medications(Keefe and Harvey, 2012). Therefore, identifying the neural substrate for these cognitive deficits is critical for the development of new therapeutic interventions. Certain cognitive deficits, such as impaired working memory, appear to emerge from altered gamma oscillations in the dorsolateral prefrontal cortex (DLPFC)(Uhlhaas and Singer, 2010). Because cortical gamma oscillations require the activity of parvalbumin-containing (PV) interneurons(Cardin et al., 2009; Sohal et al., 2009), deficient cortical PV interneuron activity could provide the neural substrate for altered prefrontal gamma oscillations and consequently impaired working memory in schizophrenia.

Lower glutamatergic drive to PV interneurons has been hypothesized to be the cause of deficient PV interneuron activity in schizophrenia(Coyle et al., 2012; Gonzalez-Burgos and Lewis, 2012; Moghaddam and Krystal, 2012). This hypothesis is based on findings that

experimental manipulations in model systems which reduce glutamatergic drive to PV interneurons result in lower PV interneuron activity accompanied by lower expression of activity-dependent gene products (e.g., PV and the GABA-synthesizing enzyme glutamic acid decarboxylase 67, GAD67), abnormal gamma oscillations and working memory deficits (Behrens et al., 2007; Belforte et al., 2010; Del Pino et al., 2013; Pelkey et al., 2015). Consistent with this hypothesis, postmortem studies have repeatedly shown lower PV and GAD67 levels in the DLPFC of schizophrenia subjects (Akbarian et al., 1995; Volk et al., 2000; Hashimoto et al., 2003; Fung et al., 2010; Curley et al., 2011), which are thought to reflect lower glutamatergic drive to a subset of PV neurons and not a loss of PV neurons in the illness (Akbarian et al., 1995; Woo et al., 1997; Hashimoto et al., 2003; Enwright et al., 2016). These deficits do not seem to be due to a global reduction in excitatory drive to all interneuron subtypes, as calretinin-containing (CR) interneurons, the most abundant interneuron subtype in the primate DLPFC (Conde et al., 1994), appear to be relatively unaffected in schizophrenia (Hashimoto et al., 2003; Fung et al., 2010; Chung et al., 2016b). However, the pathological basis for lower glutamatergic drive selectively onto PV interneurons, such as fewer excitatory synapses on these neurons, has not been identified in people with schizophrenia.

Therefore, in this study, we used multi-labeling fluorescent immunohistochemistry, confocal imaging and a custom post-image processing method to directly assess excitatory synapses on parvalbumin-positive (PV+) neurons in the DLPFC from matched pairs of schizophrenia and unaffected comparison subjects. We tested the hypotheses that 1) lower PV levels in subjects with schizophrenia reflect altered PV expression per neuron and not a loss of PV+ neurons; 2) PV+, but not calretinin-positive (CR+), neurons receive fewer excitatory

synaptic inputs in subjects with schizophrenia; and 3) fewer excitatory synapses on PV+ neurons are associated with activity-dependent down-regulation of PV and GAD67 levels.

## 3.2 MATERIALS AND METHODS

### 3.2.1 Human subjects

Brain specimens (N=40) were obtained during routine autopsies conducted at the Allegheny County Office of the Medical Examiner (Pittsburgh, PA) after consent was obtained from the next-of-kin. An independent team of clinicians made consensus DSM-IV diagnoses for each subject based on structured interviews with family members and review of medical records. The absence of a psychiatric diagnosis was confirmed in unaffected comparison subjects using the same approach. All procedures were approved by the University of Pittsburgh Committee for the Oversight of Research and Clinical Training Involving the Dead and the Institutional Review Board for Biomedical Research. The subjects were selected based on a postmortem interval (PMI) less than 24 hours in order to avoid the effect of PMI on protein immunoreactivity (**Appendix C; Supplementary Methods**). In addition, to control for the autofluorescence emitted by lipofuscin which accumulates with aging (Porta, 2002), all subjects were less than 62 years of age. To control for experimental variance and to reduce biological variance, each subject with schizophrenia or schizoaffective disorder (N=20) was paired with one unaffected comparison subject for sex and as closely as possible for age (**Appendix A; Table 3**). The mean age, PMI and tissue storage time did not differ between subject groups (**Table 2**).

**Table 2. Summary of demographic and postmortem characteristics of human subjects used in immunohistochemical assay.**

<b>Characteristic</b>	<b>Unaffected comparison</b>		<b>Schizophrenia</b>	
	<b>N</b>	<b>%</b>	<b>N</b>	<b>%</b>
<b>Sex</b>				
Male	15	75	15	75
Female	5	25	5	25
<b>Race</b>	<b>No</b>	<b>%</b>	<b>No</b>	<b>%</b>
White	16	80	14	70
Black	4	20	6	30
	<b>Mean</b>	<b>SD</b>	<b>Mean</b>	<b>SD</b>
<b>Age (years)</b>	46.3	12.1	45.2	11.8
<b>Postmortem interval (hours)</b>	16.4	5.5	15.4	6.3
<b>Freezer storage time (months)</b>	110.8	33.9	103.5	28.3

### 3.2.2 Fluorescent Immunohistochemistry

Paraformaldehyde-fixed coronal tissue sections (40 $\mu$ m) containing DLPFC area 9 were processed for fluorescent immunohistochemistry as previously described (Glausier et al., 2014). Sections were pretreated for antigen retrieval (0.01M sodium citrate for 75 minutes at 80°C) and then incubated for 72 hours in the following primary antibodies: PV (mouse, 1:1000, Swant, Bellinzona, Switzerland), CR (goat, 1:1000, Swant), post-synaptic density 95 (PSD95; rabbit, 1:250, Cell Signaling, Danvers, MA) and vesicular glutamate transporter 1 (VGlut1; guinea pig, 1:250, Millipore, Billerica, MA). Tissue sections were then incubated for 24 hours with secondary antibodies (donkey) conjugated to Alexa 488 (anti-mouse, 1:500), 568 (anti-rabbit, 1:500), 647 (anti-guinea pig, 1:500, all from Invitrogen, Carlsbad, CA) or biotin (anti-goat, 1:200, Fitzgerald, Acton, MA). Sections were then incubated with streptavidin 405 (1:200, invitrogen) for 24 hours. After washing, sections were mounted in the Prolong Gold Antifade reagent (Life technologies, Carlsbad, CA), coded to obscure diagnosis and subject number, and

stored at 4°C until imaging. All antibodies used in this study have been previously shown to specifically recognize the targeted protein (**Appendix C; Supplementary Methods**).

### **3.2.3 Image Acquisition**

Images were acquired on an Olympus (Center Valley, PA, USA) IX81 inverted microscope equipped with an Olympus spinning disk confocal unit, a Hamamatsu EM-CCD digital camera (Bridgewater, NJ, USA), and a high-precision BioPrecision2 XYZ motorized stage with linear XYZ encoders (Ludl Electronic Products Ltd, Hawthorne, NJ, USA) using a 60x 1.40 NA SC oil immersion objective. Ten image stacks (512×512 pixels; 0.25 μm z-step) in layer 2 or 4 from each section were selected using a previously published method for systematic random sampling (Sweet et al., 2009). Layer 2 or 4 was defined as 10-20% or 50-60% of the pia-to-white matter distance, respectively (Pierri et al., 1999). We sampled these two layers as layer 4 contains a high density of PV interneurons (Conde et al., 1994) and prominently lower PV mRNA levels in schizophrenia (Hashimoto et al., 2003; Chung et al., 2016b), whereas layer 2 contains a high density of CR interneurons (Gabbott et al., 1997). The very low densities of PV interneurons in layer 2 and of CR interneurons in layer 4 precluded the sampling of these neurons. Lipofuscin for each stack was imaged using a custom fifth channel (excitation wavelength: 405nm; emission wavelength: 647nm) at a constant exposure time as previously described (Rocco et al., 2015).

### 3.2.4 Post-image Processing and Object Sampling

Each fluorescent channel was deconvolved using the Autoquant's Blind Deconvolution algorithm to improve resolving power. VGlut1+ and PSD95+ puncta were used to identify the pre- and postsynaptic elements, respectively, as these molecular markers have been previously used to define excitatory synapses in PV interneurons (Chang et al., 2010; Del Pino et al., 2013; Donato et al., 2013). Masking of VGlut1+ and PSD95+ puncta was performed using the previously described method (**Appendix C; Supplementary Methods and Figure 22**). Edges of PV+ or CR+ cell bodies were segmented by the MATLAB edge function using the Canny edge detector operator (Canny, 1986). The edges of segmented objects were closed, filled and size-gated ( $>80\mu\text{m}^3$ ) to limit the boundaries of PV+ or CR+ cell bodies. All PV+ and CR+ cell body masks were manually cleaned for final analyses (**Appendix C; Figure 22**). We sampled objects that localized within the middle 80% of z-planes ( $\sim 32\ \mu\text{m}$ ), based on antibody penetration efficiency analyses to avoid edge effects (**Appendix C; Supplementary Methods**). The mean volume of tissue sampled did not differ between subject groups (layer 2:  $t_{19}=0.3$ ,  $p=0.776$ ; layer 4:  $t_{19}=0.03$ ,  $p=0.998$ ). The mean numbers of VGlut1+ puncta and PSD95+ puncta sampled in layer 2 or layer 4 did not differ between subject groups (all  $t_{19}<|1.6|$ , all  $p>0.12$ ), indicating the absence of any group differences in cortical lamination. Numbers of VGlut1+/PSD95+ puncta per surface area of PV+ or CR+ cell bodies were calculated in order to determine the density of excitatory synapses on PV+ or CR+ neurons.

### 3.2.5 Antipsychotic-Exposed Monkeys

Male monkeys (*Macaca fascicularis*) received oral doses of haloperidol (12–14 mg), olanzapine (5.5–6.6 mg) or placebo (N=6 per each group) twice daily for 17-27 months as previously described (Dorph-Petersen et al., 2005). Trough plasma levels for haloperidol and olanzapine were within the range associated with clinical efficacy in humans (Dorph-Petersen et al., 2005). Monkeys were euthanized in triads (one monkey from each of the three groups) on the same day. Coronal sections (40  $\mu$ m) containing DLPFC area 9 from each monkey were processed for fluorescent immunohistochemistry as described above.

### 3.2.6 Statistics

Two analyses of covariance (ANCOVA) models were used to assess the main effect of diagnosis on the dependent measures. The paired ANCOVA model included subject pair as a blocking factor, and PMI and tissue storage time as covariates. This paired model accounts both for our attempts to balance diagnostic groups for sex and age and for the parallel tissue processing of both subjects in a pair, but is not a true statistical paired design. Therefore, we also used an unpaired ANCOVA model that included sex, age, PMI and storage time as covariates. Most covariates were not significant and therefore were not included in the final analyses; exceptions included an effect of tissue storage time on the mean density of PSD95+ puncta on PV+ cell bodies ( $F_{1,35}=5.5$ ;  $p=0.025$ ) by unpaired ANCOVA and an effect of storage time on the mean surface area of CR+ cell bodies ( $F_{1,18}=6.5$ ;  $p=0.021$ ) and on the mean density of VGlu1+/PSD95+ puncta on CR+ cell bodies ( $F_{1,18}=8.8$ ;  $p=0.008$ ) by paired ANCOVA.

The potential influence of co-morbid factors (e.g., diagnosis of schizoaffective disorder; history of substance dependence or abuse; nicotine use, antidepressant, or benzodiazepine and/or sodium valproate use at time of death; death by suicide) in the schizophrenia subjects was assessed by an ANCOVA model with each factor as the main effect and sex, age, PMI and storage time as covariates. Pearson's correlation analysis was performed to assess the relationships between the density of VGlut1+/PSD95+ puncta on PV+ cell bodies and somal PV immunoreactivity levels or PV and GAD67 mRNA levels obtained from previously published studies (Kimoto et al., 2014; Volk et al., 2015). For the antipsychotic-exposed monkeys, an ANCOVA was used to assess the main effect of antipsychotic treatment on the dependent measures with triad as a blocking factor.

### 3.3 RESULTS

#### 3.3.1 PV levels are lower in a subset of PV interneurons in schizophrenia

We sampled PV+ neurons in DLPFC layer 4 (**Figure 6A,B**), as lower PV mRNA levels in schizophrenia are prominent in this layer (Hashimoto et al., 2003; Chung et al., 2016b). Consistent with those findings, mean PV protein levels in PV+ cell bodies were significantly 34% lower in subjects with schizophrenia (**Figure 6C**). The mean numbers of PV+ neurons in identical volumes of sampled tissue did not differ between subject groups (**Figure 6D**). Finally, we observed a left shift in the frequency distribution of PV levels per PV+ cell body in schizophrenia subjects relative to comparison subjects (**Figure 6E**). Together, these findings

suggest that lower PV levels in schizophrenia reflect lower PV expression in a subset of PV neurons and not a deficit in PV neuron number.

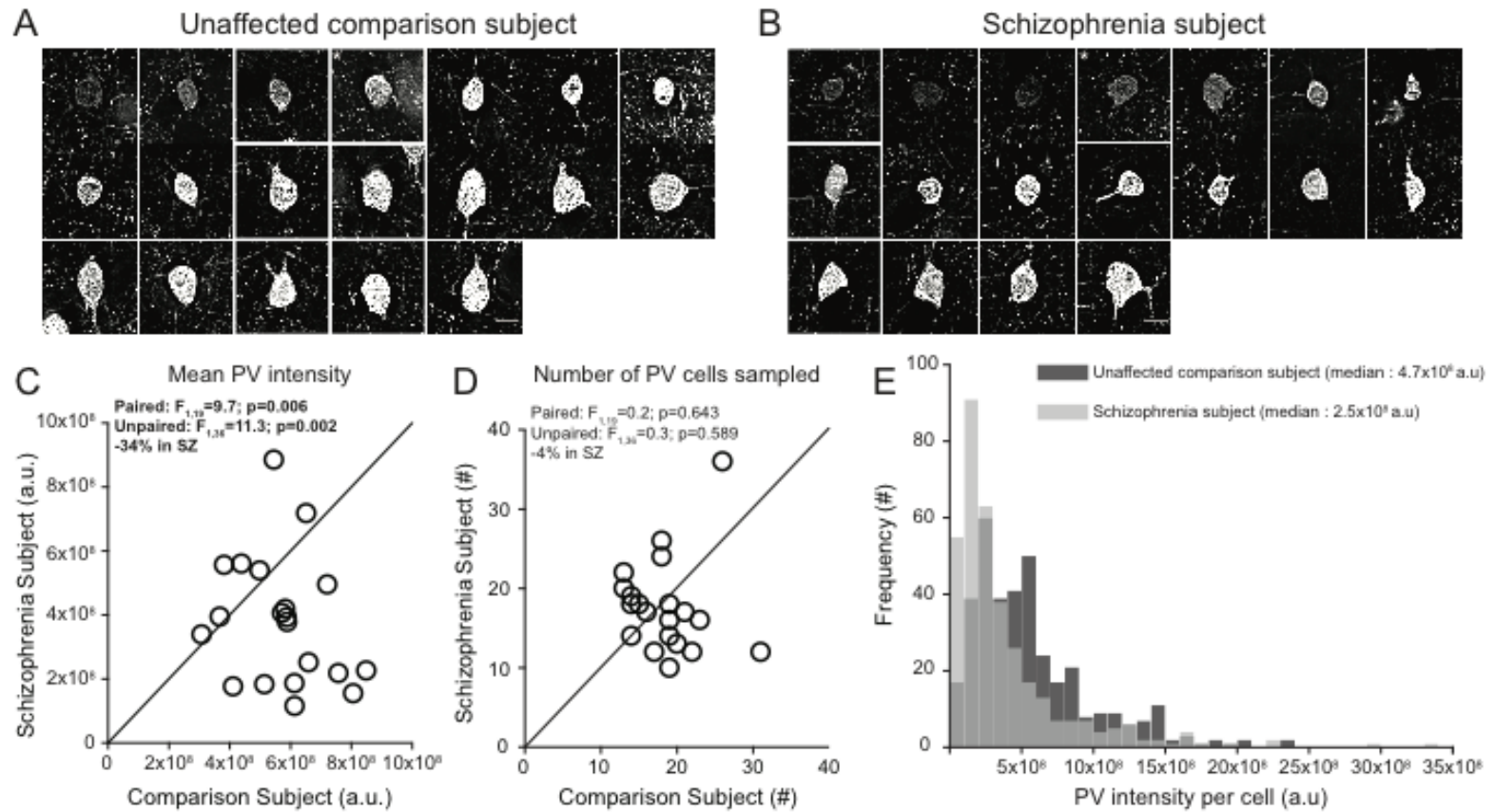


**Figure 6. Levels of PV immunoreactivity are significantly lower in PV interneurons in schizophrenia.**

(A, B) Representative sampling of PV+ neurons, illustrating the range of PV intensity levels, from one subject pair used in this study (healthy comparison subject: Hu1543, 19 cells collected; schizophrenia subject: Hu10026, 18 cells collected). \* denotes PV+ neurons shown in Figure 1. Scale bars = 10  $\mu$ m. (C-F) Scatter plots show the levels of dependent measures (indicated in the heading of each graph) for each healthy comparison and schizophrenia subject in a pair (open circles). Data points below the diagonal unity line indicate a lower level in the schizophrenia subject relative to the matched healthy comparison subject. Statistics from both paired and unpaired ANCOVA analyses are shown for each dependent measure. (C) Mean ( $\pm$ SD) somal PV immunoreactivity levels in PV+ cell bodies were significantly lower in schizophrenia subjects relative to comparison subjects (schizophrenia:  $3.8 \times 10^8 \pm 2.0 \times 10^8$ , comparison:  $5.7 \times 10^8 \pm 1.5 \times 10^8$ ), (D) whereas the mean numbers of PV+ neurons sampled did not differ between subject groups (schizophrenia:  $17.7 \pm 6.0$ , comparison:  $18.5 \pm 4.6$ ). (E) The frequency distributions of somal PV intensity values of PV+ neurons sampled from schizophrenia subjects (light gray) and healthy comparison subjects (dark gray). Each bin represents  $1 \times 10^8$  a.u.

### 3.3.2 PV interneurons receive fewer excitatory synaptic inputs in schizophrenia

The pre- and postsynaptic elements of excitatory synapses on PV+ neurons were identified by VGlut1+ puncta and PSD95+ puncta, respectively (**Figure 7A, B**). Excitatory synapses were defined by the overlap of VGlut1+ and PSD95+ (VGlut1+/PSD95+) puncta. The mean density of VGlut1+/PSD95+ puncta on PV+ cell bodies was significantly 18% lower in schizophrenia subjects (**Figure 7C**). The mean densities of VGlut1+ or PSD95+ puncta on PV+ cell bodies were also significantly 12% or 19% lower, respectively, in schizophrenia subjects (**Figure 7D, E**), reflecting fewer pre- and postsynaptic glutamatergic structures on PV+ neurons.

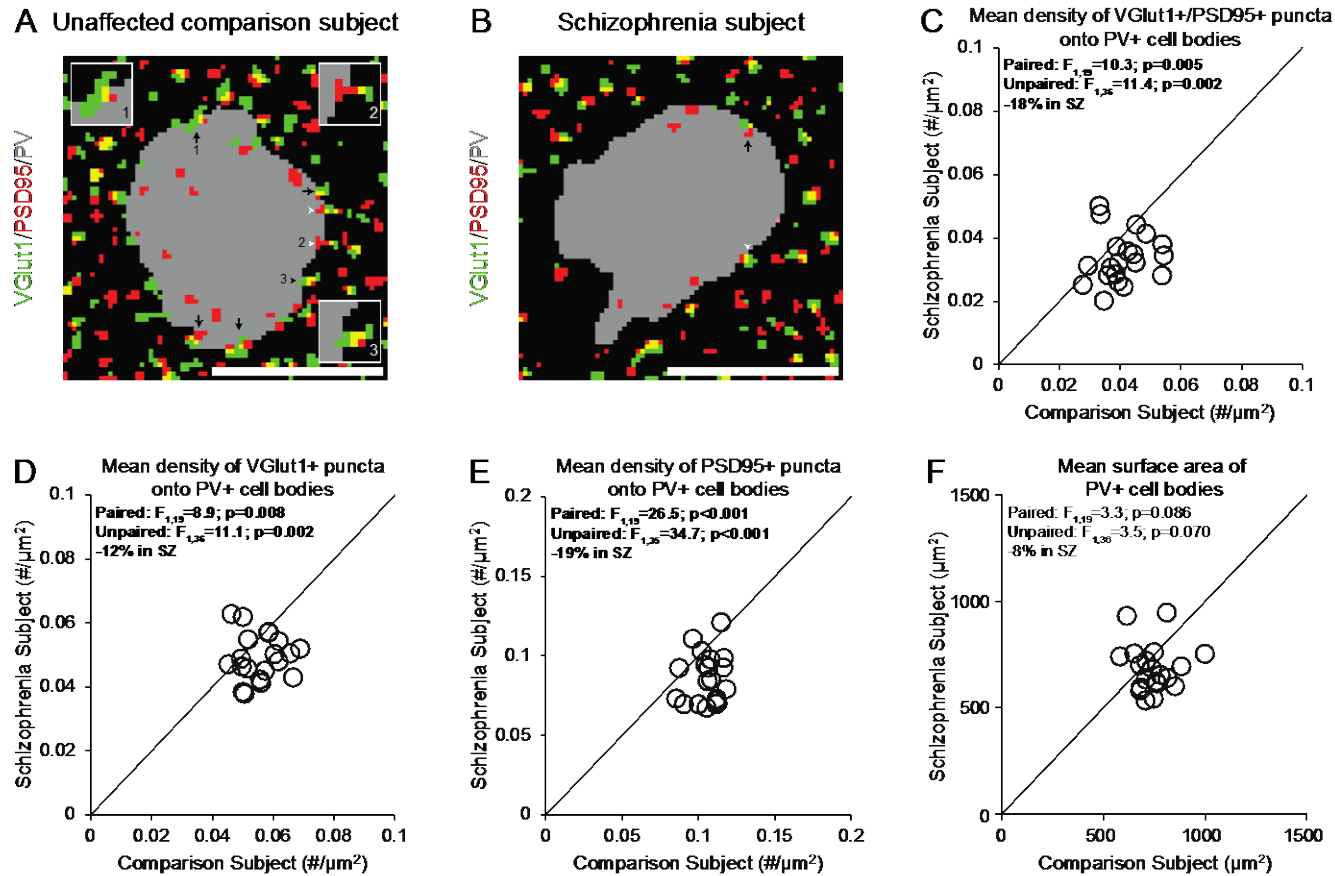


**Figure 7. Density of excitatory synaptic inputs to PV interneurons is significantly lower in schizophrenia**

(A, B) Representative masked images of VGlut1+ puncta (green), PSD95+ puncta (red) and PV+ cell bodies (gray) from the subject pair shown in Figure 6. Excitatory synaptic inputs to PV+ neurons were identified by the overlap of VGlut1+/PSD95+ puncta (yellow) within a PV+ cell body (black arrows, inset image #1). Overlapping VGlut1+/PSD95+ where only the PSD95+ puncta (white arrowheads, inset image #2) or VGlut1+ puncta (black arrowheads, inset image #3) were located within a PV cell body were not included as excitatory inputs. Scale bars = 10  $\mu$ m. (C) Mean ( $\pm$ SD) density of VGlut1+/PSD95+ puncta (schizophrenia:  $0.0335 \pm 0.008$ , comparison:  $0.0409 \pm 0.008$ ), (D) VGlut1+ puncta (schizophrenia:  $0.0492 \pm 0.007$ , comparison:  $0.0558 \pm 0.007$ ) and (E) PSD95+ puncta (schizophrenia:  $0.0857 \pm 0.016$ , comparison:  $0.106 \pm 0.010$ ) overlapping with PV+ cell bodies were all significantly lower in schizophrenia subjects relative to comparison subjects. (F) Mean surface area of PV+ cell bodies did not differ between subject groups (schizophrenia:  $684 \pm 111$ , comparison:  $745 \pm 96$ ).

### **3.3.3 Fewer excitatory synapses on PV interneurons are not affected by methodological confounds or disease-associated co-morbid factors**

The mean surface area of PV+ cell bodies did not differ between subject groups (**Figure 7F**), indicating that the lower density of excitatory synapses on PV+ neurons in schizophrenia is not due to a larger surface area of PV+ cell bodies. The mean VGlut1 or PSD95 protein levels in labeled puncta on PV+ cell bodies did not differ between subject groups (**Appendix C; Figure 23**), suggesting that our findings of fewer synaptic structures in schizophrenia were not biased by lower levels of synaptic markers. Finally, the mean density of VGlut1+/PSD95+ puncta on PV+ cell bodies did not differ among schizophrenia subjects as a function of assessed co-morbid factors (**Appendix C; Figure 24**) and was not altered in monkeys chronically exposed to psychotropic medications (**Appendix C; Figure 25**). Together, these findings suggest that fewer excitatory synapses on PV+ neurons reflect the disease process of schizophrenia, and are not due to methodological confounds or other factors commonly associated with the illness.

### **3.3.4 CR interneurons do not receive fewer excitatory synaptic inputs in schizophrenia**

In order to determine the cell type-specificity of fewer excitatory synapses on PV+ neurons, we measured the density of excitatory synapses on CR+ neurons. The mean numbers of sampled CR+ neurons, mean somal CR protein levels and mean surface area of CR+ cell bodies did not differ between subject groups (**Figure 8A-C**). The mean density of VGlut1+/PSD95+ puncta on CR+ cell bodies was non-significantly 9% higher in schizophrenia subjects (**Figure 8D**), demonstrating that the number of excitatory synapses on CR+ neurons is not lower in the

illness.

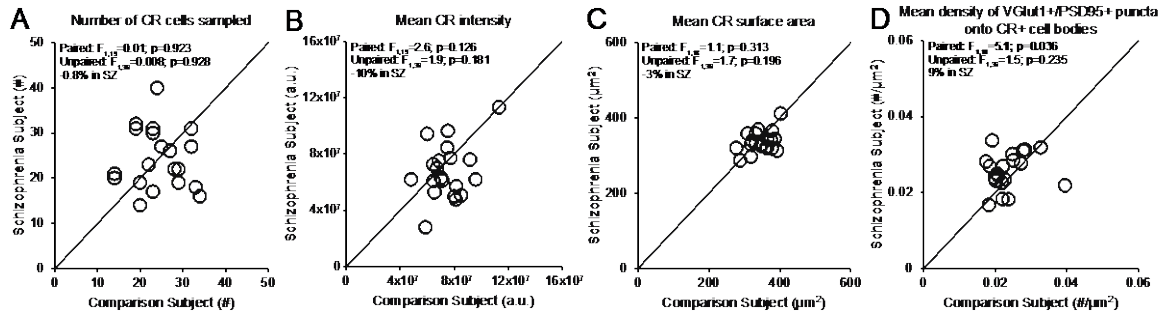


**Figure 8. Density of excitatory synaptic inputs to CR interneurons is modestly higher in schizophrenia**

(A-C) Mean numbers of sampled CR+ neurons (schizophrenia:  $24.3 \pm 6.7$ , comparison:  $24.5 \pm 5.9$ ), mean CR immunoreactivity levels in CR+ cell bodies (schizophrenia:  $6.8 \times 10^7 \pm 2.0 \times 10^7$ , comparison:  $7.5 \times 10^7 \pm 1.5 \times 10^7$ ) or mean surface area of CR+ cell bodies schizophrenia:  $336 \pm 28$ , comparison:  $347 \pm 34$ ) did not differ between subject groups. (D) Mean density of VGlut1+/PSD95+ puncta onto CR+ cell bodies was non-significantly higher in schizophrenia subjects (schizophrenia:  $0.0257 \pm 0.005$ , comparison:  $0.0236 \pm 0.005$ ).

### 3.3.5 Validation of methods for quantifying excitatory synaptic inputs

We have previously shown by dual-labeling electron microscopy that the density of excitatory synapses is significantly 1.90 fold higher on PV+ than CR+ neurons in the primate DLPFC (Melchitzky and Lewis, 2003). Consistent with these findings, the mean density of VGlut1+/PSD95+ puncta on PV+ cell bodies was significantly ( $t_{19} = 8.5$ ,  $p < 0.001$ ) 1.73 fold higher than on CR+ cell bodies in the comparison subjects in the present study. This finding indicates that the light microscopic methods used here provide a robust means for sampling excitatory synaptic inputs specific to PV+ or CR+ neurons.

### 3.3.6 Excitatory synapses on PV interneurons predict PV and GAD67 expression levels in human DLPFC

Finally, we assessed whether the density of excitatory synapses on PV+ neurons predicted levels of PV and GAD67, molecular markers of PV interneuron activity. Mean density of VGlut1+/PSD95+ puncta on PV+ cell bodies was positively correlated with PV and GAD67 mRNA levels in schizophrenia subjects but not in comparison subjects (**Figure 9A, B**). In addition, the mean density of VGlut1+/PSD95+ puncta on PV+ cell bodies positively predicted the mean somal PV immunoreactivity levels in schizophrenia subjects but not in comparison subjects (**Figure 9C**). Moreover, this positive correlation was evident across all sampled PV+ neurons in both subject groups (**Figure 9D**). Among these neurons, the PV+ neurons with the lowest PV levels (more than one standard deviation below the mean) had a density of VGlut1+/PSD95+ puncta significantly ( $t_{112}=-5.4$ ;  $p<0.001$ ) 42% lower than the PV+ neurons with the highest PV levels (more than one standard deviation above the mean).

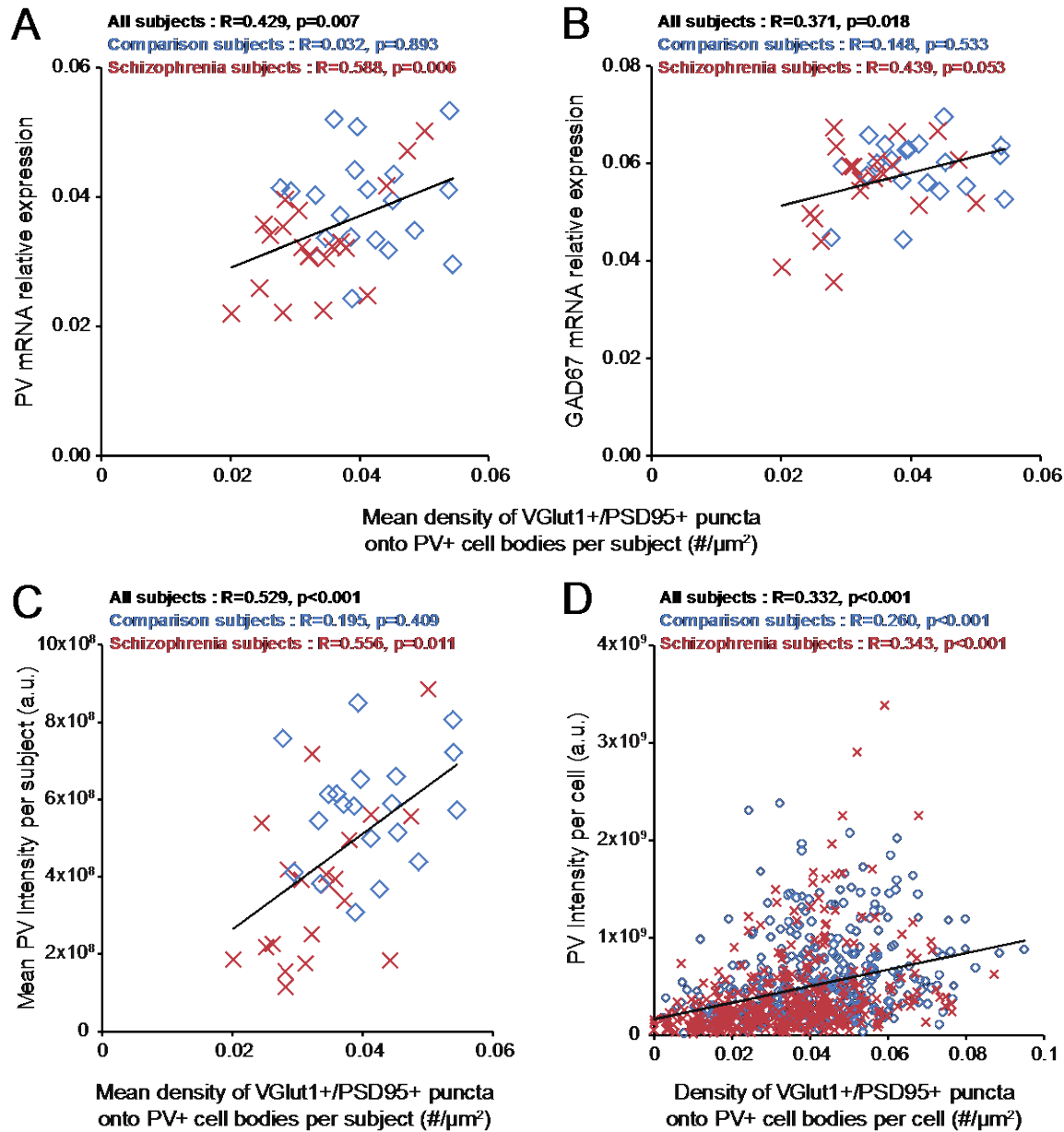


**Figure 9. Lower density of excitatory synaptic inputs to PV interneurons is associated with lower PV and GAD67 expression in human DLPFC**

(A, B) Across all subjects, the mean density of VGlut1+/PSD95+ puncta onto PV+ cell bodies positively predicted the relative levels of PV and GAD67 mRNAs. (C) Across all subjects and (D) across all sampled PV+ neurons (N=725), the density of VGlut1+/PSD95+ puncta onto PV+ cell bodies positively predicted somal PV immunoreactivity levels.

### 3.4 DISCUSSION

A pathological substrate for reduced glutamatergic drive onto PV interneurons in schizophrenia has not been previously identified due to the technical challenges of resolving synaptic abnormalities in a cell type-specific manner in postmortem human brain. Here, we report for the first time that the neuropathology of schizophrenia includes a lower number of excitatory synapses on PV interneurons. This deficit appears to reflect the disease process of schizophrenia and is not due to methodological confounds or other factors commonly associated with the illness. First, fewer excitatory synapses on PV+ neurons were evident from lower numbers of both pre- and postsynaptic markers, validating deficits in the synaptic structures. Second, these deficits were not confounded by either a larger surface area of PV+ cell bodies or undetectable levels of protein markers within existing synaptic structures in schizophrenia subjects. Third, none of the assessed schizophrenia-associated co-morbid factors accounted for these deficits. Fourth, long-term exposure to psychotropic medications did not alter the density of excitatory synapses on PV+ neurons in the DLPFC of non-human primates; the effect of antipsychotics could not be assessed in humans as only one schizophrenia subject had not been exposed to these medications. Fifth, the density of excitatory synapses on CR+ neurons was not lower in the illness, consistent with a prominent pathology of PV interneurons in schizophrenia. Finally, the density of excitatory synapses on PV+ neurons predicted levels of the activity-dependent gene products PV and GAD67 selectively in the schizophrenia subjects. Together, these findings support the hypothesis that fewer excitatory synapses selectively on cortical PV interneurons provide a pathological substrate for deficient excitatory drive to these interneurons in schizophrenia.

PV interneurons comprise two main subtypes: PV basket neurons target the proximal dendrites and cell bodies of pyramidal neurons and PV chandelier neurons synapse onto the axon initial segment of pyramidal neurons(Williams et al., 1992). Although both populations of PV interneuron subtypes are active during gamma oscillations, gamma rhythms are more strongly coupled to the activity of PV basket neurons(Dugladze et al., 2012; Massi et al., 2012). Given the much greater prevalence of PV basket neurons in the middle layers of the primate DLPFC(Krimer et al., 2005; Zaitsev et al., 2005), most of the PV+ neurons sampled in our study are likely to be PV basket neurons.

Our sampling of excitatory synapses on PV+ neurons is limited in two respects. First, we did not sample vesicular glutamate transporter 2-containing excitatory inputs that represent projections from the thalamus(Fremeau et al., 2001). However, thalamic axons represent a small minority (<10%) of excitatory terminals in the cortex(Latawiec et al., 2000) and only a small percentage of thalamic inputs target PV interneurons(Rotaru et al., 2005), suggesting that the excitation of PV interneurons is mostly driven by cortical excitatory inputs. Second, we did not sample synaptic inputs to dendrites of PV interneurons due to the few dendrites originating from PV+ cell bodies, with detectable PV immunoreactivity. Although the density of excitatory synapses is higher onto dendrites than cell bodies of PV interneurons (30), depolarization of the cell body of PV interneurons is much stronger for somal than dendritic excitatory inputs (31,32). However, despite these limitations, the density of excitatory cortical synapses on PV+ cell bodies in the present study predicted activity-dependent PV expression across all PV+ neurons. Therefore, our approach was sufficiently sensitive to detect an apparently functionally meaningful deficit in excitatory synaptic inputs to PV+ neurons in schizophrenia subjects.

Multiple signaling pathways regulate the formation of excitatory synapses on PV interneurons. For example, the ErbB4 signaling pathway induces the formation of excitatory synapses on PV interneurons (Ting et al., 2011; Del Pino et al., 2013; Mei and Nave, 2014) and the release of neuronal pentraxin 2 (Narp) from pyramidal cells recruits excitatory synapses selectively on PV interneurons in an activity-dependent manner (Chang et al., 2010). Both an abnormal shift in ErbB4 splicing at the JM locus (Law et al., 2007; Joshi et al., 2014) and lower Narp transcript levels have been shown in the DLPFC of subjects with schizophrenia, including those included in the present study (Kimoto et al., 2015; Chung et al., 2016b). Across these subjects, the density of VGlut1+/PSD95+ puncta on PV+ cell bodies was significantly correlated with the ratio of ErbB4 JM-a to JM-b splice variants in cortical layer 4 ( $R=-0.436$ ,  $p=0.005$ ) and with Narp mRNA levels in total gray matter ( $R=0.351$ ,  $p=0.026$ ). These findings suggest that alterations in the ErbB4 and/or Narp signaling pathways could be upstream of the deficit in excitatory synaptic inputs to, and consequently the lower activity of, PV interneurons in schizophrenia.

Consistent with the idea that PV interneuron activity is reduced in the illness, activity-dependent expression levels of GAD67 are lower in the DLPFC of subjects with schizophrenia, and specifically in PV interneurons (Volk et al., 2000; Curley et al., 2011). Experimental reductions of GAD67 in PV interneurons decrease inhibitory synaptic transmission in pyramidal cells and alter cortical network activity (Brown et al., 2015; Lazarus et al., 2015; Georgiev et al., 2016). Strong inhibition of pyramidal cells by PV interneurons is required for the generation of gamma oscillations in the DLPFC associated with working memory. Thus, the lower density of excitatory synapses on PV+ neurons and the corresponding deficit in GAD67 expression found in the present study could provide a pathological substrate for deficient inhibition of pyramidal

cells by PV interneurons, which in turn would result in impaired gamma oscillations and working memory deficits in people with schizophrenia.

Discovering pathological entities that bridge etiopathogenic pathways to the core features of the illness is essential for understanding the disease process of schizophrenia. For example, disruptions in the ErbB4 or Narp signaling pathways in the DLFPC could be upstream of the deficits in excitatory synaptic inputs to PV interneurons in schizophrenia. Given that PV interneuron activity is essential for gamma oscillations, these deficits could underlie the downstream pathophysiology of impaired gamma oscillations and consequently working memory dysfunction in schizophrenia. Therefore, fewer excitatory synapses on PV interneurons might serve as a common pathological locus upon which diverse streams of etiopathogenic pathways converge in order to produce a core pathophysiological feature of schizophrenia from which cognitive dysfunction emerges.

## **4.0 DEVELOPMENTAL PRUNING OF EXCITATORY INPUTS TO PARVALBUMIN INTERNEURONS IN MONKEY PREFRONTAL CORTEX: CONTRIBUTION OF ERBB4 SPLICING**

### **4.1 INTRODUCTION**

In primates, certain complex cognitive processes, such as working memory, depend in part on the proper activation of specific neural circuits in the dorsolateral prefrontal cortex (DLPFC) (Goldman-Rakic, 1995). In both monkeys and humans, recruitment of DLPFC activity and performance during working memory tasks continue to improve through adolescence (Alexander, 1982; Goldman-Rakic, 1987; Luna et al., 2010). During this period, excitatory synapses and their principal targets, pyramidal neuron dendritic spines, massively decline in number in the primate DLPFC (Huttenlocher, 1979; Bourgeois et al., 1994; Anderson et al., 1995; Petanjek et al., 2011). Synaptic pruning is thought to eliminate unwanted or imprecise connections and to strengthen the remaining connections (Lichtman and Colman, 2000; Holtmaat and Svoboda, 2009), suggesting that this process could contribute to the maturation of working memory function during adolescence.

Working memory is thought to emerge from oscillatory activity of DLPFC neurons at gamma frequency (30-80 Hz) (Fries, 2009), which requires the activity of local GABAergic interneurons that express the calcium binding protein parvalbumin (PV) (Cardin et al., 2009;

Sohal et al., 2009). During working memory tasks, excitation from pyramidal neurons recruits PV interneurons, which in turn provide phasic inhibition that synchronizes the firing of pyramidal neurons at gamma frequency (Gonzalez-Burgos et al., 2015a). Due to the narrow time window of PV interneuron recruitment during gamma oscillations, PV interneurons require efficient detection of glutamatergic inputs with high precision (Jonas et al., 2004; Hu et al., 2014). Therefore, pruning of unnecessary synaptic connections and strengthening of the remaining excitatory inputs to PV interneurons during development could play a crucial role in improving PV interneuron recruitment during gamma oscillations and consequently in the maturation of working memory function. However, evidence for pruning of excitatory synapses on PV interneurons in the DLPFC, and the molecular mechanisms that could regulate cell type-specific pruning, have not been reported.

Excitatory synapses on PV interneurons are modulated in part by receptor tyrosine kinase ErbB4 (Rico and Marin, 2011; Mei and Nave, 2014). Activation of ErbB4 increases the number of excitatory synapses (Ting et al., 2011) and the loss of ErbB4 results in fewer excitatory synapses on PV interneurons (Del Pino et al., 2013). Moreover, ErbB4 transcripts are alternatively spliced at two loci, generating four different splice variants with distinct downstream signaling pathways (Veikkolainen et al., 2011). Although their functional consequences are not known in PV interneurons, major and minor ErbB4 variants exert opposing physiological effects in non-neuronal cells (Muraoka-Cook et al., 2009; Sundvall et al., 2010). Thus, shifts in the expression level and/or splicing of ErbB4 in PV interneurons during adolescence might function as a developmental switch regulating the pruning of excitatory synapses on these neurons.

In this study, we tested the hypotheses that 1) excitatory synapses on PV interneurons are pruned during postnatal development in monkey DLPFC and 2) this pruning process is attributable to shifts in the expression levels and/or splicing of ErbB4 transcripts. We found that excitatory synapses on PV interneurons undergo pruning during adolescence in monkey DLPFC. Moreover, total ErbB4 expression did not change but the alternative splicing of ErbB4 transcripts shifted from the major to minor variants with age. Overexpression of ErbB4 major variant increased the number of excitatory synapses on PV neurons, whereas the minor variant had no effect. Finally, the ratio of minor to major splice variants predicted the pruning of excitatory synapses on PV interneurons across all monkeys. Thus, our findings indicate that shifts in ErbB4 splicing in PV interneurons modulate the pruning of excitatory synapses on these neurons during postnatal development.

## **4.2 MATERIALS AND METHODS**

### **4.2.1 Animals and tissue preparation**

We studied 13 female rhesus monkeys (*Macacca mulatta*) of two age groups: postnatal 3 to 9 months (Pre-pubertal group; n=7) and 42 to 46 months (Post-pubertal group; n=6); these age groups capture the plateau phase and the declining phase, respectively, of excitatory synapse density in the primate DLPFC (Bourgeois et al., 1994). Housing and experimental procedures were conducted in accordance with guidelines set by the United States Department of Agriculture and the National Institutes of Health Guide for the Care and Use of Laboratory Animals and with the approval of the University of Pittsburgh's Institutional Animal Care and

Use Committee. Animals were perfused transcardially with ice-cold artificial cerebrospinal fluid following ketamine and pentobarbital-induced anesthesia. The brain was removed and the right hemisphere was blocked coronally, frozen in isopentane on dry ice and stored at -80°C. The left hemisphere was blocked coronally, immersed in phosphate-buffered 4% paraformaldehyde at 4°C for 48 hours, washed in sucrose solutions at 4°C and stored at -30°C in a cryoprotectant solution containing glycerin and ethylene glycol (Gonzalez-Burgos et al., 2015b).

#### **4.2.2 Layer-specific RNA Extraction and qPCR**

Cryostat sections (12  $\mu\text{m}$ ) containing right DLPFC area 46 were mounted on glass polyethylene naphthalate membrane slides (Leica Microsystems, Bannockburn, IL), fixed in ethanol/sodium acetate, stained in 0.5% thionin and dehydrated with ethanol. The boundaries of layer 4 were determined on the basis of the size and packing density of stained neurons (Chung et al., 2016b). A Leica microdissection system (LMD 6500, Leica Microsystems, Wetzlar, Germany) was used to collect  $\sim 3 \times 10^6 \mu\text{m}^2$  of tissue from layer 4 of each monkey. The collected tissue samples were lysed by vortexing for 30 seconds in 200  $\mu\text{l}$  of RLTplus buffer (Qiagen, Valencia, CA). RNA was extracted using the RNeasy Plus Micro Kit (Qiagen, Germantown, MD), and complementary DNA was synthesized using the qScript cDNA SuperMix (Quanta Bioscience, Gaithersburg, MD). The qPCR reactions were performed in quadruplicate using an ABI StepOnePlus Real-Time PCR System (Applied Biosystems, Foster City, CA) with previously described primer sets for PV, four ErbB4 splicing variants (JM-a, JM-b, CYT-1, CYT-2), and pan-ErbB4 (Chung et al., 2016b). Beta-actin and cyclophilin A were used as reference genes to normalize the expression levels of transcripts, as these house-keeping genes have stable levels of expression across postnatal development in monkey DLPFC (Volk et al.,

2012a). The delta cycle thresholds (dCTs) were calculated for each sample by using the geometric mean of the two endogenous reference genes as the normalizing factor. Then the expression level for each transcript was calculated as the expression ratio value (expression ratio= $2^{-dCTs}$ ).

### **4.2.3 Fluorescent Immunohistochemistry**

Cryostat sections (40  $\mu$ m) containing left DLPFC area 46 were pretreated for antigen retrieval (0.01M sodium citrate for 75 minutes at 80°C) and then incubated for 72 hours at 4°C in the following primary antibodies: PV (mouse, 1:1000, Swant, Bellinzona, Switzerland), postsynaptic density 95 (PSD95; rabbit, 1:250, Cell Signaling, Danvers, MA) and vesicular glutamate transporter 1 (VGlut1; guinea pig, 1:250, Millipore, Billerica, MA). Tissue sections were washed three times in phosphate-buffered saline (PBS) and then incubated for 24 hours at 4°C with secondary antibodies (donkey) conjugated to Alexa 488 (anti-mouse, 1:500, Invitrogen, Carlsbad, CA), 568 (anti-rabbit, 1:500, Invitrogen) or 647 (anti-guinea pig, 1:500, Millipore). After washing three times in PBS, sections were mounted in the Prolong Gold Antifade reagent (Life Technologies, Carlsbad, CA) and stored at 4°C until imaging. The specificity of these antibodies has been described previously (Chung et al., 2016a).

### **4.2.4 ErbB4 Plasmid Cloning**

Full length cDNAs encoding ErbB4 JM-a/CYT-1 variant (Huang et al., 2000) (a gift from Dr. Lin Mei) or JM-b/CYT-1 variant (Sardi et al., 2006) (a gift from Dr. Gabriel Corfas) were amplified using a primer pair ErbB4\_Exon1\_Bgl II\_F (ACGTAGATCTATGAAGCCGGCGAC

AGGACTTTGG) and ErbB4\_Exon28\_Sal I\_R (ACGTGTCGACTTACACCACAGTATTCCG GTGTCTG). The amplified products were digested with *Bgl* II and *Sal* I and ligated with T4 ligase (Invitrogen) into Pires2-DsRed-Express2 vector (Clontech, Mountain View, CA). Pires2 vector contains an internal ribosome entry site (IRES) between cloning sites and fluorescent protein coding region, which allows both the gene of interest and the fluorescent protein to be translated from a single mRNA in mammalian cells (Chung et al., 2011). In order to generate cDNA encoding the JM-b/CYT-2 variant, the DNA sequence corresponding to exon 26 of JM-b/CYT-1 was deleted using the QuikChange Lightning Site-Directed Mutagenesis Kit (Agilent Technologies, Santa Clara, CA) with a primer pair Del172-219\_F (ATCTCGGTATACAAACT GGTTCCTATTCGAGTCAATTCTTGC) and Del172-219\_R (GCAAGAATTGACTCGAATA GGAACCAGTTTGTATACCGAGAT). The DNA sequence of all constructs was verified by sequencing.

#### **4.2.5 Dissociated Neuronal Culture and Immunocytochemistry**

Dissociated rat cortical neurons were prepared from postnatal day 1 Long-Evans rats (Charles River Laboratories, Inc., Wilmington, MA). In 24-well plates, cortical neurons were placed at  $1 \times 10^5$  cells per well on acid-washed coverslips coated with poly-D-lysine (20  $\mu\text{g}/\text{mL}$ ) and laminin (3.4  $\mu\text{g}/\text{mL}$ ). Cortical neurons were maintained in Neurobasal Medium supplemented with B27 (all from Invitrogen), penicillin/streptomycin (100 U/mL and 100 mg/mL, respectively), and 2mM glutamine. One half of the media in each well was replaced every 4 days. At 7 days *in vitro* (DIV) cortical neurons were transfected with 1  $\mu\text{g}$  of DNA plasmid per well using the Lipofectamine 2000 (Invitrogen) according to the manufacturer's instructions. Neurons at 21 DIV were fixed for 8 minutes at room temperature with 4%

paraformaldehyde/4% sucrose in PBS. Fixed neurons were washed with PBS and then incubated for 24 hours at 4°C in 1X GDB (15 mM phosphate buffer [pH 7.4] containing 0.1% gelatin, 0.3% Triton X-100, and 0.25M NaCl) (Wills et al., 2012) with the following primary antibodies: PV (goat, 1:500, Swant), DsRed (rabbit, 1:500, Abcam, Cambridge, MA), PSD95 (mouse, 1:250, Synaptic Systems, Gottingen, Germany) and VGlut1 (guinea pig, 1:2000, Synaptic Systems). Neurons were washed three times in PBS and then incubated for 2 hours with secondary antibodies (donkey) conjugated to Alexa 405 (anti-goat, 1:500, Abcam), 488 (anti-mouse, 1:500, Invitrogen), 568 (anti-rabbit, 1:500, Invitrogen) and 647 (anti-guinea pig, 1:500, Millipore). Coverslips were mounted using the Fluoromount-G (Southern Biotech, Birmingham, AL). All antibodies have been shown to specifically recognize the targeted protein as reported by the manufacturer.

#### **4.2.6 Image Acquisition**

Images containing monkey sections were acquired on an Olympus (Center Valley, PA) IX81 microscope with a spinning disk confocal unit and a Hamamatsu EM-CCD digital camera (Bridgewater, NJ) at 60x magnification. Ten image stacks (512×512 pixel; 0.25 μm z-step) in layer 4, defined as 50-60% of the pia-to-white matter distance, per each section were selected using a previously published method for systematic random sampling (Sweet et al., 2009). The mean numbers of PV-immunoreactive neurons sampled in the same volume of tissue did not differ between age groups ( $t_{11}=0.06$ ,  $p=0.952$ ). Images containing primary neurons were acquired on a Nikon (Melville, NY) A1R laser scanning confocal microscope at 60x magnification. In each experiment, all image stacks (1024x1024 pixels; 0.5 μm z-step) were acquired with identical settings for laser power, detector gain and amplifier offset, with pinhole diameters set

for 1.2 airy unit. Images were rendered using a maximal intensity projection algorithm. Each experimental condition comprised 10 to 12 DsRed+/PV+ neurons and the final data sets comprised 3 independent experiments.

#### **4.2.7 Post-image Processing**

For images containing monkey sections, each fluorescent channel was deconvolved using the Autoquant's Blind Deconvolution algorithm to improve image contrast by reducing out-of-focus fluorescence. Pre- and postsynaptic elements of excitatory synapses were defined as VGlut1+ and PSD95+ puncta, respectively. Masking of VGlut1+ and PSD95+ puncta and PV cell body was performed using the previously described method (See **Appendix D; Supplementary Methods**) (Chung et al., 2016a). Excitatory synapses on PV interneurons were defined by the overlap of VGlut1+ and PSD95+ (VGlut1+/PSD95+) puncta within PV cell bodies (**Fig. 10**). The validity of this approach was confirmed by a prior comparison of the data from the same approach (Chung et al., 2016a) and the results from a previous electron microscopy (EM) study (Melchitzky and Lewis, 2003). For images containing primary neurons, the VGlut1+ and PSD95+ puncta were masked using the binary threshold function in NIS-Elements AR software (Nikon). The proximal dendrites were defined as neurites containing PSD95+ puncta within 30 $\mu$ m from the PV+/DsRed+ cell body as previously characterized (Ting et al., 2011). The cell body and one randomly selected proximal dendrite from each sampled PV+/DsRed+ neuron were manually masked.

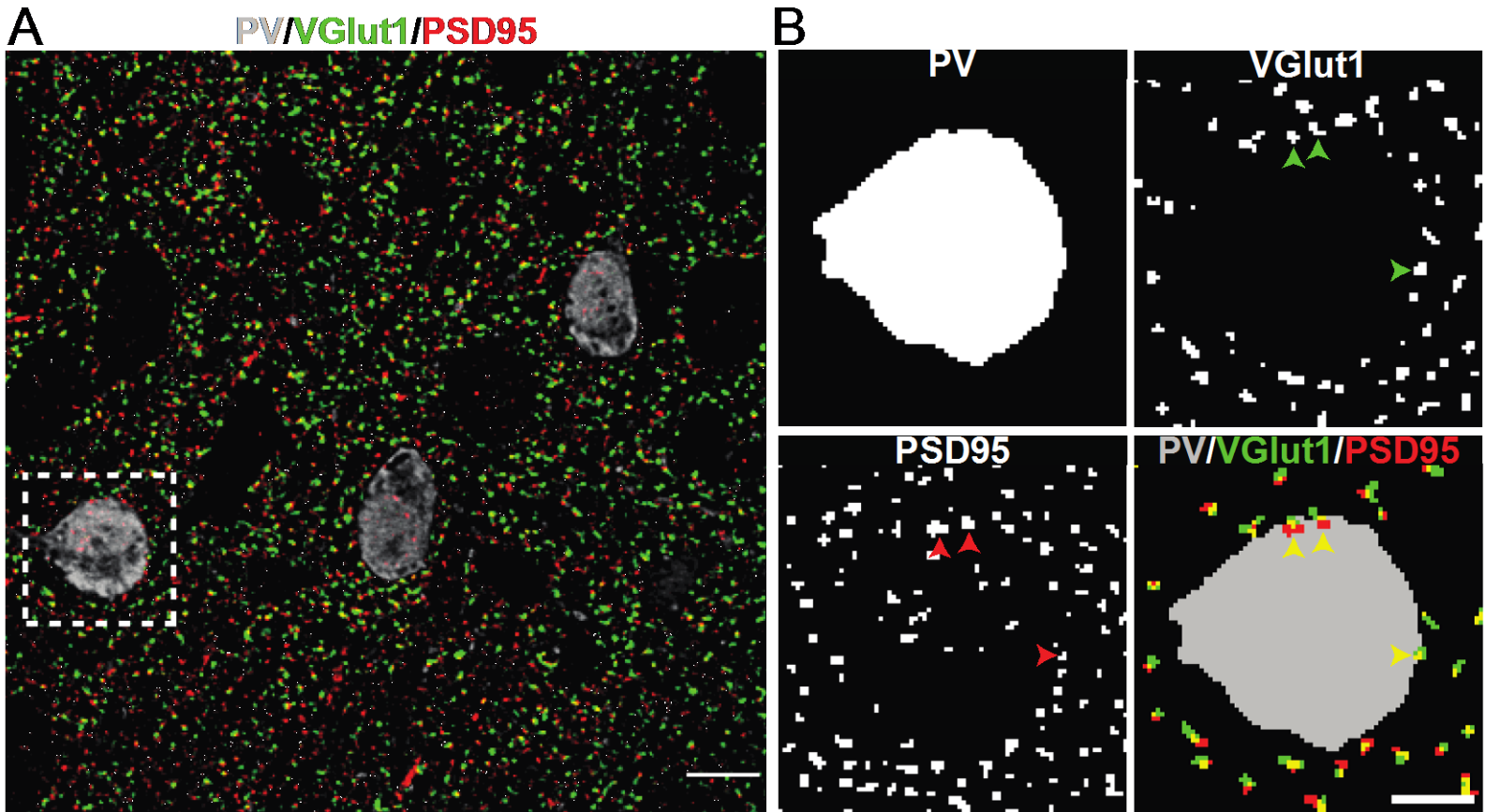


**Figure 10. Sampling of excitatory synapses on PV interneurons in monkey DLPFC layer 4**

(A) Representative deconvolved image of monkey DLPFC layer 4 labeled with antibodies against PV (gray), VGlut1 (green) and PSD95 (red). Scale bar = 10  $\mu\text{m}$ . (B) Single (white) and combined (color) mask images of PV cell body, VGlut1+ puncta and PSD95+ puncta from the boxed area in (A). Combined mask image displays only overlapping VGlut1+ and PSD95+ puncta (yellow). Excitatory synapses on PV cell bodies were defined by the VGlut1+/PSD95+ puncta within a PV cell body, as indicated by yellow arrowheads. Overlapping VGlut1+/PSD95+, where only the PSD95+ puncta or the VGlut1+ puncta were located within a PV cell body, were not counted as excitatory synapses. Scale bar = 5  $\mu\text{m}$ .

#### 4.2.8 Statistics

Student's t-tests were performed to compare the dependent measures between age groups. Pearson's correlation analyses were performed to assess the association between the ErbB4 splice variant ratios and the density of VGlut1+, PSD95+ or VGlut1+/PSD95+ puncta on PV cell bodies across all animals. One-way analysis of variance (ANOVA) was used to assess the main effect of Pires2 constructs on the dependent measures in primary neuronal culture.

### 4.3 RESULTS

#### 4.3.1 Developmental pruning of excitatory synapses on PV interneurons in layer 4 of monkey DLPFC

PV neurons were sampled in DLPFC layer 4 as this cortical layer has been shown to contain the highest density of PV neurons in monkey DLPFC (Conde et al., 1994). The mean ( $\pm$ SD) density of VGlut1+/PSD95+ puncta on PV cell bodies was significantly ( $t_{11}=2.4$ ,  $p=0.034$ ) 26% lower in the post-pubertal ( $0.026\pm 0.005$  per  $\mu\text{m}^2$ ) relative to the pre-pubertal group ( $0.035\pm 0.007$  per  $\mu\text{m}^2$ ; **Fig. 11A**), indicating that excitatory synapses on PV interneurons are pruned during adolescence. Consistent with the mean group difference, the frequency distribution of VGlut1+/PSD95+ puncta density on individual PV cell bodies was shifted to the left in post-pubertal relative to pre-pubertal animals (**Fig. 11B**). The mean surface area of PV cell bodies did not differ between age groups (Pre-pubertal:  $674\pm 64$   $\mu\text{m}^2$ , Post-pubertal:  $662\pm 73$   $\mu\text{m}^2$ ;

$t_{11}=0.3$ ,  $p=0.770$ ; **Fig. 11C**), demonstrating that the lower density of excitatory synapses on PV neurons in the post-pubertal animals is not due to a larger surface area of PV cell bodies. Moreover, the density of total VGlut1+/PSD95+ puncta in DLPFC layer 4 did not differ between age groups (Pre-pubertal:  $0.061\pm 0.011$  per  $\mu\text{m}^3$ , Post-pubertal:  $0.056\pm 0.008$  per  $\mu\text{m}^3$ ;  $t_{11}=0.9$ ,  $p=0.368$ ; **Fig. 11D**), suggesting that the pruning of excitatory synapses during adolescence is more pronounced on PV interneurons than on other neural elements in DLPFC layer 4. Finally, the mean synaptic levels (i.e., relative fluorescence intensities within VGlut1+/PSD95+ puncta on PV cell bodies) of VGlut1 (Pre-pubertal:  $6.0\times 10^5\pm 1.3\times 10^5$  a.u., Post-pubertal:  $7.9\times 10^5\pm 2.1\times 10^5$  a.u.;  $t_{11}=-2.0$ ,  $p=0.069$ ; **Fig. 11E**) and PSD95 (Pre-pubertal:  $2.7\times 10^5\pm 0.7\times 10^5$  a.u., Post-pubertal:  $3.9\times 10^5\pm 0.7\times 10^5$  a.u.;  $t_{11}=-3.1$ ,  $p=0.010$ ; **Fig. 11F**) proteins were 32% and 43% higher, respectively, in the post-pubertal group. These findings suggest that the maturation of excitatory synaptic inputs to cortical PV interneurons during adolescence involves the pruning of a subset of synapses and higher levels of VGlut1 and PSD95 proteins in the remaining synapses.

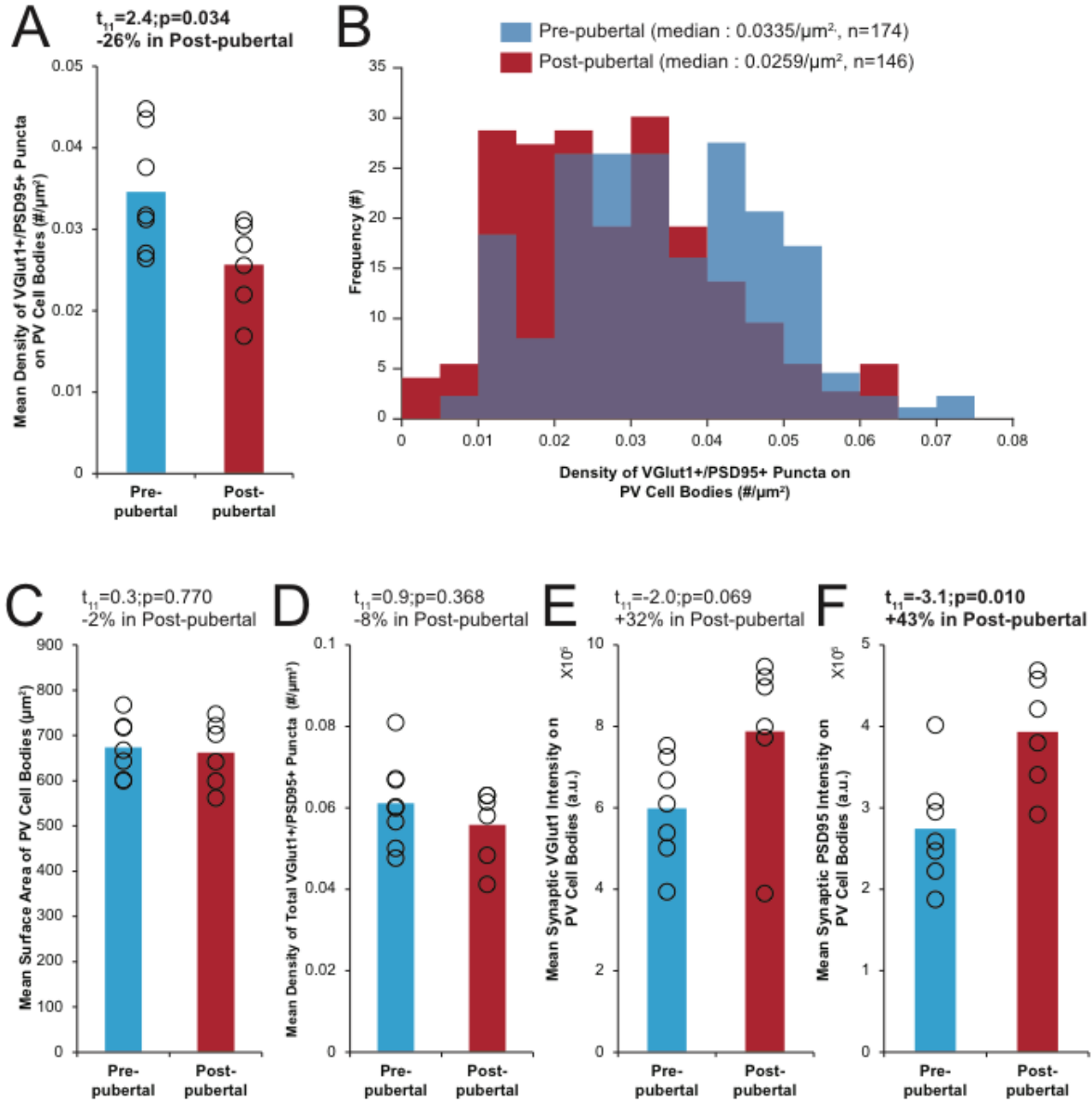


**Figure 11. Developmental pruning of excitatory synapses on PV interneurons through adolescence in layer 4 of monkey DLPFC**

(A, C-F) Group mean (bar) and individual monkey (open circles) levels of dependent measures, as indicated by the y-axis labels, in DLPFC layer 4 of monkeys in pre-pubertal group (blue) or post-pubertal group (red). Statistics from student's t-test for each dependent measures are shown above the corresponding graph. (A) Mean density of VGlut1+/PSD95+ puncta on PV cell bodies was significantly lower in the post-pubertal group. (B) The frequency distributions of VGlut1+/PSD95+ puncta density on PV cell bodies sampled from pre-pubertal monkeys (blue) and post-pubertal monkeys (red). Each bin represents 0.05 puncta per  $\mu\text{m}^2$ . (C-D) The mean surface area of PV cell bodies (C) and the density of total VGlut1+/PSD95+ puncta in DLPFC layer 4 (D) did not differ between age

groups. (E-F) Mean VGlut1 (E) and PSD95 (F) levels within VGlut1+/PSD95+ puncta on PV cell bodies were higher in the post-pubertal group.

#### 4.3.2 Association between maturation of excitatory synapses on PV interneurons and PV levels

As PV expression depends on neuronal activity (Behrens et al., 2007; Belforte et al., 2010; Del Pino et al., 2013), we next assessed changes in PV immunoreactivity between age groups. Mean PV protein levels per neuron were significantly ( $t_{11}=-3.5$ ,  $p=0.005$ ) 73% higher in the post-pubertal ( $4.2 \times 10^8 \pm 0.7 \times 10^8$  a.u.) relative to the pre-pubertal group ( $2.4 \times 10^8 \pm 1.0 \times 10^8$  a.u.; **Fig. 12A**). Moreover, mean PV protein levels per neuron were negatively correlated with the mean density of VGlut1+/PSD95+ puncta on PV cell bodies ( $R=-0.620$ ,  $p=0.024$ ; **Fig. 12B**) and positively correlated with the mean synaptic VGlut1 ( $R=0.603$ ,  $p=0.029$ ; **Fig. 12C**) and PSD95 levels ( $R=0.720$ ,  $p=0.006$ ; **Fig. 12D**) across all animals. These data suggest that although a subset of excitatory synaptic inputs to PV interneurons is pruned during adolescence, the increase in VGlut1 and PSD95 levels in the remaining excitatory synapses contribute to the developmental up-regulation of activity-dependent PV expression.

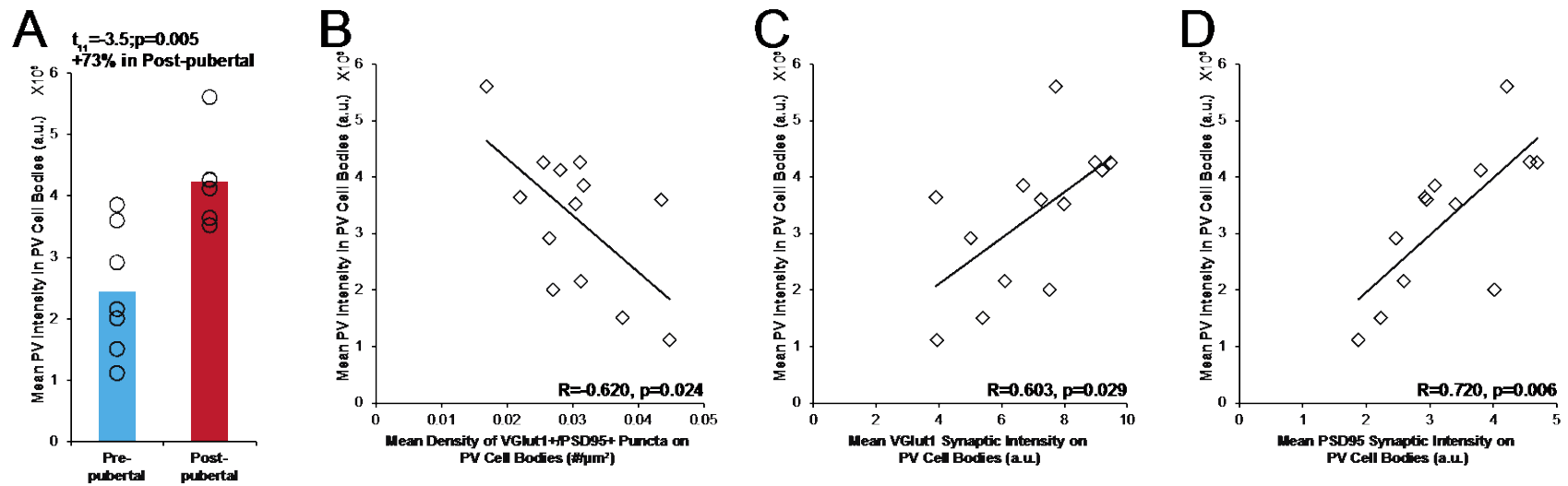


**Figure 12. Lower density of excitatory synapses on PV interneurons and higher synaptic levels of VGlu1 and PSD95 proteins predict higher PV levels across all animals**

(A) Group mean (bar) and individual monkey (open circles) levels of PV immunoreactivity in PV cell bodies for each age group. Mean PV immunoreactivity levels in PV cell bodies were significantly higher in post-pubertal group relative to pre-pubertal group. Statistic from student's t-test is shown above the graph. (B-D), Correlation graphs plotting the mean PV intensity in PV cell bodies on the y-axis and the mean density of VGlu1+/PSD95+ puncta on PV cell bodies (B), mean synaptic VGlu1 intensity (C), or mean synaptic PSD95 intensity (D) on the x-axis. Trendlines represent significant regression line across all animals (n=13).

### 4.3.3 Developmental shifts in alternative splicing of ErbB4 transcripts in layer 4 of monkey DLPFC

Next, we assessed differences in the expression level and alternative splicing of ErbB4 transcripts in PV interneurons between age groups. In the primate DLPFC, most ErbB4-positive neurons contain either PV or the calcium-binding protein calretinin (CR) (Neddens et al., 2011). Microdissection of DLPFC layer 4 yields samples highly enriched in PV relative to CR mRNA, which allows an assessment of ErbB4 expression predominantly in PV interneurons (Chung et al., 2016b). Moreover, an in situ hybridization assay (See **Appendix D; Supplementary Methods**) demonstrated that layer 4 had the highest PV mRNA levels of any layer in the DLPFC and the greatest laminar difference in PV expression between age groups (+46% in post-pubertal;  $t_6=-2.6$ ,  $p=0.042$ ; **Fig. 13A**). Thus, we micro-dissected DLPFC layer 4 (**Fig. 13B**) and quantified mRNA levels of PV and pan-ErbB4 by qPCR. Consistent with the immunohistochemistry (**Fig. 12A**) and the in situ hybridization data (**Fig. 13A**), PV mRNA levels in layer 4 were significantly ( $t_{11}=-3.4$ ,  $p=0.006$ ) 57% higher in the post-pubertal ( $0.071\pm 0.015$ ) relative to the pre-pubertal group ( $0.045\pm 0.012$ ; **Fig. 13C**). In contrast, pan-ErbB4 mRNA levels in layer 4 did not differ between age groups (Pre-pubertal:  $0.032\pm 0.011$ , Post-pubertal:  $0.038\pm 0.014$ ;  $t_{11}=-1.7$ ,  $p=0.362$ ; **Fig. 13D**).

We then assessed shifts in ErbB4 splicing between age groups in layer 4. ErbB4 transcripts are alternatively spliced at two loci (**Fig. 13E**) (Veikkolainen et al., 2011). Splicing at the juxtamembrane (JM) locus produces the minor JM-a variant and the major JM-b variant based on the inclusion of exon 16 or 15b, respectively. Inclusion or exclusion of exon 26 at the cytoplasmic (CYT) locus yields the minor CYT-1 variant and the major CYT-2 variant,

respectively. To investigate shifts in splicing, we assessed the ratio of minor to major splicing variant levels at each locus (i.e., JM-a:JM-b ratio and CYT-1:CYT-2 ratio). The JM-a:JM-b ratio (Pre-pubertal:  $0.073 \pm 0.020$ , Post-pubertal:  $0.117 \pm 0.048$ ;  $t_{11} = -3.0$ ,  $p = 0.013$ ; **Fig. 13F**) and the CYT-1:CYT-2 ratio (Pre-pubertal:  $0.253 \pm 0.090$ , Post-pubertal:  $0.446 \pm 0.168$ ;  $t_{11} = -3.5$ ,  $p = 0.005$ ; **Fig. 13G**) were significantly 62% and 76% higher, respectively, in the post-pubertal group, demonstrating a developmental shift in ErbB4 splicing from the major JM-b/CYT-2 to minor JM-a/CYT-1 variants during adolescence.

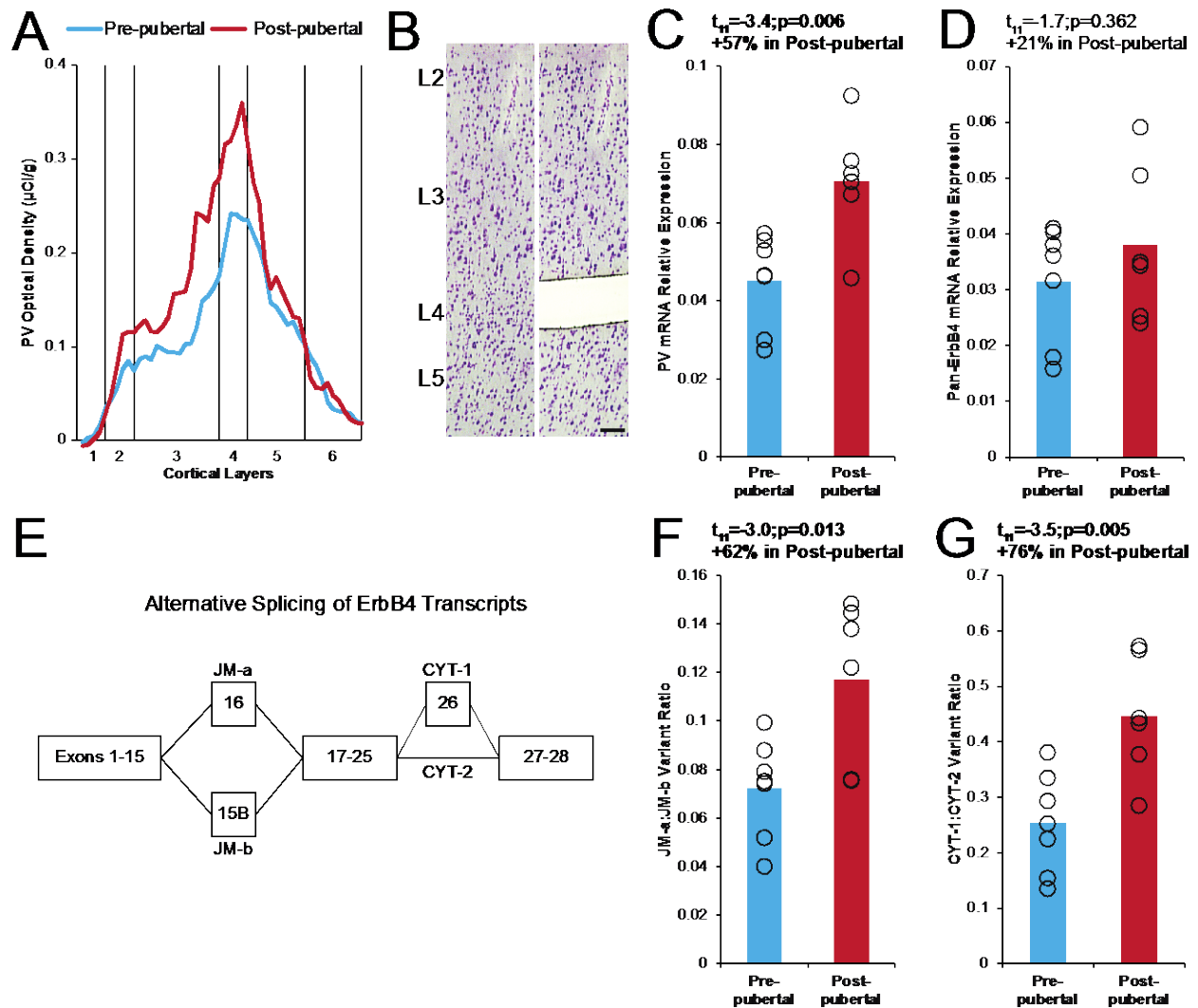


**Figure 13. Developmental shifts in alternative splicing of ErbB4 transcripts through adolescence in layer 4 of monkey DLPFC**

(A) Mean PV mRNA optical density as a function of cortical layer in monkey DLPFC for pre-pubertal (blue) and post-pubertal (red) groups. (B) A representative image of a thionin-stained coronal section before and after microdissection of layer 4. Layer 4 was identified based on the size and packing density of stained cells. Scale bar = 100µm. (C,D,F,G) Group mean (bar) and individual monkey (open circles) levels of dependent measures, as indicated by the y-axis labels, in DLPFC layer 4. Statistics from student's t-test for each dependent measures are shown above the corresponding graph. (C) Mean PV mRNA levels were significantly higher in the post-pubertal group, (D) whereas mean pan-ErbB4 levels did not differ. (E) A schematic diagram depicting the alternative splicing loci of ErbB4. (F-G) The JM-a:JM-b variant ratio (E) and the CYT-1:CYT-2 variant ratio (F) were significantly higher in the post-pubertal group.

#### 4.3.4 Differential regulation of excitatory synapse number on PV interneurons by ErbB4 splice variants

To investigate whether ErbB4 major JM-b/CYT-2 and minor JM-a/CYT-1 splice variants differentially regulate the number of excitatory synapses on PV interneurons, we transfected constructs expressing either ErbB4 JM-a/CYT-1 or JM-b/CYT-2 in rat primary neurons (**Fig. 14A**). Each construct bicistronically translates an ErbB4 splice variant and DsRed from a single mRNA, so that the intensity of DsRed reflects the levels of the transfected ErbB4 variant. The DsRed levels did not differ in PV neurons transfected with each construct (cell body:  $F_{2,113}=1.5$ ,  $p=0.225$ ; proximal dendrites:  $F_{2,113}=0.8$ ,  $p=0.463$ ; **Fig. 14B**), suggesting that the expression levels of these inserts are comparable in PV neurons. Labeling with an anti-ErbB4 antibody confirmed the presence of these inserts in transfected neurons (data not shown). The surface areas of cell bodies and proximal dendrites did not differ in PV<sup>+</sup>/DsRed<sup>+</sup> neurons transfected with each construct (cell body:  $F_{2,113}=2.2$ ,  $p=0.115$ ; proximal dendrites:  $F_{2,113}=0.09$ ,  $p=0.912$ ; **Fig. 14C**). Overexpression of the JM-b/CYT-2 variant increased the density of VGlut<sup>+</sup>/PSD95<sup>+</sup> puncta on the proximal dendrites of PV neurons relative to DsRed controls, whereas JM-a/CYT-1 overexpression had no discernable effect ( $F_{2,113}=5.4$ ,  $p=0.006$ ; **Fig. 14D**). A similar pattern was observed in the cell bodies of PV neurons, although it did not achieve statistical significance ( $F_{2,113}=1.9$ ,  $p=0.159$ ; **Fig. 14D**). These findings suggest that the JM-b/CYT-2 variant primarily drives the ErbB4 signaling effect on the number of excitatory inputs to PV interneurons, whereas the JM-a/CYT-1 variant does not contribute to this effect.

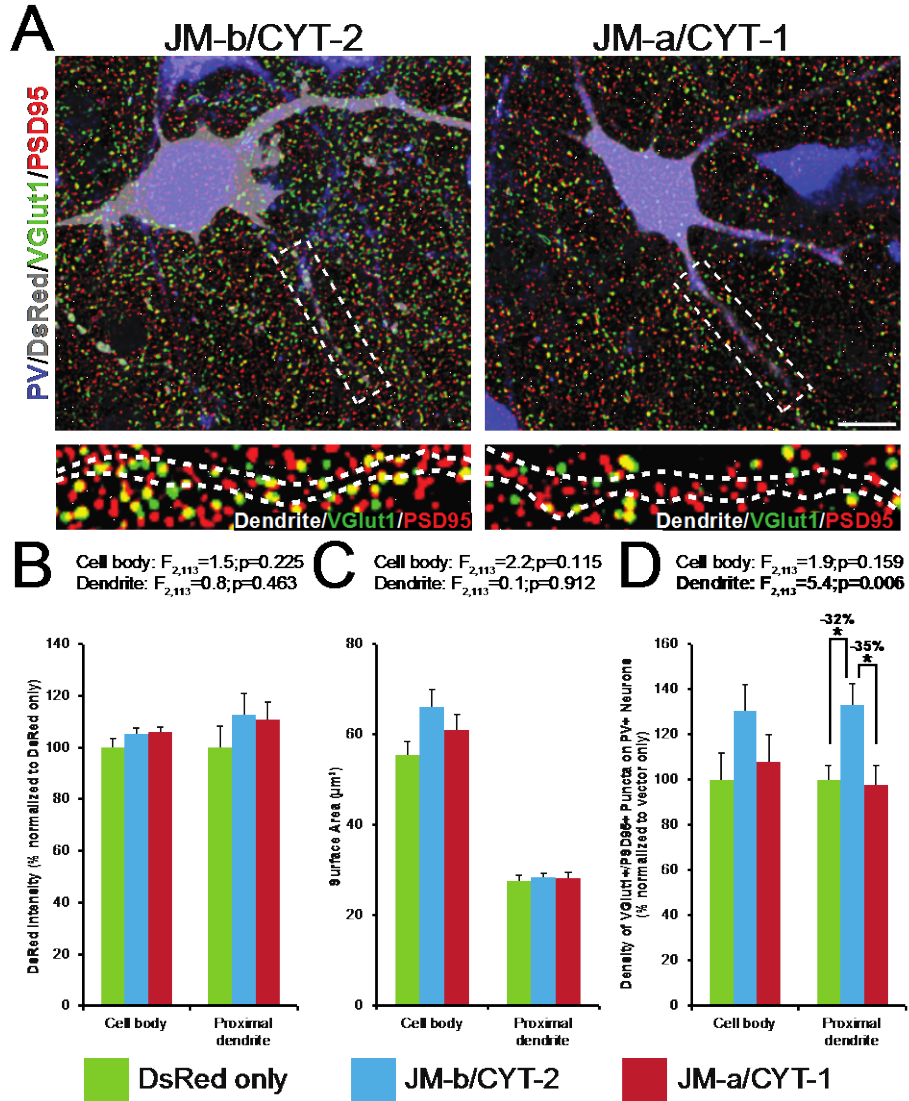


**Figure 14. Differential regulation of excitatory synapse number on PV interneurons by ErbB4 splice variants in rat primary neuronal culture**

(A) Representative images of cultured cortical neurons transfected with either JM-b/CYT-2 variant or JM-a/CYT-1 variant and labeled with antibodies against PV (blue), DsRed (gray), VGlut1 (green) and PSD95 (red). Transfected neurons are labeled with bicistronic DsRed expression. Scale bar = 5 $\mu\text{m}$ . Below are the masked images of VGlut1+ (green) and PSD95+ (red) puncta within PV dendrites (outlined with dotted lines) from the boxed area. (B-D) Bar graphs showing the levels of dependent measures, as indicated by the y-axis labels, in the cell bodies (left) and the proximal dendrites (right) of PV+/DsRed+ neurons overexpressing DsRed only (green bar), JM-b/CYT-2 (blue bar) or JM-a/CYT-1 (red bar). Data shown are mean percentage (+standard error of mean) from three individual experiments normalized to DsRed only (DsRed only: n=37, JM-b/CYT-2: n=43, JM-a/CYT-1: n=36). One-way ANOVA statistics for each dependent measures are shown above the corresponding graph. Asterisks indicate  $p < 0.05$  from Tukey's post-hoc test.

### **4.3.5 Association between ErbB4 splicing shifts and pruning of excitatory synapses on PV interneurons in monkey DLPFC**

Finally, in order to investigate whether the differential effects of ErbB4 splice variants on the number of excitatory inputs to PV neurons are reflected during pruning in primate DLPFC, we assessed the relationships between ErbB4 splicing shifts and the density of excitatory synapses on PV interneurons across all monkeys. Previous studies have demonstrated that ErbB4 signaling regulates the formation of excitatory synapses on PV interneurons primarily by its effect on synaptic recruitment of PSD95 (Huang et al., 2000; Ting et al., 2011; Seshadri et al., 2015). Consistent with these findings, the JM-a:JM-b ( $R=-0.612$ ,  $p=0.026$ ) and CYT-1:CYT-2 ( $R=-0.642$ ,  $p=0.018$ ) ratios were both significantly negatively correlated with the mean density of PSD95+ puncta on PV cell bodies across all animals.

## **4.4 DISCUSSION**

In this study, we tested the hypotheses that excitatory synapses on cortical PV interneurons are pruned during adolescence and this pruning process is attributable to shifts in ErbB4 expression and/or splicing. In layer 4 of monkey DLPFC, the density of VGlut1+/PSD95+ puncta on PV neurons was lower in post-pubertal relative to pre-pubertal monkeys, demonstrating that excitatory synapses on cortical PV interneurons undergo pruning through adolescence. Moreover, although pan-ErbB4 mRNA levels did not differ between age groups, the JM-a:JM-b and CYT-1:CYT-2 variant ratios were higher in post-pubertal monkeys. Furthermore, these ratios were negatively correlated with the density of PSD95+ puncta on PV

neurons across all animals; these findings suggest that pruning of excitatory synapses on cortical PV interneurons might be regulated by developmental shifts in ErbB4 splicing. This interpretation was supported by findings that overexpression of JM-b/CYT-2 variant increased the density of VGlut1+/PSD95+ puncta on the proximal dendrites of PV neurons, whereas overexpression of JM-a/CYT-1 variant had no effects.

Our findings indicate that PV protein levels increase in association with the pruning of excitatory synapses on PV interneurons in primate DLPFC. These results might seem contradictory with prior findings that 1) PV expression is activity-dependent (Behrens et al., 2007; Belforte et al., 2010; Del Pino et al., 2013), and 2) the density of excitatory synapses on PV neurons positively predicts PV immunoreactivity levels in mouse hippocampus (Donato et al., 2013) and human DLPFC (Chung et al., 2016a). However, we also found that the excitatory synapses remaining after pruning have higher levels of VGlut1 and PSD95 proteins. Higher levels of VGlut1 and PSD95 have been shown to increase the amplitude of excitatory postsynaptic currents and to correlate with the maturation of excitatory synapses (El-Husseini et al., 2000; Wilson et al., 2005). Consequently, the excitatory synapses on PV interneurons that remain after pruning likely represent mature synaptic connections with stronger excitatory neurotransmission. Therefore, our findings suggest that the maturation of excitatory synaptic inputs to PV interneurons during adolescence involves a reduction in the total number of synapses and a strengthening of the remaining synapses. More refined and mature glutamatergic inputs to PV interneurons could support more precise excitation of these neurons during gamma oscillations and consequently contribute to the improvement of working memory function during adolescence.

Our results demonstrate that the transcription of ErbB4 does not change with age, but that shifts in ErbB4 splicing from the JM-b/CYT-2 to JM-a/CYT-1 variants occur in PV interneurons during adolescence in primate DLPFC. The ErbB4 signaling pathway has been associated with multiple aspects of neuronal development (Mei and Xiong, 2008), including the positive modulation of excitatory synapse number on PV interneurons (Rico and Marin, 2011; Mei and Nave, 2014). Similar to other genes that are involved in neurodevelopment (Norris and Calarco, 2012), the functional consequence of ErbB4 signaling in PV neurons could be modulated by alternative splicing of ErbB4 transcripts. For example, our study demonstrates that the JM-b/CYT-2 variant increases the number of excitatory synapses on PV interneurons, whereas the JM-a/CYT-1 variant has no effects. These data suggest that normal ErbB4 signaling in PV neurons is mainly mediated by the major JM-b/CYT-2 variant, whereas the JM-a/CYT-1 variant serves as an inactive form of ErbB4. Consequently, shifts in ErbB4 splicing from the normal JM-b/CYT-2 variant to the inactive JM-a/CYT-1 variant could collectively result in a loss of ErbB4 signaling, which has been shown to reduce the number of excitatory synapses on PV interneurons (Ting et al., 2011; Del Pino et al., 2013). In support of this idea, we found that the density of PSD95+ puncta on PV interneurons was negatively correlated with the JM-a:JM-b and CYT-1:CYT-2 variants ratios across all animals. Thus, our findings suggest that developmental shifts in ErbB4 splicing could function as a molecular switch triggering the pruning of excitatory synapses on PV interneurons during adolescence.

Existing data suggest that the JM-a/CYT-1 variant might inactivate normal ErbB4 signaling, and thus contribute to the pruning of excitatory synapses on PV interneurons, through the following mechanisms. The JM-a variant, unlike the JM-b variant, contains the juxtamembrane domain that is susceptible to multiple cleavages, generating soluble extracellular and intracellular

truncated peptides (Rio et al., 2000; Ni et al., 2001). The extracellular peptide could competitively block the binding of ErbB4 ligand neuregulin-1 and inhibit normal ErbB4 signaling. Moreover, the intracellular peptide contains both the PDZ-binding and kinase motifs of ErbB4 (Maatta et al., 2006; Sundvall et al., 2010), both of which are necessary to induce stable synaptic localization of PSD-95 (Garcia et al., 2000; Huang et al., 2000; Ting et al., 2011). Upon cleavage, the intracellular peptides are displaced to the nucleus (Sardi et al., 2006), which would result in a loss of interaction between ErbB4 and PSD-95 at the synapse, and subsequent pruning of excitatory synapses on PV interneurons. Finally, unlike the CYT-2 variant, the CYT-1 variant contains a binding site for Nedd4, an E3 ubiquitin ligase (Zeng et al., 2009). Binding of Nedd4 to CYT-1 results in an increased ubiquitination and a subsequent degradation of ErbB4, which could also contribute to a decrease in ErbB4 signaling and loss of synapses.

Other molecules that converge onto ErbB4 signaling pathway could also participate in the pruning of excitatory synapses on PV interneurons (Jaaro-Peled et al., 2009). For example, Disrupted-in-schizophrenia 1 (DISC1) can interfere with the interaction between ErbB4 and PSD95, resulting in an inhibition of ErbB4 signaling in GABAergic interneurons (Seshadri et al., 2015). Similar to ErbB4, alternative splicing of the DISC1 transcript is developmentally regulated and may modulate the functional consequences of DISC1 signaling pathway (Nakata et al., 2009). Thus, if shifts in DISC1 expression and/or splicing occur in PV interneurons during adolescence, DISC1 could trigger the pruning of excitatory synapses on these neurons synergistically with the developmental changes in ErbB4 splicing.

Several methodological issues are important to consider in interpreting the results of this study. First, our sampling of excitatory synapses excluded the VGlut2-containing thalamocortical excitatory synapses (Fremeau et al., 2001). However, previous EM studies demonstrated

that thalamic excitatory inputs represent only ~10% of total excitatory synapses in the cortex (Latawiec et al., 2000) and only a small percentage (~2%) of thalamic inputs innervate PV interneurons (Rotaru et al., 2005). Second, we excluded sampling of synapses on the dendrites of PV interneurons in monkey DLPFC due to the lack of PV immunoreactivity within these structures. Although PV neurons receive excitatory inputs more frequently on their dendrites than cell bodies (Hioki, 2015), somal excitatory inputs produce much stronger depolarization in PV neurons than dendritic excitatory inputs (Hu et al., 2010; Norenberg et al., 2010). Moreover, the densities of excitatory inputs to the dendrites (Donato et al., 2013) and the cell bodies (Chung et al., 2016a) of PV neurons both similarly predict activity-dependent PV levels. Thus, these findings suggest that our sampling approach sufficiently captures functionally important excitatory synapses on PV interneurons.

In conclusion, our study demonstrates a previously unrecognized role of synaptic pruning in the maturation of excitatory synapses on cortical PV interneurons during adolescence that is mediated by a shift in ErbB4 splicing. Deficits in cortical PV interneuron maturation have been linked to several neuropsychiatric disorders including schizophrenia (Lewis et al., 2012). In the DLPFC of individuals with schizophrenia, a pathogenic shift in ErbB4 splicing from the JM-b to JM-a variants has been associated with fewer excitatory synaptic inputs to PV interneurons (Chung et al., 2016a; Chung et al., 2016b), which could reflect an exaggerated pruning process in these neurons. Therefore, findings from our study support the view that schizophrenia is a neurodevelopmental disorder with disturbances in the normal maturation process of prefrontal inhibitory circuits (Lewis et al., 2004).

## **5.0 GENERAL DISCUSSION**

### **5.1 SUMMARY OF FINDINGS**

In this dissertation, I provided evidence for perturbations of certain transcriptional, molecular and synaptic elements of prefrontal cortical circuitry in schizophrenia and their contribution to PV interneuron maturation during adolescence. In this section, I will summarize findings from each chapter and then consider how these findings could support the disease model I presented in the general introduction section.

In chapter 2, I investigated dysregulated ErbB4 splicing in schizophrenia and its selective effect on PV expression. Levels of JM-a and CYT-1 variants were higher and levels of JM-b and CYT-2 variants were lower selectively in layer 4, where PV neurons are enriched, but not in layer 2, where CR neurons are enriched, in the DLPFC of schizophrenia subjects relative to comparison subjects. Moreover, the JM-a:JM-b variant ratio was negatively correlated with PV mRNA levels selectively in layer 4 of schizophrenia subjects. Finally, MIAT levels were higher preferentially in PV interneurons in subjects with schizophrenia. This evidence supports the hypotheses that 1) schizophrenia is associated with abnormal shifts in ErbB4 splicing from the JM-b/CYT-2 to JM-a/CYT-1 variants selectively in PV but not in CR interneurons; 2) dysregulated ErbB4 splicing at the JM locus is associated with lower PV mRNA levels in

schizophrenia; and 3) higher MIAT level is associated with dysregulated ErbB4 splicing in schizophrenia.

In chapter 3, I investigated pathological basis for deficient excitatory drive to PV interneurons in schizophrenia and the contribution of ErbB4 splicing in this process. The density of excitatory synaptic inputs to PV but not CR interneurons was lower in the DLPFC of schizophrenia subjects. Furthermore, fewer excitatory synapses on PV interneurons predicted lower levels of activity-dependent PV and GAD67 levels selectively in schizophrenia subjects. Finally, dysregulated ErbB4 splicing at the JM locus predicted fewer excitatory synapses on PV interneurons in schizophrenia subjects. These findings support the hypotheses that 1) schizophrenia is associated with a loss of excitatory synapses on PV interneurons; 2) deficits in excitatory synaptic inputs to PV interneurons predict reduced PV interneuron activity; and 3) dysregulated ErbB4 splicing may contribute to fewer excitatory synapses on PV interneurons in schizophrenia.

In chapter 4, I investigated developmental pruning of excitatory synapses on PV interneurons in postnatal monkeys and the contribution of ErbB4 splicing to this process. The density of excitatory synaptic inputs to PV interneurons was lower in the DLPFC of post-pubertal monkeys relative to pre-pubertal monkeys. The excitatory synapses remaining on PV neurons after pruning contained higher levels of VGlut1 and PSD95 proteins. Moreover, shifts in ErbB4 splicing at the JM and the CYT loci predicted a lower density of excitatory synapses on PV interneurons across all animals. Finally, overexpression of the ErbB4 JM-b/CYT-2 variant in primary neuronal cultures increased, whereas JM-a/CYT-1 had no effect on the number of excitatory synapses on PV interneurons. These findings support the hypotheses that 1) excitatory synapses on PV interneurons are pruned during adolescence and the remaining synapses are

strengthened; 2) this developmental pruning is associated with shifts in alternative splicing of ErbB4 in PV interneurons; and 3) the ErbB4 JM-a/CYT-1 variant does not contribute to the normal effect of ErbB4 signaling. Thus, ErbB4 splicing shifts from the JM-b/CYT-2 to JM-a/CYT-1 could be associated with the loss of ErbB4 signaling and consequently fewer excitatory synaptic inputs to PV interneurons.

In concert, these findings from primary neuronal culture, postnatal monkeys and human subjects support the hypothesis proposed in the introductory model that developmental shifts in ErbB4 splicing contribute to the pruning of excitatory synaptic inputs to PV interneurons and that disturbances in this process could induce fewer excitatory synapses onto, and consequently reduced activity of, PV interneurons in schizophrenia (**Figure 15**). Findings from my dissertation collectively suggest that for a given individual, a shift in ErbB4 splicing from the JM-b/CYT-2 to JM-a/CYT-1 splice variant occurs in PV interneurons during adolescence. This splicing shift results in a mild loss of ErbB4 signaling, which in turn triggers the pruning of superfluous excitatory synapses on PV interneurons. In schizophrenia, the ErbB4 splicing shift is dysregulated and results in abnormally high levels of the JM-a/CYT-1 variant and low levels of the JM-b/CYT-2 variant. This molecular shift leads to a pathological impairment in ErbB4 signaling and an exaggerated pruning process, resulting in a loss of normal excitatory synapses on PV interneurons. In the following sections I will discuss the potential implications of the ErbB4 splicing shifts and pruning of excitatory inputs to PV interneurons in cortical circuitry maturation and schizophrenia.

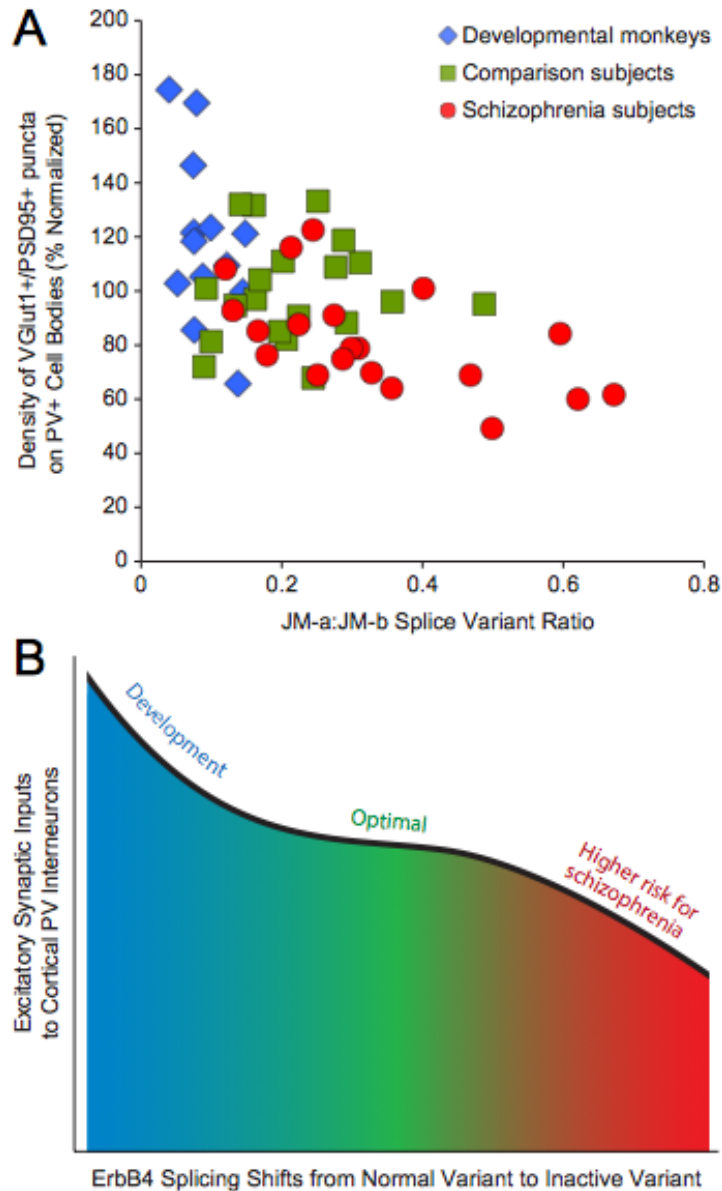


**Figure 15. Proposed role of ErbB4 splicing shifts in regulating the number of excitatory synaptic inputs to PV interneurons in development and schizophrenia**

(A) Data points compiled from studies in chapters 2 and 3 representing the relationship between the JM-a:JM-b splice variant ratio and the density of VGlut1+/PSD95+ puncta on PV+ cell bodies across postnatal monkeys, unaffected comparison subjects and schizophrenia subjects. The data points from postnatal monkeys were normalized to the mean of the post-pubertal group, whereas the data points from human subjects were normalized to the mean of the comparison group. (B) In postnatal development, a shift in ErbB4 splicing from the normal JM-b/CYT-2 to inactive JM-a/CYT-1 splice variants occurs in PV interneurons. This splicing shift results in a mild loss of ErbB4 signaling, which triggers the pruning of superfluous excitatory synapses on PV interneurons. In schizophrenia, the ErbB4 splicing shift is dysregulated and results in abnormally high levels of inactive JM-a/CYT-1 variant and low levels of normal JM-b/CYT-2 variant. This in turn induces a pathogenic loss of ErbB4 signaling and an exaggerated pruning process, resulting in a loss of normal excitatory synapses on PV interneurons.

## 5.2 IMPLICATIONS IN CORTICAL CIRCUITRY MATURATION AND SCHIZOPHRENIA

Our findings introduce a potential mechanism that allows PV interneurons to regulate their excitatory synapse density in response to changes in neuronal activity. A recent study identified a non-coding RNA MIAT that modulates alternative splicing of ErbB4 pre-mRNA in an activity-dependent manner (Barry et al., 2014). This study demonstrated that MIAT normally sequestered splicing factors such as QKI and SRSF1, restricting their access to ErbB4 pre-mRNA. Upon neuronal activation, the expression level of MIAT was reduced, presumably resulting in a release of splicing factors to ErbB4 pre-mRNA. Moreover, a knock down of MIAT in human induced pluripotent stem cell derived neuronal culture led to higher levels of ErbB4 JM-a and CYT-1 variants. This phenotype reflects the changes we observed in PV interneurons in schizophrenia (**Figure 4**). Finally, the expression levels of MIAT were shown to be reduced in the superior temporal gyrus of subjects with schizophrenia. Thus, findings from this study suggest that activity-dependent expression of MIAT regulates the alternative splicing of ErbB4 transcripts and deficits in MIAT levels in schizophrenia induces dysregulated ErbB4 splicing.

However, data from this study should be interpreted with caution. For example, this study found lower levels of MIAT in the superior temporal gyrus of schizophrenia subjects whereas our study detected higher levels of MIAT in the DLPFC of subjects with schizophrenia; such a discrepancy might come from differences in the human cohorts and the brain regions from which the MIAT levels were quantified. Nevertheless, as the neuronal activity is thought to be dampened in schizophrenia (Driesen et al., 2008) and the expression of MIAT is shown to be inhibited by neuronal activity in an experimental system, the expression level of MIAT is expected to be higher in schizophrenia. Moreover, the primer pairs used in Barry et al to detect

ErbB4 splice variants in the MIAT knock-down assay seem to non-specifically detect other ErbB4 variants. Therefore, although this study has identified a splicing regulator MIAT that is expressed in an activity-dependent manner, it lacked the proper resolution to determine how MIAT directly affects the alternative splicing of ErbB4 transcripts.

Despite these limitations in interpreting the data from Barry et al, the hypothesis that ErbB4 splicing is regulated by neuronal activity is intriguing, since such a mechanism could provide PV interneurons with the machinery that triggers the developmental pruning of superfluous excitatory synaptic inputs in response to the maturation of functionally-relevant synaptic connections with pyramidal neurons. Moreover, in mature neuronal circuits, this mechanism could be utilized to maintain excitation/inhibition (E/I) balance by re-adjusting the number of excitatory inputs to PV interneurons and consequently PV-mediated inhibition in response to changes in pyramidal neuron activity. ErbB4 splicing shifts are unlikely to be the only means by which neuronal activity participates in this process, as the alternative splicing of ErbB4 ligand neuregulin-1 (Nrg-1) is also regulated in an activity-dependent manner (Liu et al., 2011). Thus, neuronal activity seems to orchestrate the effect of Nrg-1/ErbB4 signaling by modulating the alternative splicing of both ligand and the receptor. Nevertheless, because functional consequences of different Nrg-1 isoforms are not clear in PV interneurons, I will solely focus on the effect of neuronal activity in regulating ErbB4 splicing shifts.

Our data demonstrate that the activity-dependent PV expression levels and ErbB4 splicing shifts are correlated positively during postnatal development and negatively in schizophrenia. These findings would argue paradoxically that the ErbB4 splicing shift from the JM-b/CYT-2 to JM-a/CYT-1 variants is induced by increasing neuronal activity during development, but in schizophrenia reduced neuronal activity triggers this splicing shift. In order

to explain the opposing relationship between PV interneuron activity and ErbB4 splicing shifts in development and disease, I propose the “developmental arrest model” (**Figure 16**). In this model, the splicing shift from the JM-b/CYT-2 to JM-a/CYT-1 variant is induced by a splicing factor 1 (Factor 1) and inhibited by a splicing factor 2 (Factor 2), which are both expressed in PV interneurons. The promoters of Factor 1 and Factor 2 are both activated by neuronal activity but the Factor 2 promoter is activated only by high neuronal activity.

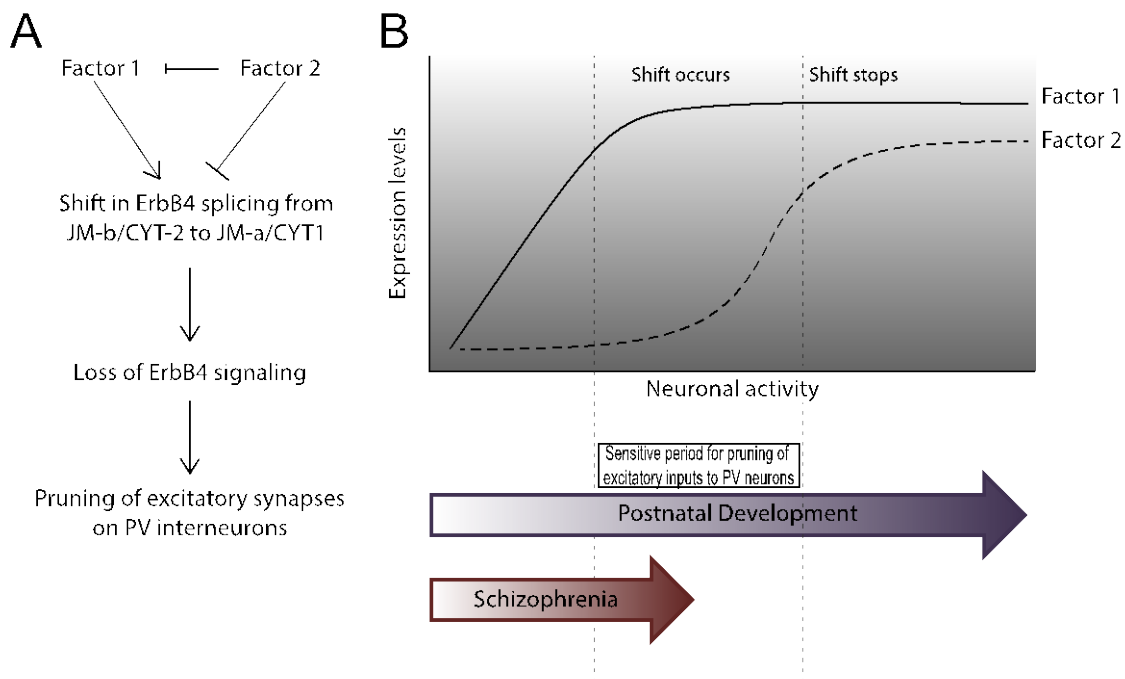


**Figure 16. Developmental arrest model for activity-dependent regulation of ErbB4 splicing shifts**

(A) Hypothetical activity-dependent signaling pathway that leads to pruning of excitatory inputs to PV neurons. Findings from this dissertation suggest that shifts in ErbB4 splicing from the JM-b/CYT-2 to JM-a/CYT-1 variants result in a loss of ErbB4 signaling and pruning of excitatory synapses on PV neurons. This model introduces an activity-regulated “factor 1” and “factor 2” that induces or inhibits, respectively, shifts in ErbB4 splicing to the JM-a/CYT-1 variant. (B) In this model, the expression of factor 1 is induced in PV interneurons by increasing neuronal activity during postnatal development. Factor 1 induces ErbB4 splicing shifts and initiates pruning of excitatory inputs to PV neurons. Into early adulthood, the neuronal activity of mature PV interneuron induces the expression of Factor 2, which inhibits the shifts in ErbB4 splicing and stops the pruning process. Therefore, the sensitive period for the maturation of excitatory inputs to PV interneuron would be based upon changes in the ratio of factor 1 to factor 2 expression levels, which defines the onset and the closure of the pruning process. In schizophrenia, PV interneuron activity does not reach the adult level, resulting in a failure to establish closure of the sensitive period.

In this model, developmental strengthening of the functionally-relevant synaptic connections between pyramidal neurons and PV interneurons increases PV interneuron activity, as evidenced by a robust increase in activity-dependent PV expression early in human postnatal development (Fung et al., 2010). Increasing PV interneuron activity activates the expression of Factor 1 and induces a shift in ErbB4 splicing from JM-b/CYT-2 to JM-a/CYT-1 variants. This splicing shift triggers an elimination of superfluous and non-relevant synaptic connections in PV interneurons during adolescence. Into early adulthood, the neuronal activity of mature PV interneurons induces the expression of Factor 2, which inhibits the shifts in ErbB4 splicing and the pruning process. The balance between expression levels of Factor 1 and Factor 2 would allow PV interneurons to achieve an optimal level of excitatory synaptic number in adulthood. Thus, the onset and the closure of sensitive period for proper pruning of excitatory inputs to PV interneuron would be defined by the initiation and the termination of ErbB4 splicing shifts, respectively.

In schizophrenia, previous studies have shown that for most GABA-related transcripts, including PV mRNA, the changes in expression level with postnatal development were in the opposite direction of the differences observed between schizophrenia and comparison subjects (Fung et al., 2010; Hoftman et al., 2015). Based on this observation, it was proposed that the developmental trajectory of prefrontal inhibition is blunted and does not reach the adult level in schizophrenia (Hoftman et al., 2015). Therefore, if PV interneuron activity does not reach the mature level and is arrested at an earlier developmental stage, presumably at the adolescent period, this in turn would fail to induce the expression of Factor 2, resulting in a persistently predominant expression of Factor 1. Failure to achieve the balance between Factor 1 and Factor 2 expression levels would result in a continued shifting of ErbB4 splicing to JM-a/CYT-1

variants, causing a pathological elimination of mature excitatory synapses on PV interneurons. Consequently, the loss of excitatory inputs to and reduced activity of PV interneurons in schizophrenia might be the result of a failure to establish the closure of sensitive period during adolescence. In section 5.4, I will discuss potential experiments that can test the validity of this model.

I would like to emphasize that Factors 1 and 2 in this model are hypothetical molecules based on the interpretation of the existing data, but a similar activity-dependent mechanism does exist for regulating the alternative splicing of Neurexin-1 transcripts. Neurexin-1 is an autism susceptibility gene that participates in the formation of excitatory synapses (Craig and Kang, 2007). At moderate neuronal activity, alternative splicing of Neurexin-1 transcripts is shifted towards the Neurexin-1 4(+) variant that includes exon 20, which favors synaptic formation (Uemura et al., 2010). High neuronal activity activates the RNA binding protein SAM68, which inhibits an inclusion of exon 20 (Iijima et al., 2011). This renders Neurexin-1 to have a stronger interaction with its receptor neuroligin-1B thereby stabilizing the synaptic connections.

In the following sub-sections, I will first review some of the putative causal factors that might arrest the maturation of PV interneuron activity in schizophrenia, and then I will provide potential implications of the developmental arrest model that could explain the relationship between such causal factors and ErbB4 splicing shifts. The term “reduced PV interneuron activity” as used here indicates a lower level of PV interneuron activity (due to developmental arrest; see boundary defined by the two dotted vertical lines in Figure 2B), that is sufficient to induce the factor 1 but not enough to express the factor 2. This notion is supported by findings that PV mRNA expression levels in schizophrenia subjects are greater than those found in

normal neonates and infants but less than those found in adult comparison subjects (Fung et al., 2010).

### **5.2.1 Perineuronal net disruption**

Alterations in perineuronal net (PNN) formation could reduce the activity of PV interneurons and might function as an upstream cause for abnormal ErbB4 splicing shifts in schizophrenia. PNNs are aggregates of extracellular matrix that preferentially encapsulate the proximal neurites and cell body of PV interneurons (Berretta et al., 2015). During postnatal development, PNNs stabilize synaptic connections and restrict synaptic plasticity (Dityatev and Schachner, 2003). Moreover, disrupting PNNs reduces AMPA receptor clustering and excitatory drive to PV interneurons, induces a disinhibition of pyramidal neurons and produces abnormal gamma oscillations in animal models (Chang et al., 2010; Shah and Lodge, 2013; Steullet et al., 2014). In human DLPFC, the number of PNN-positive PV interneurons increases during adolescence and the intensity levels of extracellular matrix within PNNs are reduced in the DLPFC of individuals with schizophrenia (Mauney et al., 2013; Enwright et al., 2016). Finally, schizophrenia-associated redox dysregulation and oxidative stress (Emiliani et al., 2014), which are known to impair PV interneuron activity (Cabungcal et al., 2014), also disrupt PNN formation (Cabungcal et al., 2013a). Thus, dysregulated PNN formation during adolescence in schizophrenia could trigger an initial reduction in excitatory drive to PV neurons, which in turn induces abnormal ErbB4 splicing shifts and further loss of excitatory inputs to these neurons.

While these data suggest the role of PNN disruption in the pathogenesis of schizophrenia, it is important to note that in the human DLPFC, PNNs are localized primarily in layers 3 and 5 but virtually absent in layer 4 (Mauney et al., 2013), where PV neurons are predominantly

localized (**Figure 13A**). Consequently, laminar PNN deficits in schizophrenia seem to be more pronounced in cortical layers 3 and 5 whereas the loss of PNN is not observed in layer 4 (Mauney et al., 2013). In contrast to this data, the greatest deficit in PV expression is observed in cortical layer 4 of schizophrenia (Hashimoto et al., 2003). Thus, although it is possible that PNN disruptions may influence the activity of some PV interneurons in cortical layers 3 and 5, it is unlikely that they contribute to the activity regulation in majority of PV neurons in schizophrenia. Alternatively, based on the existing data, it would be more plausible to hypothesize that the absence of PNN in DLPFC layer 4 renders PV neurons in this layer preferentially vulnerable to oxidative stress and redox dysregulation. Consequently, these neurons would be affected to a greater degree in schizophrenia than PV interneurons in other cortical layers. Consistent with this idea, chronic redox dysregulation that produces oxidative stress has been shown to preferentially affect PV interneurons without PNNs in an animal model (Cabungcal et al., 2013b).

### **5.2.2 NMDAR hypofunction**

Reduced PV interneuron activity in schizophrenia could be a consequence of hypoactive N-methyl-D-aspartate receptors (NMDAR) in these neurons. Studies in animal models show that systemic administration of NMDAR antagonists decreases PV and GAD67 expression levels and disinhibits pyramidal cell firing (Behrens et al., 2007; Homayoun and Moghaddam, 2007). Also, an early postnatal knockout of NMDAR core subunit NR1 in GABAergic interneurons results in reduced PV and GAD67 expression levels, abnormal gamma oscillations and behavioral deficits that are associated with schizophrenia (Belforte et al., 2010). Consistent with these data, administration of NMDAR antagonists, such as phencyclidine and ketamine, have been shown to

transiently reproduce full range of symptoms associated with schizophrenia in human subjects (Krystal et al., 1994; Coyle et al., 2012). Taken together, these multiple lines of evidence suggest that deficits in NMDAR function in PV interneurons might serve as an upstream casual factor for dysregulated ErbB4 splicing.

Nevertheless, recent studies demonstrate that the excitation of PV interneurons is driven predominantly by calcium permeable  $\alpha$ -amino-3-hydroxy-5-methyl-4-isoxazolepropionic acid receptor (AMPA) with a minimal contribution from NMDAR (Wang and Gao, 2009; Rotaru et al., 2011). Consistent with this notion, a PV-specific NR1 knockout does not recapitulate many of the schizophrenia-associated deficits seen in an animal model with interneuron-specific NR1 knockout (Korotkova et al., 2010; Saunders et al., 2013). In contrast to the medial ganglionic eminence-derived neurons including PV neurons, the excitation of caudal ganglionic eminence-derived interneuron subtypes, such as those containing vasoactive intestinal peptide (VIP), is mainly driven by NMDAR (Matta et al., 2013). Interestingly, VIP interneurons have been shown to disinhibit the activity of PV neurons by providing inhibitory inputs to somatostatin (SST) neurons that normally inhibit PV neurons (Pfeffer et al., 2013; Pi et al., 2013). Thus, reduced PV neuron activity due to the interneuron-specific NR1 knockout as mentioned above could be a consequence of hypoactive NMDAR in VIP neurons, which would increase the inhibitory effect of SST neurons on PV neurons. However, as these data are solely from rodent models, it is critical to investigate whether the selective enrichment of AMPAR and NMDAR in different interneuron subtypes is conserved in the primate DLPFC.

### 5.2.3 Dendritic spine deficits

Reduced PV neuron activity in schizophrenia could be a consequence of deficits in dendritic spines and hypoactive pyramidal neurons. Dendritic spines are morphologically and biochemically discrete synaptic compartments that protrude from the dendritic shafts of cortical pyramidal neurons and are the site of most excitatory synapses in the cortex (DeFelipe and Farinas, 1992). Reduced density of dendritic spines in layer deep 3 (L3D) pyramidal neurons has been consistently replicated in the DLPFC of schizophrenia (Garey et al., 1998; Glantz and Lewis, 2000; Konopaske et al., 2014). This deficit seems to be a cell type-specific and DLPFC-prominent pathology as spine density is not lower in layer 5 pyramidal neurons or in layer 3 pyramidal neurons in the primary visual cortex. Moreover, the levels of gene products that are associated with CDC42 pathway, which normally participates in dendritic spine formation, have been shown to be altered in L3D pyramidal neurons in subjects with schizophrenia (Hill et al., 2006; Ide and Lewis, 2010; Datta et al., 2015). Finally, de novo mutations and common alleles that are associated with schizophrenia were shown to be enriched for genes that are involved in dendritic spine formation and glutamatergic neurotransmission (Fromer et al., 2014; Schizophrenia Working Group of the Psychiatric Genomics, 2014). These data collectively demonstrate that schizophrenia is associated with dendritic spine deficits and hypoactive L3D pyramidal neurons.

PV interneurons receive excitatory inputs primarily from local pyramidal neurons (Thomson and Lamy, 2007). The strength of excitatory inputs to cortical layer 4 PV neurons from local pyramidal neurons is likely to be reduced in the illness because these pyramidal neurons are thought to be less active due to deficits in their dendritic spines (Lewis et al., 2012; Arion et al., 2015). In schizophrenia, a consequence of reduced excitatory inputs from

hypoactive pyramidal neurons may involve dysregulated ErbB4 splicing in PV interneurons, which would trigger a further reduction of excitatory inputs to and the activity of PV interneurons in order to decrease feedback inhibition to pyramidal neurons. This process could restore the excitation/inhibition (E/I) balance in the DLPFC circuitry of schizophrenia that is initially disrupted by hypoactive pyramidal neurons. Consistent with this idea, the loss of ErbB4 signaling in PV interneurons results in a lower number of perisomatic inhibitory inputs to and reduced inhibitory transmission in pyramidal neurons (Woo et al., 2007; Fazzari et al., 2010).

The maturation of dendritic spines involves pruning of superfluous spines and strengthening of remaining spines, both of which seem to be regulated by neuronal activity (Huttenlocher, 1979; Bourgeois et al., 1994; Anderson et al., 1995; Segal et al., 2000; Gonzalez-Burgos et al., 2008; Petanjek et al., 2011; Bian et al., 2015). These findings suggest that the maturation processes of both dendritic spines and excitatory inputs to PV neurons might involve 1) activity-dependent regulation, 2) pruning of synapses and 3) strengthening of the remaining synapses. Such similarities raise three important speculations regarding how they might contribute to maintaining E/I balance in development and schizophrenia. First, during postnatal development, the maturation processes of dendritic spines and excitatory inputs to PV interneurons might induce each other by activity-dependent regulation in order to maintain the E/I balance within DLPFC circuitry. This notion is supported by the temporal overlap between pruning processes of dendritic spines and of excitatory inputs to PV neurons over adolescent period in the primate DLPFC (Anderson et al., 1995) (**Figure 11A**). Second, at least our findings in chapter 3 suggest that the schizophrenia-associated changes in excitatory inputs to PV neurons involve fewer number of synapses without strengthening of remaining synapses. Although there is currently no direct evidence, we can also speculate that the dendritic spine deficits in

schizophrenia is not accompanied by strengthening of remaining spines, since pyramidal neurons in the illness seem to be hypoactive (Arion et al., 2015). Thus, the changes in excitatory synapses to pyramidal and PV neurons in schizophrenia, unlike in development, might only involve a reduction in the number without affecting the strength of synapses, which collectively would result in reduced excitatory drive to each cell type. Finally, the above two speculations converge onto the hypothesis that the pathogenic loss of excitatory inputs to either pyramidal neurons or PV interneurons in schizophrenia could trigger over-pruning of excitatory inputs to the other neuron through activity-dependent regulation in order to restore E/I balance (see **Figure 17** for further explanation).

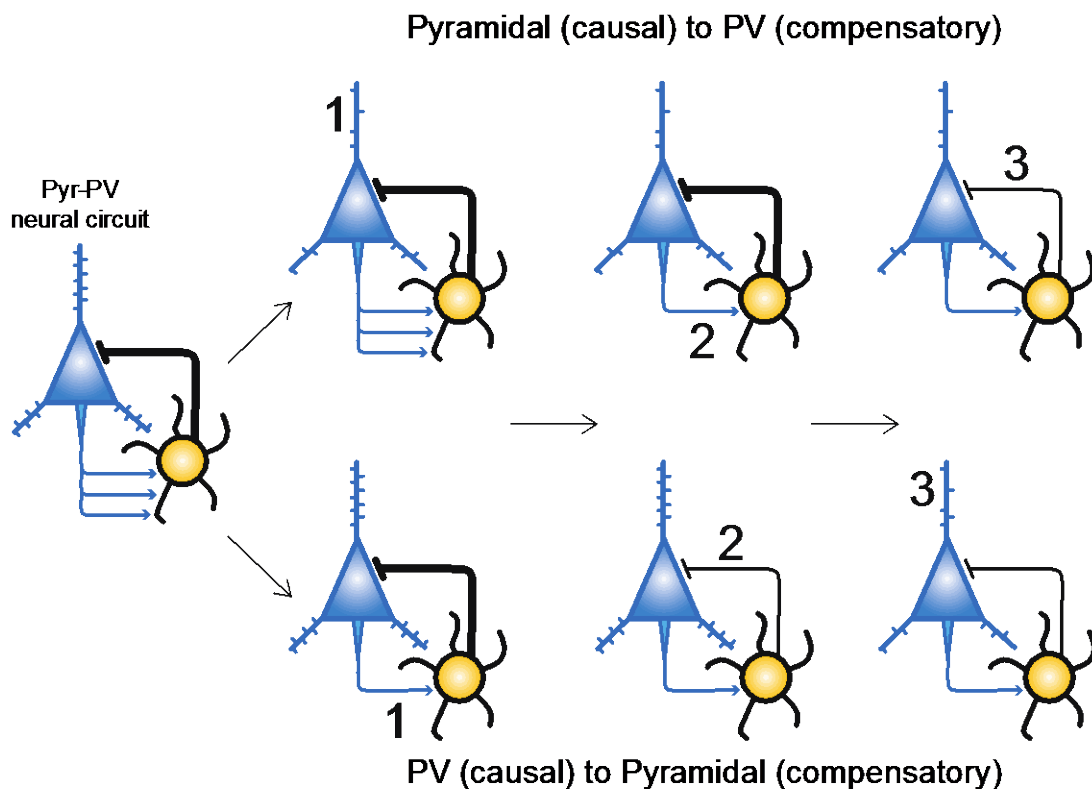


**Figure 17. Proposed E/I balance adjustment by activity-dependent synaptic pruning in response to deficits in either pyramidal (top) or PV neurons (bottom) in schizophrenia**

Each image shows a simple neural circuit composed of a pyramidal neuron (blue) and a PV neuron (yellow) connected to each other (Pyr-PV neural circuit). Top: 1) Cell autonomous dendritic spine deficits result in a hypoactive pyramidal neuron. 2) Hypoactive pyramidal neuron sends reduced glutamatergic drive to a PV neuron

which in turn triggers ErbB4 splicing shifts and compensatory downregulation of excitatory synapses on PV neuron. 3) PV neuron with reduced activity sends lower feedback inhibition to pyramidal neuron. Bottom: 1) Cell autonomous deficits in PV neuron activity triggers ErbB4 splicing shifts, which in turn results in a loss of excitatory inputs to PV neuron. 2) A hypoactive PV neuron sends reduced inhibitory drive to pyramidal neuron. 3) Disinhibited pyramidal neuron triggers activity-dependent dendritic spine pruning that results in compensatory downregulation of pyramidal neuron activity.

Although in this section I hypothesized that the over-pruning of excitatory inputs to PV neurons is a compensatory response to the upstream dendritic spine deficits, some unknown PV-specific etiological factors could induce dysregulated ErbB4 splicing and a reduction in the number of excitatory inputs to PV interneurons. Then, in this event the loss or over-pruning of dendritic spines would function as a homeostatic mechanism that reduces pyramidal neuron activity in response to reduced inhibition from PV interneurons. Consistent with this idea, impairing glutamatergic drive to PV interneurons by knocking out ErbB4 in these neurons has been shown to reduce the density of dendritic spines in animal models (Del Pino et al., 2013; Yin et al., 2013a).

The end result of either event, in which the dendritic spine deficit or the loss of excitatory inputs to PV neurons provides an upstream cause, would both reflect the DLPFC circuitry alterations seen in schizophrenia (**Figure 17**). Nevertheless, determining which cell type, pyramidal neurons or PV neurons, provides the upstream cause in the disease is not only important for deciding where the dysregulated ErbB4 splicing might fit in the pathogenesis of schizophrenia, but also critical for developing new therapeutic strategies. There are a number of limitations to using animal studies to directly address this question, since an isolated disruption in either excitatory activity (Han et al., 2013) or inhibitory activity (Del Pino et al., 2013; Yin et al., 2013a) causes disruptions in the other system in order to maintain E/I balance. Although such studies could elucidate basic mechanisms by which neural circuit maintains E/I balance, these studies may not tell us which side of E/I disruption is the upstream cause in schizophrenia.

Given that the pathology of schizophrenia is thought to reflect a disruption in normal developmental processes of prefrontal cortical circuitry (Lewis, 1997), perhaps we may need to take a step back and first understand how the maturation processes of dendritic spines and excitatory inputs to PV neurons might contribute to triggering each other during normal development in the primate DLPFC. For example, if the onset of spine pruning precedes that of pruning of excitatory inputs to PV neurons during postnatal development, this finding would suggest that the maturation of dendritic spines and increased pyramidal neuron activity trigger the downstream activity-dependent maturation of excitatory inputs to PV neurons. This in turn would provide a greater feedback inhibition to the mature pyramidal neurons. Thus, this finding would support the hypothesis that the directionality of normal E/I balance adjustment during development is from pyramidal neurons to PV interneurons. The opposite would be supported by the findings that the pruning of excitatory inputs to PV neurons precedes the dendritic spine pruning during postnatal development. PV interneurons receive inputs predominantly from local pyramidal neurons (Lee et al., 2013), whereas the source of excitatory inputs to DLPFC pyramidal neurons include intrinsic as well as cortical and subcortical areas that mature earlier than DLPFC (Kritzer and Goldman-Rakic, 1995; Melchitzky et al., 1999). Therefore, it is likely that the maturation processes of dendritic spines and excitatory inputs to PV neurons initiate at different developmental time points. In section 5.4 I will introduce potential experiments that can test the validity of this model.

In this section, I discussed the potential role of ErbB4 splicing shifts and pruning of excitatory inputs to PV neurons in cortical circuitry maturation and schizophrenia. In the next section, I will expand upon the implication of my findings in the context of working memory function using the basic mechanisms discussed in this section in order to speculate how ErbB4

splicing shifts and pruning of excitatory inputs to PV neurons could be associated with working memory maturation and how alterations in these processes may result in working memory deficits in schizophrenia.

### **5.3 IMPLICATION IN WORKING MEMORY MATURATION AND SCHIZOPHRENIA**

The cellular basis of working memory within DLPFC circuitry was identified from the studies on spatial working memory performance using *in vivo* electrophysiology in rhesus monkeys (Goldman-Rakic, 1995). In these studies, a monkey was subjected to the oculomotor delayed response (ODR) task in which the animal was trained to briefly view a spatial cue and then remember the position over a delay period of several seconds. At the end of the delay period, the monkey could make a hand or eye movement to the remembered direction. *In vivo* recordings demonstrated that the DLPFC activity during the delay period of this task was predominantly generated by the excitation of L3D pyramidal neurons (Kritzer and Goldman-Rakic, 1995). Thus, these neurons were thought to represent and maintain the information about visual space in the absence of sensory stimulation. Importantly, clusters of neighboring L3D pyramidal neurons within a micro-column were spatially tuned together, firing together across the delay period when the direction of stimulus coincides with the neurons' preferred direction (Funahashi et al., 1989).

Subsequent studies have shown that fast-spiking (FS) interneurons also possessed spatially tuned delay activity similar to that of L3D pyramidal neurons (Rao et al., 1999, 2000). Interestingly, connected pairs of a L3D pyramidal neuron and an adjacent FS interneuron were

isodirectionally tuned, suggesting that a network of pyramidal cells and interneurons could be clustered based on their propensity to respond to certain spatial stimuli. If such a clustering exists for the neuronal network of pyramidal neurons and PV interneurons, it would facilitate the effective generation of gamma oscillations towards a specific stimulus without incorporating out-of-tune signals from other neurons, thus establishing an anatomical organization for spatial memory fields similar to the receptive fields found in motor and sensory cortices.

ErbB4 splicing shifts and synaptic pruning could provide a mechanism that contributes to establishing the spatial tuning of PV interneurons that is coherent with that of nearby cluster of pyramidal neurons (**Figure 18A**). In this model, a cluster of L3D pyramidal neurons tuned to 90-degree angle make excitatory projections to local PV interneurons. These PV neurons initially receive additional inputs from pyramidal neurons that are tuned to zero-degree angle and thus fail to achieve isodirectional tuning with either clusters of pyramidal neurons. During postnatal development, recurring recruitment of PV interneurons from the 90 degree-tuned L3D pyramidal neurons results in an activity-dependent stabilization and maturation of synaptic connections between these two neuronal populations. Increasing activity of PV interneurons triggers developmental shifts in ErbB4 splicing from the JM-b/CYT-2 to JM-a/CYT-1 variants in these neurons, which induces pruning of weak and immature excitatory synaptic inputs from the zero degree-tuned pyramidal neurons. These processes would collectively result in increases in the strength and the precision of PV interneuron recruitment by the spatially-tuned pyramidal neuron cluster. As the effective recruitment of PV interneurons is critical for generating cortical gamma oscillations (Jonas et al., 2004), this model may provide a circuit-based mechanism for the maturation of gamma oscillations during adolescence in primate DLPFC (Cho et al., 2015).

In schizophrenia, perhaps the loss of dendritic spines in the 90 degree-tuned pyramidal neurons might reduce PV interneuron activity, which would trigger abnormal shifts in ErbB4 splicing and an exaggerated pruning process that eliminates the excitatory inputs from the 90 degree-tuned L3D pyramidal neurons. This exaggerated pruning process would result in a further reduction of PV neuron activity and consequently lower feedback inhibition to hypoactive 90 degree-tuned L3D pyramidal neurons. However, reduction in the strength of excitatory drive to PV neurons would impair the proper recruitment of PV neurons by the 90 degree-tuned L3D pyramidal neurons, and consequently would result in deficient cortical gamma oscillations and working memory dysfunction in schizophrenia. Collectively, the degree of effective PV interneuron recruitment would form an inverted U-shaped curve as a function of ErbB4 splicing shifts (**Figure 18B**). Intriguingly, animal models that recapitulate the abnormal loss or gain of ErbB4 signaling both exhibit synaptic dysfunction and behavioral deficits (Marin and Rico, 2013; Yin et al., 2013b; Agarwal et al., 2014). These observations led to the hypothesis that there is an optimal range for ErbB4 signaling in the brain and either too much or too little ErbB4 signaling is sufficient to impair neuronal development and synaptic plasticity (**Figure 18C**) (Mei and Nave, 2014). Therefore, our model suggests that maintaining the optimal range of ErbB4 splicing shifts and pruning of excitatory inputs to PV neurons in the DLPFC could serve as molecular and synaptic substrates for the inverted U-shaped effect of NRG-1/ErbB4 signaling pathway on working memory performance and potentially other cognitive function. In section 5.4 I will discuss potential experiments that could at least partly test the validity of this model.

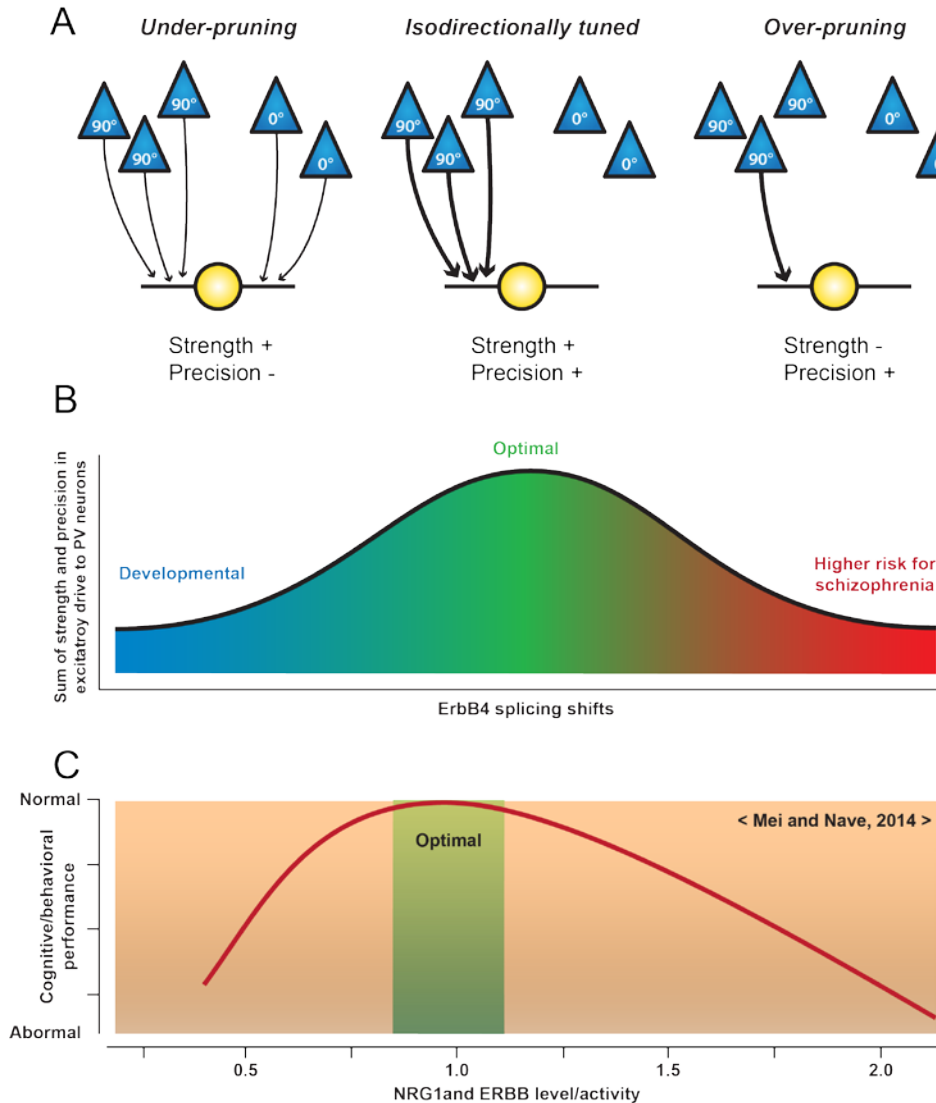


**Figure 18. Proposed role of ErbB4 splicing shifts and pruning of excitatory inputs to PV interneurons in working memory maturation and schizophrenia**

(A) Simplified DLPFC microcircuitry depicting L3D pyramidal neurons (blue) that maintain persistent firing across the delay period for the neuron's preferred direction (either 90° or 0°) and PV interneuron (yellow) that receives excitatory inputs from L3D pyramidal neurons. *Under-pruning*: Prior to adolescence, PV neuron receives excitatory inputs from both 90° and 0° preferred L3D neurons and therefore this PV neuron can be recruited by both populations of L3D neurons. *Isodirectionally tuned*: During adolescence, maturation of synaptic connection between PV neuron and 90° preferred L3D neurons triggers shifts in ErbB4 splicing and pruning of excitatory inputs from 0° preferred L3D neurons. Consequently, this PV neuron is recruited selectively by 90° preferred L3D neurons. *Over-pruning*: In schizophrenia, an exaggerated pruning process eliminates synaptic connections between PV neuron and 90° preferred L3D neurons and therefore this PV neuron is recruited weakly by 90° preferred L3D neurons. (B) Collectively, the recruitment of PV neuron by 90° preferred L3D neurons would be less efficient prior to adolescence and in schizophrenia, due to the lack of precision or strength, respectively, in excitatory drive to PV neuron. (C) As efficient PV neuron recruitment is critical for generating cortical gamma oscillations and working memory performance, ErbB4 splicing shifts and pruning of excitatory inputs to PV neurons may contribute to the proposed inverted-U shaped effect of ErbB4 signaling on cognitive function. Figure 4C is adapted from Mei L, Nave KA (2014) *Neuron* 83:27-49.

## 5.4 CONCLUDING REMARKS: FUTURE STUDIES

In this general discussion section, I have postulated potential role of ErbB4 splicing shifts and pruning of excitatory inputs to PV interneurons in maintaining E/I balance of cortical circuitry, working memory maturation and schizophrenia. First, I proposed that alternative splicing of ErbB4 could be regulated in an activity-dependent manner, allowing PV interneurons to regulate the excitatory input number they receive in response to changes in neuronal activity. Second, I proposed that dendritic spine plasticity might trigger ErbB4 splicing shifts in PV interneurons and pruning of excitatory inputs to these neurons in order to restore E/I balance in development and schizophrenia. Third, I proposed that ErbB4 splicing shifts and pruning of excitatory inputs to PV neurons could provide molecular and synaptic substrates for the inverted U-shaped effect of NRG-1/ErbB4 signaling pathway on working memory function. I would like to conclude my dissertation by providing three aims and sets of hypotheses for each aim that could test, at least partly, the validity of those models that are proposed in the discussion sections.

In the first aim, I propose that alternative splicing of ErbB4 transcripts in PV interneurons is regulated in an activity-dependent manner. In order to investigate this aim, I propose the following sets of hypotheses that can be tested in rat cortex and primary neuronal culture, similar to the previous study that investigated the effect of neuronal activity on alternative splicing of neuregulin-1 transcripts (Liu et al., 2011). First, I hypothesize that the four ErbB4 splice variants (JM-a, JM-b, CYT-1, CYT-2) are expressed in adult rat cortex and the relative ratios of minor to major variants are similar to those found in the primate DLPFC. Second, I hypothesize that ErbB4 splicing shift occurs during postnatal development and parallels with the developmental trajectory of PV expression in rat cortex (de Lecea et al., 1995).

Third, I hypothesize that in primary rat neuronal culture, shifts in ErbB4 splicing from the JM-b/CYT-2 to JM-a/CYT-1 variants occur in response to increasing concentrations of kainic acid until it reaches a plateau; the ErbB4 splicing shifts would be abolished with an overexpression of MIAT if MIAT indeed does regulate ErbB4 splicing. Finally, I hypothesize that with increasing incubation period with kainic acid, the slope of ErbB4 shifts is greater for the lower concentration than the higher concentration of kainic acid. The results from this study would elucidate whether 1) shifts in ErbB4 splicing is a conserved mechanism across developing brains of different species, 2) an activity-dependent mechanism is involved in modulating ErbB4 splicing, and 3) ErbB4 splicing shift could be differentially regulated by moderate (arrested) and high neuronal activity.

In the second aim, I propose that dendritic spine maturation precedes the maturation of excitatory inputs to PV neurons and deficits in spine maturation induce an over-pruning of excitatory inputs to PV neurons. In order to validate this aim, I propose the following sets of hypotheses that can be tested using a developmental monkey cohort expanded from chapter 4 and an existing Arp 2/3 knock out (KO) mouse model in which dendritic spine formation is impaired (Kim et al., 2015). First, I hypothesize that the onset of L3D dendritic spine pruning precedes the pruning onset of excitatory synaptic inputs to PV interneurons during postnatal development in monkey DLPFC. Second, I hypothesize that ErbB4 splicing is shifted from the JM-b/CYT-2 to JM-a/CYT-1 variants in the Arp 2/3 KO mouse compared to the wild type mouse. Third, I hypothesize that the density of VGlut1+/PSD95+ puncta on PV+ neurons is lower in the Arp 2/3 KO mouse compared to the wild type mouse. Finally, I hypothesize that inhibitory transmission is reduced in pyramidal neurons of the Arp 2/3 KO mouse compared to the wild type mouse. The results from this study would elucidate whether 1) the maturation onset

of dendritic spines and excitatory inputs to PV neuron coincides or differs, 2) the deficits in dendritic spine maturation could provide an upstream cause for dysregulated ErbB4 splicing shifts and the loss of excitatory inputs to PV neurons and 3) these downstream processes could contribute to reduced feedback inhibition to hypoactive pyramidal neurons.

Finally, in the third aim, I propose that the ErbB4 splicing shifts and pruning of excitatory synaptic inputs to PV neurons contribute to the inverted U-shaped effect of NRG-1/ErbB4 signaling on cognitive function. In order to validate this aim, I propose the following sets of hypotheses that can be tested by using an existing mouse model in which NRG-1 is overexpressed in order to induce an abnormally high level of ErbB4 activation (ctoNrg1 mouse) (Yin et al., 2013b). I first hypothesize that in ctoNrg1 mouse, PV interneurons receive a greater number of excitatory synaptic inputs than those in control mouse. Second, I hypothesize that reducing Nrg1 to normal levels results in pruning of excitatory synaptic inputs to PV interneurons. Third, I hypothesize that shifts in ErbB4 splicing accompany those changes in the density of excitatory synapses on PV interneurons. The results from this study would elucidate whether 1) the gain of ErbB4 signaling is associated with an under-pruning of excitatory inputs to PV neurons, 2) the under-pruning of excitatory inputs to PV neurons could contribute to cognitive dysfunction and 3) ErbB4 splicing shifts could provide underlying mechanisms to these processes.

The ultimate goal of schizophrenia research is to develop more effective treatments and preventative measures for patients with this illness, which requires greater knowledge of the underlying disease process. In order to understand the disease process of schizophrenia, it is critical to identify an abnormality in the brain that is associated with the clinical syndrome (pathology), investigate pathogenic mechanisms underlying this pathology (pathogenesis) and

understand how such pathology can give rise to alterations in brain function (pathophysiology) (Lewis et al., 2005). Rational therapeutic strategy then can be developed that either interrupts or reverses the pathophysiological processes and pathogenetic mechanisms, respectively (Lewis and Sweet, 2009). In this dissertation, I have identified fewer excitatory inputs to PV interneurons as a novel pathology of schizophrenia, implicated developmental disturbances in ErbB4 splicing shifts and pruning of excitatory inputs to PV neurons as the underlying pathogenic mechanisms and speculated the potential role of these processes in the emergence of the pathophysiological element that is associated with the core clinical feature of schizophrenia. Therefore, further elucidating the role of abnormal ErbB4 splicing shifts and an exaggerated pruning of excitatory inputs to PV neurons in schizophrenia, and investigating how these processes can be interrupted or reversed along the course of illness, may provide critical insights for development of new therapeutic interventions for individuals with schizophrenia.

**APPENDIX A**

**TABLE 3. DEMOGRAPHIC, POSTMORTEM, AND CLINICAL CHARACTERISTICS  
OF HUMAN SUBJECTS USED IN THIS DISSERTATION.**

Subject Group <sup>a</sup>	Case #	S/R/A <sup>b</sup>	PMI <sup>c</sup>	pH	RIN	Storage time <sup>d</sup>	Cause of death <sup>e</sup>	DSM IV Diagnoses <sup>f</sup> Primary Substance <sup>g</sup>	Anti- psychotics ATOD	Anti- depressants ATOD	BZ/VPA ATOD <sup>h</sup>
1	C	592	M/B/41	22.1	6.7	9	216	ASCVD	N		
	S	533	M/W/40	29.1	6.8	8.4	225	Accidental Asphyxiation	US	Y	N
2	C	567	F/W/46	15	6.7	8.9	220	Mitral valve prolapse	N		
	S	537	F/W/37	14.5	6.7	8.6	225	Suicide by hanging	SA	N	N
3	C	516	M/B/20	14	6.9	8.4	227	Homicide by gun shot	N		
	S	547	M/B/27	16.5	7	7.4	223	Heat stroke	SA	Y	Y
4	C	630	M/W/65	21.2	7	9	210	ASCVD	N		
	S	566	M/W/63	18.3	6.8	8	220	ASCVD	US	AAR	Y
5	C	604	M/W/39	19.3	7.1	8.6	213	Hypoplastic coronary artery	N		
	S	581	M/W/46	28.1	7.2	7.9	218	Accidental combined drug overdose	PS	ADC; OAC	Y
6	C	546	F/W/37	23.5	6.7	8.6	224	ASCVD	N		
	S	587	F/B/38	17.8	7	9	216	Myocardial hypertrophy	US	AAR	Y
7	C	551	M/W/61	16.4	6.6	8.3	222	Cardiac tamponade	N		
	S	625	M/B/49	23.5	7.3	7.6	210	ASCVD	DS	AAC	Y
8	C	685	M/W/56	14.5	6.6	8.1	203	Hypoplastic coronary artery	N		
	S	622	M/W/58	18.9	6.8	7.4	210	Right MCA infarction	US		N
9	C	681	M/W/51	11.6	7.2	8.9	203	Hypertrophic cardiomyopathy	N		
	S	640	M/W/49	5.2	6.9	8.4	208	Pulmonary embolism	PS		Y
10	C	806	M/W/57	24	6.9	7.8	182	Pulmonary embolism	N		
	S	665	M/B/59	28.1	6.9	9.2	206	Intestinal hemorrhage	PS	ADC	Y
11	C	822	M/B/28	25.3	7	8.5	179	ASCVD	N		
	S	787	M/B/27	19.2	6.7	8.4	185	Suicide by gun shot	SA	ODC	Y
12	C	727	M/B/19	7	7.2	9.2	196	Trauma	N		
	S	829	M/W/25	5	6.8	9.3	177	Suicide by drug overdose	SA	ADC; OAR	N
13	C	871	M/W/28	16.5	7.1	8.5	169	Trauma	N		
	S	878	M/W/33	10.8	6.7	8.9	168	Myocardial fibrosis	DS	ADC	Y
14	C	575	F/B/55	11.3	6.8	9.6	218	ASCVD	N		
	S	517	F/W/48	3.7	6.7	9.3	227	Intracerebral hemorrhage	DS	ADC	Y
15	C	700	M/W/42	26.1	7	8.7	200	ASCVD	N		
	S	539	M/W/50	40.5	7.1	8.1	224	Suicide by combined drug overdose	SA	ADR	Y
16	C	988	M/W/82	22.5	6.2	8.4	147	Trauma	N		
	S	621	M/W/83	16	7.3	8.7	211	Accidental asphyxiation	US		N

Subject Group <sup>a</sup>		Case #	S/R/A <sup>b</sup>	PMI <sup>c</sup>	pH	RIN	Storage time <sup>d</sup>	Cause of death <sup>e</sup>	DSM IV Diagnoses <sup>f</sup> Primary Substance <sup>g</sup>	Anti- psychotics ATOD	Anti- depressants ATOD	BZ/VPA ATOD <sup>h</sup>
17	C	686	F/W/52	22.6	7	8.5	202	ASCVD	N			
	S	656	F/B/47	20.1	7.3	9.2	207	Suicide by gun shot	SA	ADC	Y	N
18	C	634	M/W/52	16.2	7	8.5	209	ASCVD	N			
	S	722	M/B/45	9.1	6.7	9.2	197	Upper GI bleeding	US	ODR; OAR	Y	N
19	C	852	M/W/54	8	6.8	9.1	172	Cardiac tamponade	N			
	S	781	M/B/52	8	6.7	7.7	187	Peritonitis	SA	ADR	Y	Y
20	C	987	F/W/65	21.5	6.8	9.1	147	ASCVD	N			
	S	802	F/W/63	29	6.4	9.2	182	Right ventricular dysplasia	SA	ADC; ODR	Y	N
21	C	818	F/W/67	24	7.1	8.4	180	Anaphylactic reaction	N			
	S	917	F/W/71	23.8	6.8	7	160	ASCVD	US		Y	N
22	C	857	M/W/48	16.6	6.7	8.9	170	ASCVD	N			
	S	930	M/W/47	15.3	6.2	8.2	157	ASCVD	DS	ADR; OAR	Y	N
23	C	739	M/W/40	15.8	6.9	8.4	195	ASCVD	N			
	S	933	M/W/44	8.3	5.9	8.1	156	Myocarditis	DS		Y	Y
24*#+	C	1047	M/W/43	13.8	6.6	9	129	ASCVD	N			
	S	1209	M/W/35	9.1	6.5	8.7	110	Diphenhydramine overdose	SA		Y	N
25*#	C	1086	M/W/51	24.2	6.8	8.1	123	ASCVD	N			
	S	10025	M/B/52	27.1	6.7	7.8	102	ASCVD	DS	OAR	N	N
26*#+	C	1092	F/B/40	16.6	6.8	8	123	Mitral valve prolapse	N			
	S	1178	F/B/37	18.9	6.1	8.4	114	Pulmonary embolism	SA		Y	N
27*	C	10005	M/W/42	23.5	6.7	7.4	111	Trauma	N			
	S	1256	M/W/34	27.4	6.4	7.9	103	Hanging	US		Y	N
28*#	C	1336	M/W/65	18.4	6.8	8	88	Cardiac tamponade	N			
	S	1173	M/W/62	22.9	6.4	7.7	114	ASCVD	DS	ADR	Y	N
29*#+	C	1122	M/W/55	15.4	6.7	7.9	119	Cardiac tamponade	N			
	S	1105	M/W/53	7.9	6.2	8.9	121	ASCVD	SA		Y	N
30*+	C	1284	M/W/55	6.4	6.8	8.7	98	ASCVD	N			
	S	1188	M/W/58	7.7	6.2	8.4	113	ASCVD	US	AAR; OAR	Y	N
31*+	C	1191	M/B/59	19.4	6.2	8.4	112	ASCVD	N			
	S	1263	M/W/62	22.7	7.1	8.5	102	Asphyxiation	US	ADR	Y	Y
32*#	C	970	M/W/42	25.9	6.4	7.2	141	ASCVD	N			
	S	1222	M/W/32	30.8	6.4	7.5	108	Combined drug overdose	US	AAC	Y	Y
33*+	C	10003	M/W/49	21.2	6.5	8.4	112	Trauma	N			
	S	1088	M/W/49	21.5	6.5	8.1	124	Combined drug overdose	US	ADC; OAC	Y	Y
34*+	C	1247	F/W/58	22.7	6.4	8.4	104	ASCVD	N			
	S	1240	F/B/50	22.9	6.3	7.7	105	ASCVD	US	ADR	Y	N

Subject Group <sup>a</sup>	Case #	S/R/A <sup>b</sup>	PMI <sup>c</sup>	pH	RIN	Storage time <sup>d</sup>	Cause of death <sup>e</sup>	DSM IV Diagnoses <sup>f</sup>		Anti- psychotics ATOD	Anti- depressants ATOD	BZ/VPA ATOD <sup>h</sup>
								Primary Substance <sup>g</sup>				
35*#	C	1324	M/W/43	22.3	7	7.3	90	Aortic dissection	N			
	S	10020	M/W/38	28.8	6.6	7.4	104	Salicylate overdose	PS	AAC; OAC	Y	Y
36*#+	C	1099	F/W/24	9.1	6.5	8.6	122	Cardiomyopathy	N			
	S	10023	F/B/25	20.1	6.7	7.4	103	Suicide by drowning	DS		Y	N
37*#+	C	1307	M/B/32	4.8	6.7	7.6	93	ASCVD	N			
	S	10024	M/B/37	6	6.1	7.5	103	ASCVD	PS		N	N
38*#+	C	1391	F/W/51	7.8	6.6	7.1	79	ASCVD	N			
	S	1189	F/W/47	14.4	6.4	8.3	113	Combined drug overdose	SA	AAR	Y	Y
39*#	C	1282	F/W/39	24.5	6.8	7.5	99	ASCVD	N			
	S	1211	F/W/41	20.1	6.3	7.8	110	Sudden unexpected death	SA		Y	Y
40*#+	C	1159	M/W/51	16.7	6.5	7.6	116	ASCVD	N			
	S	1296	M/W/48	7.8	6.5	7.3	96	Pneumonia	US		Y	Y
41*#+	C	1326	M/W/58	16.4	6.7	8	90	ASCVD	N			
	S	1314	M/W/50	11	6.2	7.2	93	ASCVD	US		Y	Y
42*#	C	902	M/W/60	23.6	6.7	7.7	155	ASCVD	N			
	S	1361	M/W/63	23.2	6.4	7.7	85	Cardiomyopathy	SA	ODC	Y	N
43*	C	1374	M/W/43	21.7	6.6	7.2	85	ASCVD	N			
	S	904	M/W/33	28	6.2	7.1	156	Pneumonia	SA		Y	N
44*+	C	1555	M/W/17	15.1	6.9	7.9	50	Trauma	N			
	S	1649	M/B/17	21.4	6.9	8.1	35	Hanging	US		Y	Y
45*+	C	1268	M/B/49	19.9	7.1	7.9	102	ASCVD	N			
	S	1230	M/W/50	16.9	6.6	8.2	108	Doxepin overdose	US		Y	Y
46*	C	1466	F/B/64	20	6.7	8.8	67	Trauma	N			
	S	1341	F/W/44	24.5	6.6	8.8	89	Trauma	SA	ODC	Y	N
47*	C	1518	M/W/50	20.7	6.4	7.7	56	ASCVD	N			
	S	1367	M/W/47	28.9	6.6	7.2	86	Combined drug overdose	SA	ADC; ODR	N	N
48*+	C	1386	M/W/46	21.2	6.7	8.3	82	ASCVD	N			
	S	1420	M/W/47	23.4	6.8	8.2	75	Jump	SA	AAR; ODC; OAR	Y	Y
49*+	C	1472	M/W/61	23.8	6.5	8	66	Pulmonary embolism	N			
	S	1453	M/W/62	11.1	6.4	8.2	69	Trauma	PS	ADR	Y	N
50*	C	1026	M/W/59	19.8	6.3	7.4	134	ASCVD	N			
	S	1454	M/W/59	24.1	6.1	7.6	69	Trauma	PS	AAR; ODC	Y	Y
51*+	C	694	M/W/38	20.7	7	7.7	195	Subarachnoid hemorrhage	N			
	S	1455	M/W/42	8.2	6.4	7.7	69	Peritonitis	PS	AAR; OAC	Y	N
52*	C	1350	M/W/21	24.2	6.4	7.3	88	Trauma	N			
	S	1474	M/W/37	39.9	6.7	7	66	Hanging	SA	ADR	N	N

Subject Group <sup>a</sup>	Case #	S/R/A <sup>b</sup>	PMI <sup>c</sup>	pH	RIN	Storage time <sup>d</sup>	Cause of death <sup>e</sup>	DSM IV Diagnoses <sup>f</sup> Primary Substance <sup>g</sup>	Anti- psychotics ATOD	Anti- depressants ATOD	BZ/VPA ATOD <sup>h</sup>
53*	C	1792	F/W/36	28.1	6.5	7.5	10	Pulmonary embolism	N		
	S	1506	F/W/47	14.1	6.6	7.5	60	Combined drug overdose	SA	ADC	Y
54*	C	1524	M/W/66	9.4	6.4	8.1	55	Intestinal infarction	N		Y
	S	1542	M/W/65	17.4	6.7	7.8	52	Combined drug overdose	PS		Y
55*	C	1270	F/W/73	19.7	6.7	7.7	102	Trauma	N		
	S	1579	F/W/69	16.1	6.7	7.7	46	ASCVD	SA	ADR; ODC	Y
56*+	C	1372	M/W/37	20.5	6.6	9	86	Asphyxiation	N		
	S	1581	M/W/32	18.4	6.8	9	45	ASCVD	PS	ODC; OAC	Y
57*+	C	1543	F/W/45	17.9	6.8	7.4	52	Subarachnoid hemorrhage	N		
	S	10026	F/W/46	23.8	6.6	7.6	104	Thermal injuries	US		Y
58*+	C	1583	M/W/58	19.1	6.8	8.2	45	Trauma	N		Y
	S	1686	M/B/56	14.1	6.2	8.3	28	ASCVD	PS	AAR	Y
59*	C	1554	M/W/50	23.2	6.5	7.6	50	ASCVD	N		
	S	1691	M/W/51	31.9	6.6	7.7	27	Combined drug overdose	PS	ADR; ODC	Y
60*	C	1635	M/W/66	25.3	6.8	8.2	38	Cardiac tamponade	N		
	S	1706	M/B/60	28.1	6.8	8.4	23	Sepsis	SA	AAR; ODC; OAR	Y
61*	C	1384	M/W/67	21.9	6.6	7	83	ASCVD	N		
	S	1712	M/W/63	15.1	6.2	7.1	22	ASCVD	SA	ADR; ODC	Y
62*	C	1558	M/W/54	24.4	6.9	7.7	50	ASCVD	N		
	S	1734	M/W/54	28.6	6.1	7.7	19	Pneumonia	US	AAR; ODC; OAR	Y

\*: Subject pairs used for layer-specific qPCR; #: Subject pairs used for microarray; +: Subject pairs used for immunohistochemistry a: C, normal comparison; S, schizophrenia; b: A, age in years; B, black; F, female; M, male; R, race; S, sex; W, white; c: PMI, postmortem interval (hours); d: Storage time (months) at -80C; e: ASCVD, arteriosclerotic cardiovascular disease; MCA, middle coronary artery; f: DS, disorganized schizophrenia; PS, paranoid schizophrenia; SA, schizoaffective disorder; US, undifferentiated schizophrenia; g: ADC, alcohol dependence, current at time of death; ADR, alcohol dependence, in remission at time of death; AAC, alcohol abuse, current at time of death; AAR, alcohol abuse, in remission at time of death; ODC, other substance dependence, current at time of death; ODR, other substance dependence, in remission at time of death; OAC, other substance abuse, current at time of death; OAR, other substance abuse, in remission at time of death; h: BZ/VPA ATOD; BZ, benzodiazepines; VPA, Sodium valproate; ATOD, at time of death; Y, yes; N, no.

## **APPENDIX B**

### **SUPPLEMENTAL INFORMATION FOR DYSREGULATED ERBB4 SPLICING IN SCHIZOPHRENIA: SELECTIVE EFFECTS ON PARVALBUMIN EXPRESSION**

#### **B.1 SUPPLEMENTARY METHODS**

##### **Total gray matter RNA extraction**

The gray-white matter boundary of DLPFC area 9 in a tissue block from each subject was carefully scored with a scalpel blade where the gray matter had uniform thickness and the gray-white matter boundary was easily delineated. The scored gray matter region of the tissue block was then digitally photographed, and the number of tissue sections (40  $\mu\text{m}$ ) required to collect  $\sim 30 \text{ mm}^3$  of gray matter was determined for each subject. The calculated number of required tissue sections for each subject was then cut by cryostat, and gray matter was separately collected into a tube containing TRIzol reagent in a manner that ensured minimal white matter contamination and excellent RNA preservation. Complementary DNA (cDNA) was synthesized from standardized dilutions of total RNA (10  $\text{ng}/\mu\text{l}$ ) for each subject.

## **Microarray analysis**

For laser microdissection of individual neurons, cryostat sections of DLPFC area 9 were dual-labeled with lectin *Vicia villosa* agglutinin (VVA) and anti-NeuN antibody in order to visualize parvalbumin interneuron-selective perineuronal nets and all neurons, respectively. RNA was extracted from pooled samples of 360 VVA-labeled neurons, converted into cDNA, amplified, labeled with biotin, and loaded on Affymetrix GeneChip HT HG-U133+ PM Array Plate (Affymetrix, Santa Clara, CA). Scanned images were segmented and converted into DAT files, using Microarray Analysis Suite 5.0. Segmented images were normalized and log<sub>2</sub>-transformed using GeneChip Robust Multiarray Average (Georgiev et al., 2014).

## **Genotype analysis**

DNA was isolated from brain tissue using standard techniques and genotyped by the Illumina Infinium HumanOmniExpressExome array (Illumina, INC, San Diego, CA). Genotype calls were retained if they passed quality control for samples and SNPs, which yielded 767,368 SNPs for all samples. To impute a larger set of genotypes per sample, haplotypes were inferred and variants were imputed in 5Mb segments by Impute v2.3.1 (Howie et al., 2009) with the 1000 Genomes Phase 1 integrated reference panel (Genomes Project et al., 2010). Of the 4 SNPs evaluated in this study, 3 were genotyped directly and one was imputed (rs4673628). Due to missing genotype information, some subjects were excluded from the analyses.

## **Statistical analysis**

Repeated measures model was implemented in SAS PROC MIXED using the REML method in order to analyze layer-specific expression of PV, CR and ErbB4 splicing variants. In

the REML method, the Kenward-Roger degrees of freedom approximation method was used to compute the denominator degrees of freedom (Kenward and Roger, 1997). Paired and unpaired repeated measures models included mRNA level as the dependent variable; diagnosis, cortical layer, and the interaction between diagnosis and cortical level as main effects. Covariates were included in each model as described for the ANCOVA model.

The potential influence of co-morbid factors (e.g., diagnosis of schizoaffective disorder; history of substance dependence or abuse; nicotine use at time of death; antipsychotic, antidepressant or benzodiazepine and/or sodium valproate use at time of death; or death by suicide) on the levels of JM-a, JM-b, CYT-1 and CYT-2 mRNAs in layer 4 of schizophrenia subjects were assessed by using an ANCOVA model with each factor as the main effect and sex, age, brain pH, RIN, PMI, storage time as covariates.

Relationships between the ratios of minor to major ErbB4 splicing variants and CR or PV mRNA levels in layers 2 or 4, respectively, were assessed by Pearson's correlation analysis with the Bonferroni-corrected alpha level of 0.006 (Curtin and Schulz, 1998).

## B.2 SUPPLEMENTARY TABLES

Table 4. Oligonucleotide sequences of forward and reverse primers for ErbB4 splicing variants, pan-ErbB4 and MIAT.

Gene	Accession #	Forward Primer	Reverse Primer	Amplicon size (bp)	Position
CYT-1	NM_005235	TTGGACACAGCCCTCCTC	GGGCACAGACACTCCTTGT	98	3241~3338
CYT-2	NM_001042599	TGACTCGAATAGGAACCAGTTTG	GGGTGCTACTGTCCTCTTGG	206	3221~3426
JM-a	NM_001042599	TTAAAGATGGCCCAAACCTGTG	CCCGTCCATGGGTAGTAAAT	172	1846~2017
JM-b	XM_005246377	AAAGATGGCCCAAACCTGTGT	ATCAGGCCGATGCAGTCTT	161	2375~2535
Pan-ErbB4	NM_001042599	GACCAATGTCTGTCGTGTCG	TCAAACCTCCCGAAATTCACC	89	1650~1738
MIAT	NR_003491.3	GGTCCATGTGGTTAGGGTTG	GGGTTAGTTGGTTGGCAGAA	227	4971~5197

**Table 5. Summary statistics comparing the levels of transcripts between subject groups in total gray matter, layer 2 or 4 by paired ANCOVA or paired repeated measures models.**

Transcript	% change in schizophrenia			ANCOVA				Repeated Measures					
	Total Gray Matter	Layer 2	Layer 4	Total Gray Matter	Layer 2	Layer 4	Layer 2	Layer 4	Layer 2	Layer 4	Layer 2	Layer 4	
				F	p	F	p	F	p	F	p	F	p
PV		-9.9%	-19.5%			F <sub>1,38</sub> =1.35	0.253	F <sub>1,38</sub> =14.6	<0.001	F <sub>1,114</sub> =0.06	0.808	F <sub>1,114</sub> =27.2	0.001
CR		-6.1%	-0.4%			F <sub>1,38</sub> =1.95	0.171	F <sub>1,38</sub> =0.002	0.961	F <sub>1,114</sub> =2.64	0.107	F <sub>1,114</sub> =0.06	0.808
JM-a	+10.9%	+10.3%	+22.1%	F <sub>1,61</sub> =7.49	0.008	F <sub>1,38</sub> =1.71	0.199	F <sub>1,38</sub> =4.62	0.038	F <sub>1,97.3</sub> =1.41	0.238	F <sub>1,97.3</sub> =6.27	0.014
JM-b	-11.5%	-15.0%	-17.0%	F <sub>1,61</sub> =17.1	<0.001	F <sub>1,37</sub> =3.15	0.084	F <sub>1,38</sub> =15.1	0.001	F <sub>1,65.1</sub> =5.58	0.021	F <sub>1,65.1</sub> =6.54	0.013
CYT-1	+4.7%	-1.1%	+19.3%	F <sub>1,61</sub> =0.97	0.328	F <sub>1,38</sub> =0.02	0.902	F <sub>1,38</sub> =7.07	0.011	F <sub>1,75.8</sub> =0.02	0.890	F <sub>1,75.8</sub> =4.87	0.030
CYT-2	-10.0%	-3.2%	-10.2%	F <sub>1,60</sub> =12.3	<0.001	F <sub>1,38</sub> =0.23	0.635	F <sub>1,38</sub> =3.98	0.053	F <sub>1,98.3</sub> =0.29	0.592	F <sub>1,98.3</sub> =2.73	0.101
Pan-ErbB4	+3.9%	+1.3%	-6.6%	F <sub>1,61</sub> =3.39	0.071	F <sub>1,38</sub> =0.12	0.727	F <sub>1,38</sub> =1.92	0.174	F <sub>1,81.5</sub> =0.09	0.761	F <sub>1,81.5</sub> =2.28	0.135
MIAT	+12.6%			F <sub>1,60</sub> =6.79	0.012								

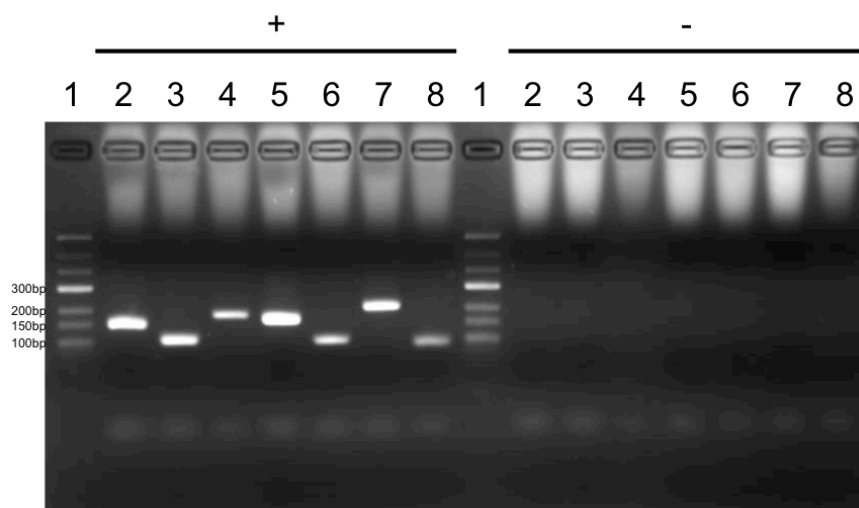
Table 6. Relationship between the ratios of ErbB4 splicing variants and the levels of CR or PV mRNA and in layer 2 or 4, respectively.

	CR in layer 2				PV in layer 4			
	Healthy Comparison		Schizophrenia		Healthy Comparison		Schizophrenia	
	r	p	r	p	r	p	r	p
<b>CYT-1/CYT-2</b>	-0.243	0.135	-0.125	0.448	-0.243	0.137	-0.127	0.442
<b>JM-a/JM-b</b>	-0.275	0.091	-0.132	0.424	0.017	0.920	<b>-0.502</b>	<b>&lt;0.001</b>

Table 7. Summary statistics displaying the main effect of genotypes and interactions between genotypes and diagnosis on the ratios of JM-a/JM-b variants or CYT-1/CYT-2 variants.

Genotype	JM-a/JM-b gray matter		JM-a/JM-b layer 4		Genotype	CYT-1/CYT-2 gray matter		CYT-1/CYT-2 layer 4	
	Main effect	Interaction with diagnosis	Main effect	Interaction with diagnosis		Main effect	Interaction with diagnosis	Main effect	Interaction with diagnosis
rs4673628	$F_{2,109}=0.289$	$F_{2,109}=0.192$	$F_{2,68}=0.767$	$F_{2,68}=1.646$	rs7598440	$F_{2,114}=0.993$	$F_{2,114}=1.026$	$F_{2,71}=0.952$	$F_{2,71}=0.855$
	$P=0.750$	$P=0.825$	$P=0.468$	$P=0.200$		$P=0.374$	$P=0.362$	$P=0.391$	$P=0.430$
					rs839523	$F_{2,114}=0.031$	$F_{2,114}=0.152$	$F_{2,71}=1.562$	$F_{2,71}=0.404$
					$P=0.969$	$P=0.859$	$P=0.271$	$P=0.669$	
					rs707284	$F_{2,114}=0.266$	$F_{2,114}=0.046$	$F_{2,71}=2.532$	$F_{2,71}=0.255$
						$P=0.767$	$P=0.955$	$P=0.087$	$P=0.776$

### B.3 SUPPLEMENTARY FIGURES

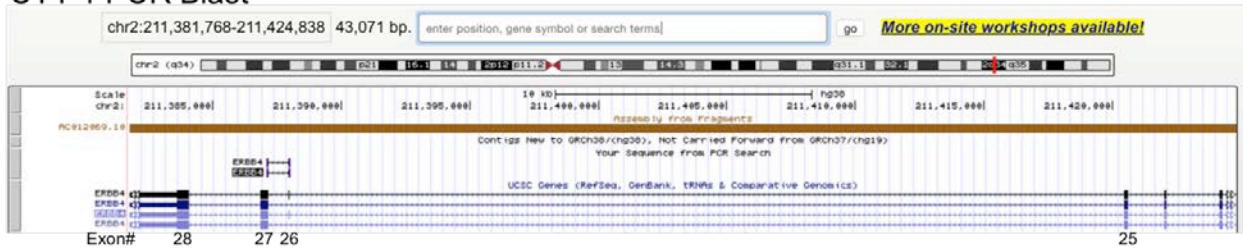


Lane	Gene	Predicted amplicon size
1	Ladder	
2	CR	145bp
3	PV	99bp
4	JM-a	172bp
5	JM-b	161bp
6	CYT-1	98bp
7	CYT-2	206bp
8	Pan-ErbB4	89bp

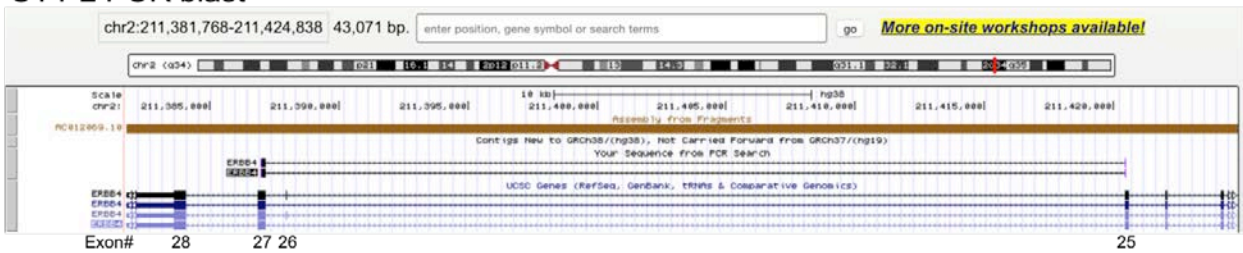
**Figure 19. Specificity of qPCR primers for calretinin, parvalbumin, ErbB4 splice variants and pan-ErbB4.**

Gel electrophoresis displaying the post-qPCR amplicon products for calretinin, parvalbumin, ErbB4 splicing variants and Pan-ErbB4 transcripts. + : qPCR with cDNA. - : qPCR without cDNA. Ladder : GeneRuler Low Range DNA Ladder, Life Technologies Cat#SM1193.

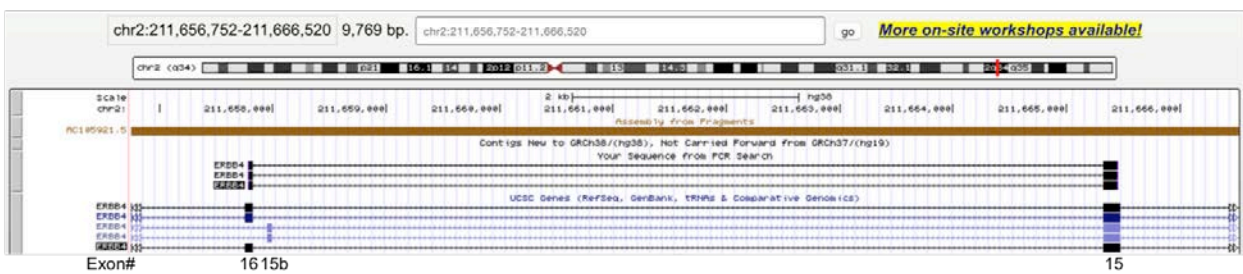
### CYT-1 PCR Blast



### CYT-2 PCR blast



### JM-a PCR blast



### JM-b PCR blast

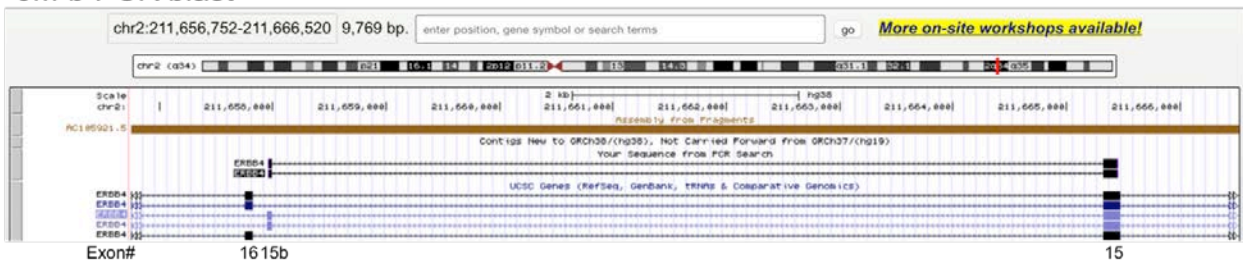


**Figure 20. qPCR amplicon products blasted to specific ErbB4 splice variants.**

Results of UCSC In-Silico PCR blast (<https://genome.ucsc.edu/cgi-bin/hgPcr>) for each primer pair targeting ErbB4 splicing variants in relation to the alternative exons of ErbB4 transcripts. Note that the primer pair targeting CYT-1 variant includes exon 26, whereas the pair targeting CYT-2 variant excludes it. The exon 16 or 15b is selectively spanned for the primer pair targeting JM-a or JM-b variants, respectively.

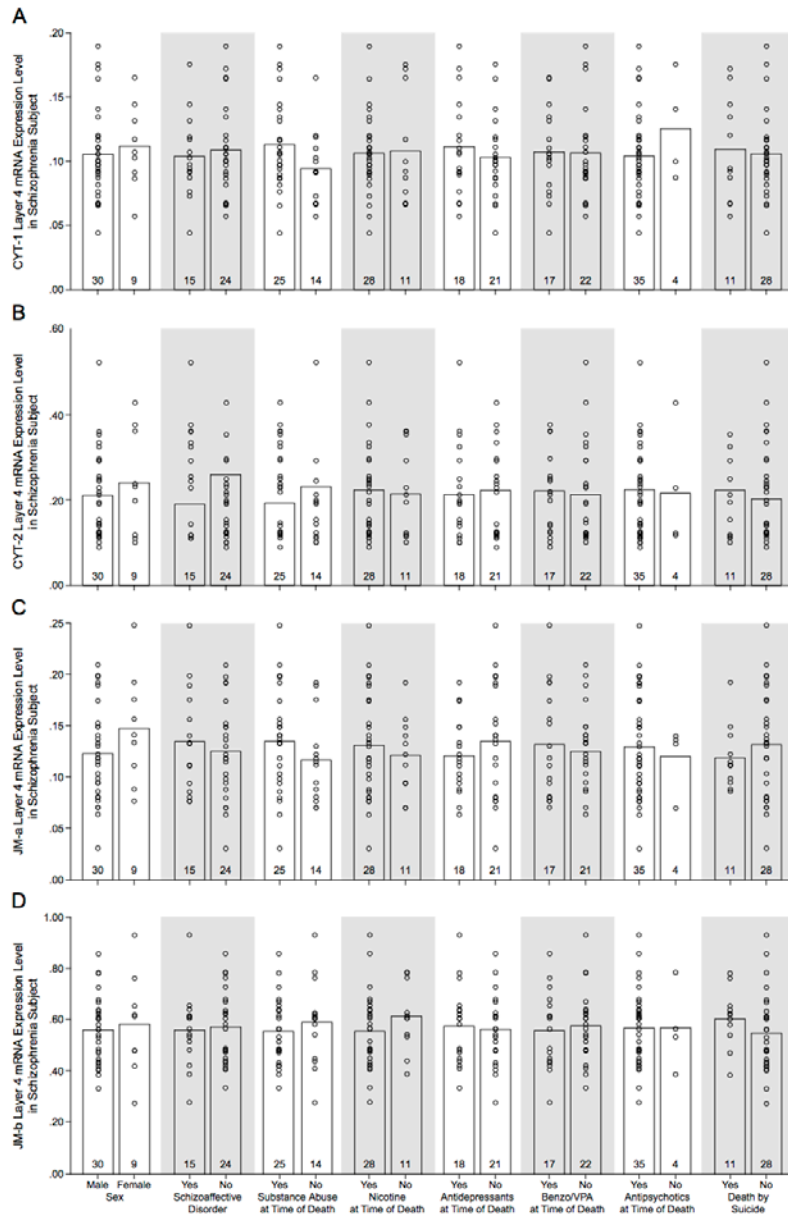


**Figure 21. No effect of co-morbid factors on the normalized ErbB4 splice variant levels in subjects with schizophrenia.**

In each pair of plots, schizophrenia subjects are grouped by potential confounding factors listed on the x-axis. Circles represent the levels of ErbB4 splicing variants for individual subjects and the bars represent mean ErbB4 splicing variant levels for the indicated group. Numbers listed for each bar represent the number of schizophrenia subjects for each condition. Levels of CYT-1 (A), CYT-2 (B), JM-a (C) and JM-b (D) in layers 4 of schizophrenia

subjects did not differ significantly (all F values  $<5.4$ , all p-values  $> 0.182$ ) as a function of sex, diagnosis of schizoaffective disorder, history of substance dependence or abuse, nicotine use at the time of death, use of antipsychotics, antidepressants, or benzodiazepines and/or sodium valproate at the time of death, or death by suicide

## **APPENDIX C**

### **SUPPLEMENTAL INFORMATION FOR PATHOLOGICAL BASIS FOR DEFICIENT EXCITATORY DRIVE TO CORTICAL PARVALBUMIN INTERNEURONS IN SCHIZOPHRENIA**

#### **C.1 SUPPLEMENTARY METHODS**

##### **Antibody Characterization**

The mouse anti-PV antibody (Cat#235, Lot#10-11F, Swant) recognized a single band at the expected size of 12 kDa by western blotting and showed an absence of immunoreactivity by immunohistochemistry in PV knockout mice (Celio et al., 1988; Schwaller et al., 1999). The goat anti-CR antibody (Cat#CG1, Lot#1ξ1, Swant) showed an absence of immunoreactivity by immunohistochemistry in CR knock-out mice (Schiffmann et al., 1999). The guinea pig anti-VGlut1 antibody (Cat#AB5905, Lot#22430498, Millipore) recognized a single band at the expected size of 60 kDa by western blotting (Melone et al., 2005) and preadsorption with the immunogen peptide abolished immunolabeling (reported by the manufacturer). The rabbit anti-PSD-95 antibody (Cat#3450s, Lot#2, Cell Signaling) recognized a single band of 95 kDa on western blots from extracts of rat brain and human cerebellum as reported by the manufacturer, and highly co-localized with immunolabeling of a well-characterized mouse monoclonal anti-

PSD-95 antibody (Neuromab cat. no. 75-028)(Soiza-Reilly and Commons, 2011). All secondary and tertiary antibodies used in this study were shown to produce minimum cross-reactivity by the manufacturers.

### **PMI effect on protein immunoreactivity**

Because PMI may affect protein immunoreactivity(Lewis, 2002), we assessed the density of VGlut1+/PSD95+ puncta onto PV+ cell bodies in 6 control subjects with PMIs ranging from 4.8 to 22.7 hours. The density of Vglut1+/PSD95+ puncta onto PV+ cell bodies was not correlated with PMI in these subjects ( $R=-0.111$ ,  $p=0.835$ ), suggesting that the detectability of excitatory inputs is not influenced by a PMI less than 24 hours.

### **Antibody Penetration Efficiency Analysis**

To check for penetration efficiency of anti-VGlut1 or anti-PSD95 antibody, we preliminarily assessed the distribution of VGlut1+ or PSD95+ masks along the Z-axis in ten random image stacks from control subjects. Z-axis per each image was divided into 10 bins, with each bin representing the 10% of total Z-axis from the top (100%) to the bottom (1%) of the section. Mean percent localization of VGlut1+ or PSD95+ masks in 1~10% and 91~100% of the Z-axis were significantly different from those in the middle 80% of the Z-axis (VGlut1:  $F_{9,90}=9.5$ ,  $p<0.001$ ; PSD95:  $F_{9,90}=20.9$ ,  $p<0.001$ ; post hoc tukey's test  $p<0.05$ ). Therefore, only the objects localized within the 80% of middle z-planes ( $\sim 32 \mu\text{m}$ ) were sampled for data analysis.

## **VGlut+ and PSD95+ puncta segmentation**

First, a custom channel was made for each deconvolved channel of VGlut1 or PSD95 by calculating a difference of Gaussians using sigma values of 0.7 and 2. Then, the Ridler-Calvard threshold value was applied to the fluorescence intensity histogram of either VGlut1+ or PSD95+ labeling and all pixels were reassigned to a binary value according to whether they were above or below the threshold value, and the resulting binary image was referred to as the object mask. Then these object masks were automatically defined as VGlut1+ or PSD95+ masks if they fell in the range of defined puncta size ( $0.06-0.7\mu\text{m}^3$ )(Fish et al., 2008). Choosing a single threshold value may not be sufficient to ensure comprehensive masking of VGlut1+ and PSD95+ puncta, as protein levels differ within synaptic structures and vary substantially as a result of disease states. Therefore, we utilized the MATLAB script, which performs multiple iterations of automated masking process that starts from the Ridler-Calvard threshold value and incrementally migrates towards the highest intensity value. The resulting object masks from each iteration were combined to represent the total population of VGlut1+ or PSD95+ puncta. Lipofuscin autofluorescence labeling was masked using the Ridler-Calvard threshold value as explained above and was subtracted from the VGlut1+ or PSD95+ masks for final analysis.

## C.2 SUPPLEMENTARY FIGURES

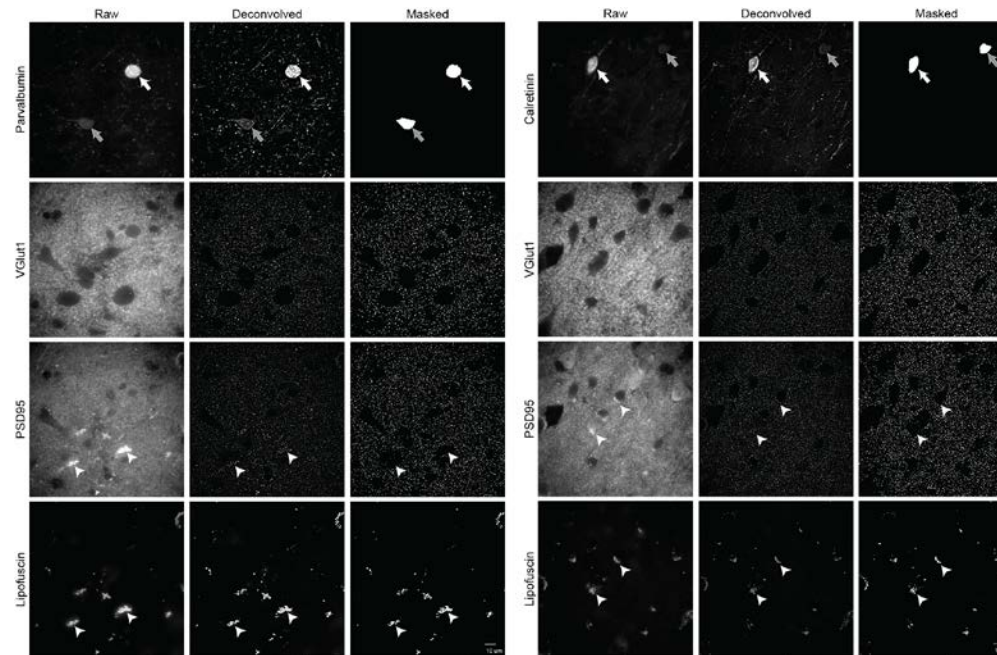


**Figure 22. Representative raw, deconvolved and masked images of PV+ cell bodies, CR+ cell bodies, VGlut1+ puncta, PSD95+ puncta and lipofuscin in human DLPFC.**

PV+ neurons with varying intensity range (white arrow – PV mean intensity: 2810 a.u., PV sum intensity: 133426234 a.u.; gray arrow – PV mean intensity: 951 a.u., PV sum intensity: 35779294 a.u.) and CR+ neurons with varying intensity range (white arrow – CR mean intensity: 3189 a.u., CR sum intensity: 50431392 a.u.; gray arrow – CR mean intensity: 1010 a.u., CR sum intensity: 7999625 a.u.) were masked as described in Methods. Lipofuscin masks (white arrowheads) were subtracted from the puncta mask for final analyses. Scale bar = 10 $\mu$ m.

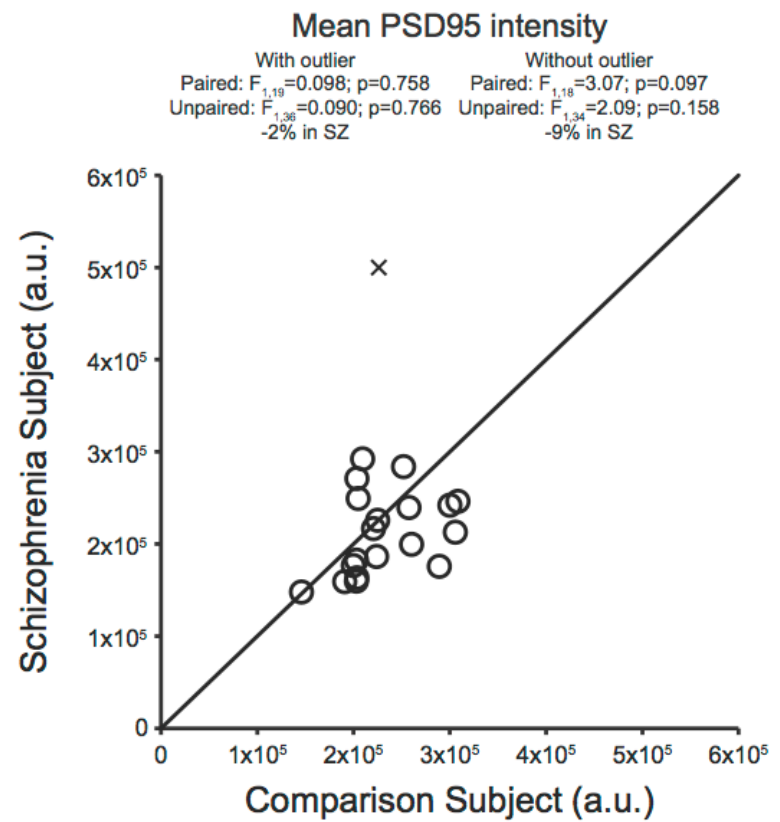
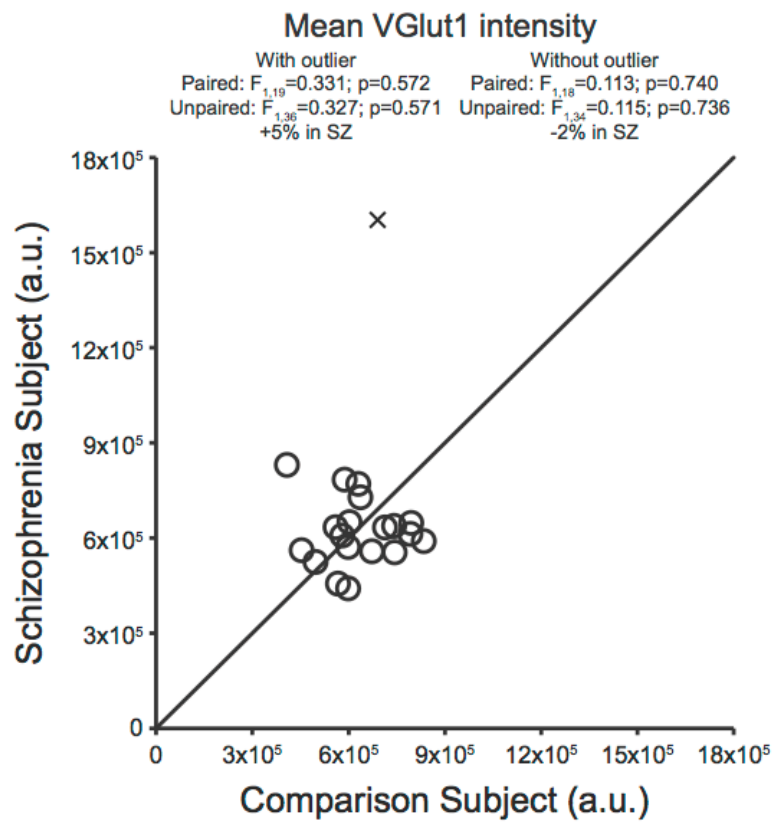


**Figure 23. Levels of VGlut1 or PSD95 immunoreactivity within VGlut1+ puncta or PSD95+ puncta, respectively, onto PV interneurons are unaltered in schizophrenia subjects.**

X denotes a subject pair identified as an outlier by the Grubbs' test ( $Z=3.38$ ,  $p<0.01$ ). Statistical analyses with and without the outlier pair are shown.

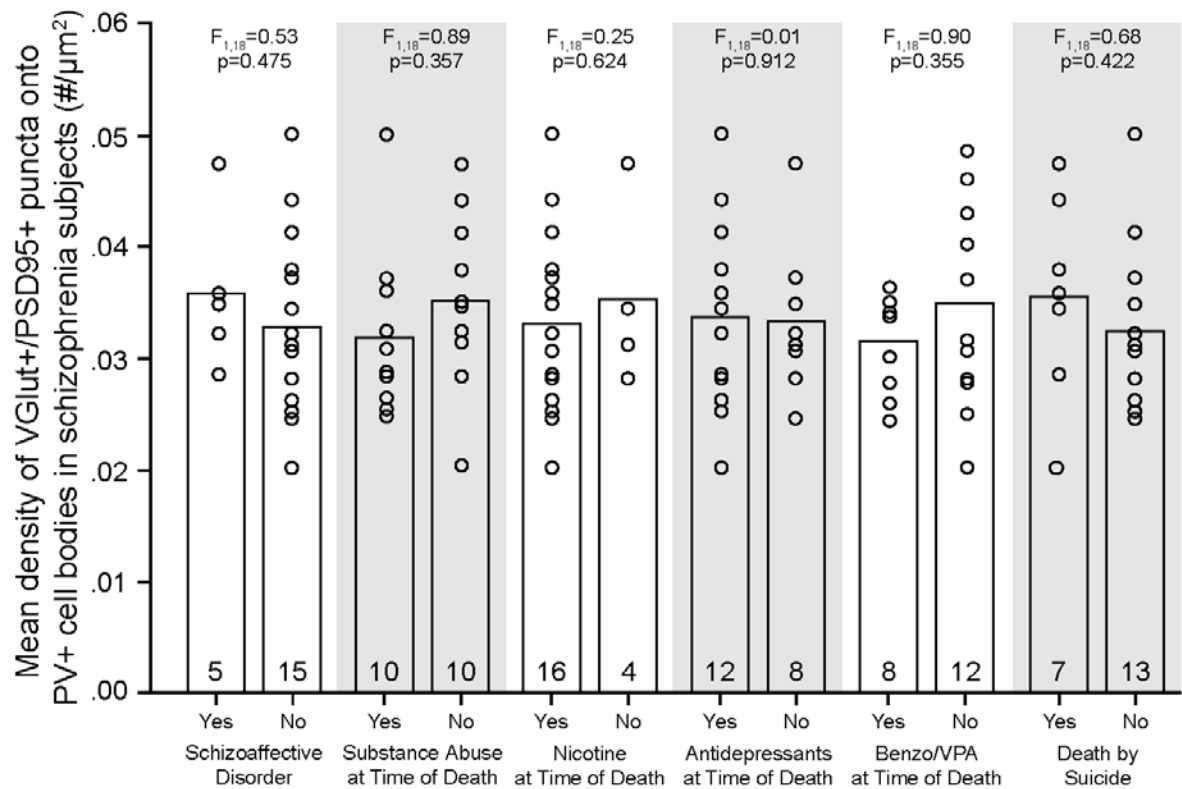


**Figure 24. No effect of co-morbid factors on the mean density of VGlut1+/PSD95+ puncta onto PV+ cell bodies in subjects with schizophrenia.**

In each pair of plots, schizophrenia subjects are grouped by the co-morbid factors listed on the x-axis. Circles represent the levels of the mean density for individual schizophrenia subjects and the bars represent mean density for the indicated group. Numbers listed for each bar represent the number of schizophrenia subjects with that condition. Mean density of VGlut1+/PSD95+ puncta onto PV+ cell bodies in schizophrenia subjects did not differ significantly as a function of diagnosis of schizoaffective disorder, history of substance dependence or abuse, nicotine use at the time of death, use of antidepressants, or benzodiazepines and/or sodium valproate at the time of death, or death by suicide.

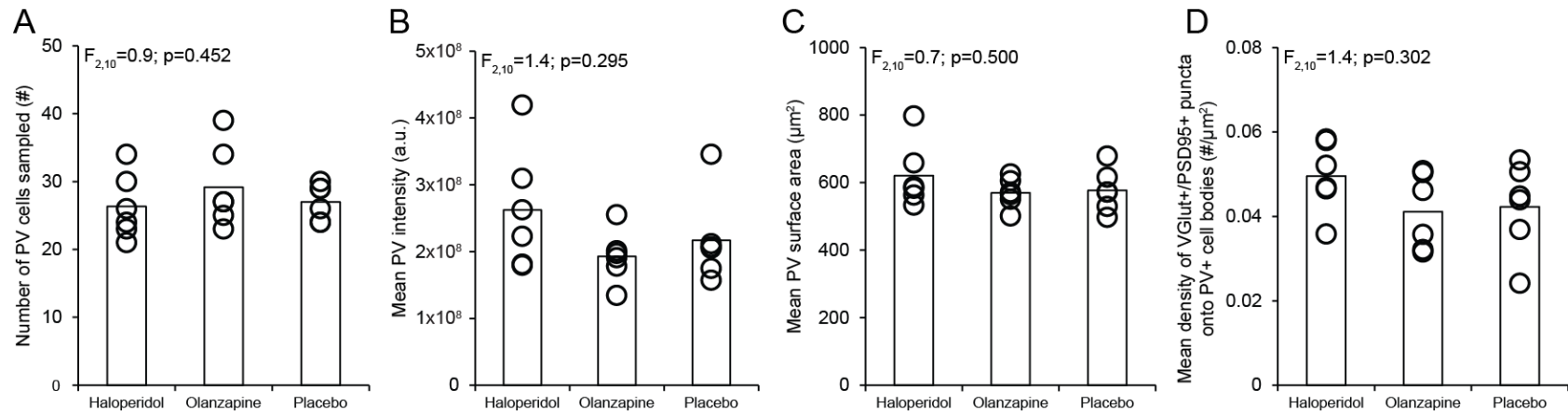


**Figure 25. Density of excitatory synaptic inputs to PV interneurons is not altered in monkeys treated with psychotropic medications.**

(A-D) Mean numbers of sampled PV+ neurons, mean PV immunoreactivity levels in PV+ cell bodies, mean surface area of PV+ cell bodies or mean density of VGlut1+/PSD95+ puncta onto PV+ cell bodies was not altered in the monkeys treated with haloperidol or olanzapine compared to the monkeys treated with placebo.

## **APPENDIX D**

### **SUPPLEMENTAL INFORMATION FOR DEVELOPMENTAL PRUNING OF EXCITATORY INPUTS TO PARVALBUMIN INTERNEURONS IN MONKEY PREFRONTAL CORTEX: CONTRIBUTION OF ERBB4 SPLICING**

#### **D.1 SUPPLEMENTARY METHOD**

##### **In situ hybridization.**

Cryostat sections (20  $\mu$ m) containing right DLPFC area 46 were mounted onto glass slides from a subset of monkeys (5 pre-pubertal and 3 post-pubertal) due to limitations in tissue availability. Sections were fixed with 4% paraformaldehyde in PBS and then acetylated with 0.25% acetic anhydride in 0.1 M triethanolamine/0.9% NaCl for 10 minutes, dehydrated through a graded ethanol series, and defatted in chloroform for 10 minutes. The sections were then hybridized with <sup>35</sup>S-labeled riboprobes ( $2 \times 10^7$  dpm/ml) targeting bases 59-403 of PV mRNA in hybridization buffer containing 50% formamide, 0.75 M NaCl, 20 mM 1,4-piperazine diethane sulfonic acid, pH 6.8, 10 mM EDTA, 10% dextran sulfate, 5X Denhardt's solution (0.2 mg/ml Ficoll, 0.2 mg/ml polyvinylpyrrolidone, 0.2 mg/ml BSA), 50 mM dithiothreitol, 0.2% SDS, and 100  $\mu$ g/ml yeast tRNA at 56°C for 16 hours. The sections were then washed in a solution containing 0.3 M NaCl, 20 mM Tris-HCl, pH 8.0, 1 mM EDTA, pH 8.0, and 50%

formamide at 63°C, treated with RNase A (20 µg/ml) at 37°C, and washed in 0.1× SSC (150 mM NaCl, 15 mM sodium citrate) at 67°C. Finally, sections were dehydrated through a graded ethanol series, air dried, and exposed to BioMax MR film (Kodak, Rochester, NY) for 72 hours. Film optical density (OD) was quantified as nanocuries per gram of tissue by reference to radioactive C-14 standards. PV mRNA expression as a function of cortical layer was quantified in approximately 1-mm-wide cortical traverses extending from the pial surface to the white matter. Each traverse was divided into 50 equal bins parallel to the pial surface and the OD was determined for each bin.

### **Masking of VGlut1+ and PSD95+ puncta and PV cell body.**

For the purpose of masking synaptic structures, a custom channel was made for each deconvolved channel of VGlut1 or PSD95 by calculating a difference of Gaussians using sigma values of 0.7 and 2. The Ridler-Calvard threshold value was applied to the fluorescence intensity histogram of either VGlut1+ or PSD95+ labeling and all pixels were reassigned to a binary value according to whether they were above or below the threshold value, and the resulting binary image was referred to as the object mask. These object masks were automatically defined as VGlut1+ or PSD95+ masks if they fell in the range of defined puncta size (0.06-0.7µm<sup>3</sup>). Multiple iteration of binary masking process was then performed with the threshold level incrementally increasing for each iteration of masking until it reached the highest intensity value. The resulting object masks from each iteration were combined to represent the total population of VGlut1+ or PSD95+ puncta. Edges of PV cell bodies were segmented by the MATLAB edge function using the Canny edge detector operator. The edges of segmented objects were closed,

filled, and size-gated ( $>80 \mu\text{m}^3$ ) to limit the boundaries of PV cell bodies. All PV cell body masks were manually cleaned for final analyses.

## BIBLIOGRAPHY

- Abe Y, Namba H, Kato T, Iwakura Y, Nawa H (2011) Neuregulin-1 signals from the periphery regulate AMPA receptor sensitivity and expression in GABAergic interneurons in developing neocortex. *J Neurosci* 31:5699-5709.
- Agarwal A et al. (2014) Dysregulated expression of neuregulin-1 by cortical pyramidal neurons disrupts synaptic plasticity. *Cell Rep* 8:1130-1145.
- Akbarian S, Kim JJ, Potkin SG, Hagman JO, Tafazzoli A, Bunney WE, Jr., Jones EG (1995) Gene expression for glutamic acid decarboxylase is reduced without loss of neurons in prefrontal cortex of schizophrenics. *Arch Gen Psychiatry* 52:258-266.
- Alexander GE (1982) Functional development of frontal association cortex in monkeys: behavioural and electrophysiological studies. *Neurosci Res Program Bull* 20:471-479.
- Anderson SA, Classey JD, Conde F, Lund JS, Lewis DA (1995) Synchronous development of pyramidal neuron dendritic spines and parvalbumin-immunoreactive chandelier neuron axon terminals in layer III of monkey prefrontal cortex. *Neuroscience* 67:7-22.
- Arion D, Corradi JP, Tang S, Datta D, Boothe F, He A, Cacace AM, Zaczek R, Albright CF, Tseng G, Lewis DA (2015) Distinctive transcriptome alterations of prefrontal pyramidal neurons in schizophrenia and schizoaffective disorder. *Mol Psychiatry*.
- Barry G, Briggs JA, Vanichkina DP, Poth EM, Beveridge NJ, Ratnu VS, Nayler SP, Nones K, Hu J, Bredy TW, Nakagawa S, Rigo F, Taft RJ, Cairns MJ, Blackshaw S, Wolvetang EJ, Mattick JS (2014) The long non-coding RNA Gomafu is acutely regulated in response to neuronal activation and involved in schizophrenia-associated alternative splicing. *Mol Psychiatry* 19:486-494.
- Beasley CL, Zhang ZJ, Patten I, Reynolds GP (2002) Selective deficits in prefrontal cortical GABAergic neurons in schizophrenia defined by the presence of calcium-binding proteins. *Biol Psychiatry* 52:708-715.
- Behrens MM, Ali SS, Dao DN, Lucero J, Shekhtman G, Quick KL, Dugan LL (2007) Ketamine-induced loss of phenotype of fast-spiking interneurons is mediated by NADPH-oxidase. *Science* 318:1645-1647.
- Belforte JE, Zsiros V, Sklar ER, Jiang Z, Yu G, Li Y, Quinlan EM, Nakazawa K (2010) Postnatal NMDA receptor ablation in corticolimbic interneurons confers schizophrenia-like phenotypes. *Nat Neurosci* 13:76-83.
- Berretta S, Pantazopoulos H, Markota M, Brown C, Batzianouli ET (2015) Losing the sugar coating: potential impact of perineuronal net abnormalities on interneurons in schizophrenia. *Schizophr Res* 167:18-27.

- Bian WJ, Miao WY, He SJ, Qiu Z, Yu X (2015) Coordinated Spine Pruning and Maturation Mediated by Inter-Spine Competition for Cadherin/Catenin Complexes. *Cell* 162:808-822.
- Bourgeois JP, Goldman-Rakic PS, Rakic P (1994) Synaptogenesis in the prefrontal cortex of rhesus monkeys. *Cereb Cortex* 4:78-96.
- Bowie CR, Reichenberg A, Patterson TL, Heaton RK, Harvey PD (2006) Determinants of real-world functional performance in schizophrenia subjects: correlations with cognition, functional capacity, and symptoms. *Am J Psychiatry* 163:418-425.
- Britsch S (2007) The neuregulin-I/ErbB signaling system in development and disease. *Adv Anat Embryol Cell Biol* 190:1-65.
- Brown JA, Ramikie TS, Schmidt MJ, Baldi R, Garbett K, Everheart MG, Warren LE, Gellert L, Horvath S, Patel S, Mirnics K (2015) Inhibition of parvalbumin-expressing interneurons results in complex behavioral changes. *Mol Psychiatry* 20:1499-1507.
- Bublil EM, Yarden Y (2007) The EGF receptor family: spearheading a merger of signaling and therapeutics. *Curr Opin Cell Biol* 19:124-134.
- Cabungcal JH, Steullet P, Kraftsik R, Cuenod M, Do KQ (2013a) Early-life insults impair parvalbumin interneurons via oxidative stress: reversal by N-acetylcysteine. *Biol Psychiatry* 73:574-582.
- Cabungcal JH, Steullet P, Morishita H, Kraftsik R, Cuenod M, Hensch TK, Do KQ (2013b) Perineuronal nets protect fast-spiking interneurons against oxidative stress. *Proc Natl Acad Sci U S A* 110:9130-9135.
- Cabungcal JH, Counotte DS, Lewis EM, Tejada HA, Piantadosi P, Pollock C, Calhoun GG, Sullivan EM, Presgraves E, Kil J, Hong LE, Cuenod M, Do KQ, O'Donnell P (2014) Juvenile antioxidant treatment prevents adult deficits in a developmental model of schizophrenia. *Neuron* 83:1073-1084.
- Canny J (1986) A Computational Approach to Edge-Detection. *Ieee Transactions on Pattern Analysis and Machine Intelligence* 8:679-698.
- Cardin JA, Carlen M, Meletis K, Knoblich U, Zhang F, Deisseroth K, Tsai LH, Moore CI (2009) Driving fast-spiking cells induces gamma rhythm and controls sensory responses. *Nature* 459:663-667.
- Celio MR, Baier W, Scharer L, de Viragh PA, Gerday C (1988) Monoclonal antibodies directed against the calcium binding protein parvalbumin. *Cell Calcium* 9:81-86.
- Chang MC, Park JM, Pelkey KA, Grabenstatter HL, Xu D, Linden DJ, Sutula TP, McBain CJ, Worley PF (2010) Narp regulates homeostatic scaling of excitatory synapses on parvalbumin-expressing interneurons. *Nat Neurosci* 13:1090-1097.
- Chen CM, Stanford AD, Mao X, Abi-Dargham A, Shungu DC, Lisanby SH, Schroeder CE, Kegeles LS (2014) GABA level, gamma oscillation, and working memory performance in schizophrenia. *Neuroimage Clin* 4:531-539.
- Cho RY, Konecky RO, Carter CS (2006) Impairments in frontal cortical gamma synchrony and cognitive control in schizophrenia. *Proc Natl Acad Sci U S A* 103:19878-19883.
- Cho RY, Walker CP, Polizzotto NR, Wozny TA, Fissell C, Chen CM, Lewis DA (2015) Development of sensory gamma oscillations and cross-frequency coupling from childhood to early adulthood. *Cereb Cortex* 25:1509-1518.
- Chung DW, Fish KN, Lewis DA (2016a) Pathological basis for deficient excitatory drive to cortical parvalbumin interneurons in schizophrenia. *Am J Psychiatry*.

- Chung DW, Rudnicki DD, Yu L, Margolis RL (2011) A natural antisense transcript at the Huntington's disease repeat locus regulates HTT expression. *Hum Mol Genet* 20:3467-3477.
- Chung DW, Volk DW, Arion D, Zhang Y, Sampson AR, Lewis DA (2016b) Dysregulated ErbB4 Splicing in Schizophrenia: Selective Effects on Parvalbumin Expression. *Am J Psychiatry* 173:60-68.
- Conde F, Lund JS, Jacobowitz DM, Baimbridge KG, Lewis DA (1994) Local circuit neurons immunoreactive for calretinin, calbindin D-28k or parvalbumin in monkey prefrontal cortex: distribution and morphology. *J Comp Neurol* 341:95-116.
- Coyle JT, Basu A, Benneyworth M, Balu D, Konopaske G (2012) Glutamatergic synaptic dysregulation in schizophrenia: therapeutic implications. *Handb Exp Pharmacol*:267-295.
- Craig AM, Kang Y (2007) Neurexin-neuroigin signaling in synapse development. *Curr Opin Neurobiol* 17:43-52.
- Curley AA, Arion D, Volk DW, Asafu-Adjei JK, Sampson AR, Fish KN, Lewis DA (2011) Cortical deficits of glutamic acid decarboxylase 67 expression in schizophrenia: clinical, protein, and cell type-specific features. *Am J Psychiatry* 168:921-929.
- Curtin F, Schulz P (1998) Multiple correlations and Bonferroni's correction. *Biol Psychiatry* 44:775-777.
- Datta D, Arion D, Corradi JP, Lewis DA (2015) Altered expression of CDC42 signaling pathway components in cortical layer 3 pyramidal cells in schizophrenia. *Biol Psychiatry* 78:775-785.
- de Lecea L, del Rio JA, Soriano E (1995) Developmental expression of parvalbumin mRNA in the cerebral cortex and hippocampus of the rat. *Brain Res Mol Brain Res* 32:1-13.
- DeFelipe J, Farinas I (1992) The pyramidal neuron of the cerebral cortex: morphological and chemical characteristics of the synaptic inputs. *Prog Neurobiol* 39:563-607.
- Del Pino I, Garcia-Frigola C, Dehorter N, Brotons-Mas JR, Alvarez-Salvado E, Martinez de Lagran M, Ciceri G, Gabaldon MV, Moratal D, Dierssen M, Canals S, Marin O, Rico B (2013) ErbB4 Deletion from Fast-Spiking Interneurons Causes Schizophrenia-like Phenotypes. *Neuron* 79:1152-1168.
- Dityatev A, Schachner M (2003) Extracellular matrix molecules and synaptic plasticity. *Nat Rev Neurosci* 4:456-468.
- Donato F, Rompani SB, Caroni P (2013) Parvalbumin-expressing basket-cell network plasticity induced by experience regulates adult learning. *Nature* 504:272-276.
- Dorph-Petersen KA, Pierri JN, Perel JM, Sun Z, Sampson AR, Lewis DA (2005) The influence of chronic exposure to antipsychotic medications on brain size before and after tissue fixation: a comparison of haloperidol and olanzapine in macaque monkeys. *Neuropsychopharmacology* 30:1649-1661.
- Driesen NR, Leung HC, Calhoun VD, Constable RT, Gueorguieva R, Hoffman R, Skudlarski P, Goldman-Rakic PS, Krystal JH (2008) Impairment of working memory maintenance and response in schizophrenia: functional magnetic resonance imaging evidence. *Biol Psychiatry* 64:1026-1034.
- Dugladze T, Schmitz D, Whittington MA, Vida I, Gloveli T (2012) Segregation of axonal and somatic activity during fast network oscillations. *Science* 336:1458-1461.
- El-Husseini AE, Schnell E, Chetkovich DM, Nicoll RA, Brecht DS (2000) PSD-95 involvement in maturation of excitatory synapses. *Science* 290:1364-1368.

- Emiliani FE, Sedlak TW, Sawa A (2014) Oxidative stress and schizophrenia: recent breakthroughs from an old story. *Curr Opin Psychiatry* 27:185-190.
- Enwright JF, Sanapala S, Foglio A, Berry R, Fish KN, Lewis DA (2016) Reduced Labeling of Parvalbumin Neurons and Perineuronal Nets in the Dorsolateral Prefrontal Cortex of Subjects with Schizophrenia. *Neuropsychopharmacology*.
- Fazzari P, Paternain AV, Valiente M, Pla R, Lujan R, Lloyd K, Lerma J, Marin O, Rico B (2010) Control of cortical GABA circuitry development by Nrg1 and ErbB4 signalling. *Nature* 464:1376-1380.
- Fish KN, Sweet RA, Deo AJ, Lewis DA (2008) An automated segmentation methodology for quantifying immunoreactive puncta number and fluorescence intensity in tissue sections. *Brain Res* 1240:62-72.
- Fremeau RT, Jr., Troyer MD, Pahner I, Nygaard GO, Tran CH, Reimer RJ, Bellocchio EE, Fortin D, Storm-Mathisen J, Edwards RH (2001) The expression of vesicular glutamate transporters defines two classes of excitatory synapse. *Neuron* 31:247-260.
- Fries P (2009) Neuronal gamma-band synchronization as a fundamental process in cortical computation. *Annu Rev Neurosci* 32:209-224.
- Fromer M et al. (2014) De novo mutations in schizophrenia implicate synaptic networks. *Nature* 506:179-184.
- Fuchs EC, Zivkovic AR, Cunningham MO, Middleton S, Lebeau FE, Bannerman DM, Rozov A, Whittington MA, Traub RD, Rawlins JN, Monyer H (2007) Recruitment of parvalbumin-positive interneurons determines hippocampal function and associated behavior. *Neuron* 53:591-604.
- Fujimoto T, Okumura E, Takeuchi K, Kodabashi A, Tanaka H, Otsubo T, Nakamura K, Sekine M, Kamiya S, Higashi Y, Tsuji M, Shimooki S, Tamura T (2012) Changes in Event-Related Desynchronization and Synchronization during the Auditory Oddball Task in Schizophrenia Patients. *Open Neuroimag J* 6:26-36.
- Funahashi S, Bruce CJ, Goldman-Rakic PS (1989) Mnemonic coding of visual space in the monkey's dorsolateral prefrontal cortex. *J Neurophysiol* 61:331-349.
- Fung SJ, Webster MJ, Sivagnanasundaram S, Duncan C, Elashoff M, Weickert CS (2010) Expression of interneuron markers in the dorsolateral prefrontal cortex of the developing human and in schizophrenia. *Am J Psychiatry* 167:1479-1488.
- Gabbott PL, Jays PR, Bacon SJ (1997) Calretinin neurons in human medial prefrontal cortex (areas 24a,b,c, 32', and 25). *J Comp Neurol* 381:389-410.
- Gallinat J, Winterer G, Herrmann CS, Senkowski D (2004) Reduced oscillatory gamma-band responses in unmedicated schizophrenic patients indicate impaired frontal network processing. *Clin Neurophysiol* 115:1863-1874.
- Garcia RA, Vasudevan K, Buonanno A (2000) The neuregulin receptor ErbB-4 interacts with PDZ-containing proteins at neuronal synapses. *Proc Natl Acad Sci U S A* 97:3596-3601.
- Garey LJ, Ong WY, Patel TS, Kanani M, Davis A, Mortimer AM, Barnes TR, Hirsch SR (1998) Reduced dendritic spine density on cerebral cortical pyramidal neurons in schizophrenia. *J Neurol Neurosurg Psychiatry* 65:446-453.
- Genomes Project C, Abecasis GR, Altshuler D, Auton A, Brooks LD, Durbin RM, Gibbs RA, Hurles ME, McVean GA (2010) A map of human genome variation from population-scale sequencing. *Nature* 467:1061-1073.

- Georgiev D, Arion D, Enwright JF, Kikuchi M, Minabe Y, Corradi JP, Lewis DA, Hashimoto T (2014) Lower gene expression for KCNS3 potassium channel subunit in parvalbumin-containing neurons in the prefrontal cortex in schizophrenia. *Am J Psychiatry* 171:62-71.
- Georgiev D, Yoshihara T, Kawabata R, Matsubara T, Tsubomoto M, Minabe Y, Lewis DA, Hashimoto T (2016) Cortical Gene Expression after a Conditional Knockout of 67 kDa Glutamic Acid Decarboxylase in Parvalbumin Neurons. *Schizophr Bull*.
- Glantz LA, Lewis DA (2000) Decreased dendritic spine density on prefrontal cortical pyramidal neurons in schizophrenia. *Arch Gen Psychiatry* 57:65-73.
- Glausier JR, Fish KN, Lewis DA (2014) Altered parvalbumin basket cell inputs in the dorsolateral prefrontal cortex of schizophrenia subjects. *Mol Psychiatry* 19:30-36.
- Goldman-Rakic PS (1987) Development of cortical circuitry and cognitive function. *Child Dev* 58:601-622.
- Goldman-Rakic PS (1995) Cellular basis of working memory. *Neuron* 14:477-485.
- Gonzalez-Albo MC, Elston GN, DeFelipe J (2001) The human temporal cortex: characterization of neurons expressing nitric oxide synthase, neuropeptides and calcium-binding proteins, and their glutamate receptor subunit profiles. *Cereb Cortex* 11:1170-1181.
- Gonzalez-Burgos G, Lewis DA (2012) NMDA receptor hypofunction, parvalbumin-positive neurons, and cortical gamma oscillations in schizophrenia. *Schizophr Bull* 38:950-957.
- Gonzalez-Burgos G, Cho RY, Lewis DA (2015a) Alterations in cortical network oscillations and parvalbumin neurons in schizophrenia. *Biol Psychiatry* 77:1031-1040.
- Gonzalez-Burgos G, Kroener S, Zaitsev AV, Povysheva NV, Krimer LS, Barrionuevo G, Lewis DA (2008) Functional maturation of excitatory synapses in layer 3 pyramidal neurons during postnatal development of the primate prefrontal cortex. *Cereb Cortex* 18:626-637.
- Gonzalez-Burgos G, Miyamae T, Pafundo DE, Yoshino H, Rotaru DC, Hoftman G, Datta D, Zhang Y, Hammond M, Sampson AR, Fish KN, Ermentrout GB, Lewis DA (2015b) Functional maturation of GABA synapses during postnatal development of the monkey dorsolateral prefrontal cortex. *Cereb Cortex* 25:4076-4093.
- Han K, Holder JL, Jr., Schaaf CP, Lu H, Chen H, Kang H, Tang J, Wu Z, Hao S, Cheung SW, Yu P, Sun H, Breman AM, Patel A, Lu HC, Zoghbi HY (2013) SHANK3 overexpression causes manic-like behaviour with unique pharmacogenetic properties. *Nature* 503:72-77.
- Hashimoto T, Bazmi HH, Mirnics K, Wu Q, Sampson AR, Lewis DA (2008a) Conserved regional patterns of GABA-related transcript expression in the neocortex of subjects with schizophrenia. *Am J Psychiatry* 165:479-489.
- Hashimoto T, Volk DW, Eggan SM, Mirnics K, Pierri JN, Sun Z, Sampson AR, Lewis DA (2003) Gene expression deficits in a subclass of GABA neurons in the prefrontal cortex of subjects with schizophrenia. *J Neurosci* 23:6315-6326.
- Hashimoto T, Arion D, Unger T, Maldonado-Aviles JG, Morris HM, Volk DW, Mirnics K, Lewis DA (2008b) Alterations in GABA-related transcriptome in the dorsolateral prefrontal cortex of subjects with schizophrenia. *Mol Psychiatry* 13:147-161.
- Hawrylycz MJ et al. (2012) An anatomically comprehensive atlas of the adult human brain transcriptome. *Nature* 489:391-399.
- Hedman AM, van Haren NE, van Baal CG, Kahn RS, Hulshoff Pol HE (2013) IQ change over time in schizophrenia and healthy individuals: a meta-analysis. *Schizophr Res* 146:201-208.

- Hill JJ, Hashimoto T, Lewis DA (2006) Molecular mechanisms contributing to dendritic spine alterations in the prefrontal cortex of subjects with schizophrenia. *Mol Psychiatry* 11:557-566.
- Hioki H (2015) Compartmental organization of synaptic inputs to parvalbumin-expressing GABAergic neurons in mouse primary somatosensory cortex. *Anat Sci Int* 90:7-21.
- Hoftman GD, Volk DW, Bazmi HH, Li S, Sampson AR, Lewis DA (2015) Altered cortical expression of GABA-related genes in schizophrenia: illness progression vs developmental disturbance. *Schizophr Bull* 41:180-191.
- Holtmaat A, Svoboda K (2009) Experience-dependent structural synaptic plasticity in the mammalian brain. *Nat Rev Neurosci* 10:647-658.
- Homayoun H, Moghaddam B (2007) NMDA receptor hypofunction produces opposite effects on prefrontal cortex interneurons and pyramidal neurons. *J Neurosci* 27:11496-11500.
- Howie BN, Donnelly P, Marchini J (2009) A flexible and accurate genotype imputation method for the next generation of genome-wide association studies. *PLoS Genet* 5:e1000529.
- Hu H, Martina M, Jonas P (2010) Dendritic mechanisms underlying rapid synaptic activation of fast-spiking hippocampal interneurons. *Science* 327:52-58.
- Hu H, Gan J, Jonas P (2014) Interneurons. Fast-spiking, parvalbumin(+) GABAergic interneurons: from cellular design to microcircuit function. *Science* 345:1255263.
- Huang YZ, Won S, Ali DW, Wang Q, Tanowitz M, Du QS, Pelkey KA, Yang DJ, Xiong WC, Salter MW, Mei L (2000) Regulation of neuregulin signaling by PSD-95 interacting with ErbB4 at CNS synapses. *Neuron* 26:443-455.
- Huttenlocher PR (1979) Synaptic density in human frontal cortex - developmental changes and effects of aging. *Brain Res* 163:195-205.
- Ide M, Lewis DA (2010) Altered cortical CDC42 signaling pathways in schizophrenia: implications for dendritic spine deficits. *Biol Psychiatry* 68:25-32.
- Iijima T, Wu K, Witte H, Hanno-Iijima Y, Glatter T, Richard S, Scheiffele P (2011) SAM68 regulates neuronal activity-dependent alternative splicing of neurexin-1. *Cell* 147:1601-1614.
- Insel TR (2010) Rethinking schizophrenia. *Nature* 468:187-193.
- Jaaro-Peled H, Hayashi-Takagi A, Seshadri S, Kamiya A, Brandon NJ, Sawa A (2009) Neurodevelopmental mechanisms of schizophrenia: understanding disturbed postnatal brain maturation through neuregulin-1-ErbB4 and DISC1. *Trends Neurosci* 32:485-495.
- Jonas P, Bischofberger J, Fricker D, Miles R (2004) Interneuron Diversity series: Fast in, fast out--temporal and spatial signal processing in hippocampal interneurons. *Trends Neurosci* 27:30-40.
- Joshi D, Fullerton JM, Weickert CS (2014) Elevated ErbB4 mRNA is related to interneuron deficit in prefrontal cortex in schizophrenia. *J Psychiatr Res* 53:125-132.
- Junttila TT, Sundvall M, Maatta JA, Elenius K (2000) ErbB4 and its isoforms: selective regulation of growth factor responses by naturally occurring receptor variants. *Trends Cardiovasc Med* 10:304-310.
- Kahn RS, Keefe RS (2013) Schizophrenia is a cognitive illness: time for a change in focus. *JAMA Psychiatry* 70:1107-1112.
- Keefe RS, Harvey PD (2012) Cognitive impairment in schizophrenia. *Handb Exp Pharmacol*:11-37.
- Kenward MG, Roger JH (1997) Small sample inference for fixed effects from restricted maximum likelihood. *Biometrics* 53:983-997.

- Khandaker GM, Barnett JH, White IR, Jones PB (2011) A quantitative meta-analysis of population-based studies of premorbid intelligence and schizophrenia. *Schizophr Res* 132:220-227.
- Kim IH, Rossi MA, Aryal DK, Racz B, Kim N, Uezu A, Wang F, Wetsel WC, Weinberg RJ, Yin H, Soderling SH (2015) Spine pruning drives antipsychotic-sensitive locomotion via circuit control of striatal dopamine. *Nat Neurosci* 18:883-891.
- Kimoto S, Bazmi HH, Lewis DA (2014) Lower expression of glutamic acid decarboxylase 67 in the prefrontal cortex in schizophrenia: contribution of altered regulation by Zif268. *Am J Psychiatry* 171:969-978.
- Kimoto S, Zaki MM, Bazmi HH, Lewis DA (2015) Altered Markers of Cortical gamma-Aminobutyric Acid Neuronal Activity in Schizophrenia: Role of the NARP Gene. *JAMA Psychiatry*.
- Kinney JW, Davis CN, Tabarean I, Conti B, Bartfai T, Behrens MM (2006) A specific role for NR2A-containing NMDA receptors in the maintenance of parvalbumin and GAD67 immunoreactivity in cultured interneurons. *J Neurosci* 26:1604-1615.
- Konopaske GT, Lange N, Coyle JT, Benes FM (2014) Prefrontal cortical dendritic spine pathology in schizophrenia and bipolar disorder. *JAMA Psychiatry* 71:1323-1331.
- Korotkova T, Fuchs EC, Ponomarenko A, von Engelhardt J, Monyer H (2010) NMDA receptor ablation on parvalbumin-positive interneurons impairs hippocampal synchrony, spatial representations, and working memory. *Neuron* 68:557-569.
- Krimer LS, Zaitsev AV, Czanner G, Kroner S, Gonzalez-Burgos G, Povysheva NV, Iyengar S, Barrionuevo G, Lewis DA (2005) Cluster analysis-based physiological classification and morphological properties of inhibitory neurons in layers 2-3 of monkey dorsolateral prefrontal cortex. *J Neurophysiol* 94:3009-3022.
- Kritzer MF, Goldman-Rakic PS (1995) Intrinsic circuit organization of the major layers and sublayers of the dorsolateral prefrontal cortex in the rhesus monkey. *J Comp Neurol* 359:131-143.
- Krystal JH, Karper LP, Seibyl JP, Freeman GK, Delaney R, Bremner JD, Heninger GR, Bowers MB, Jr., Charney DS (1994) Subanesthetic effects of the noncompetitive NMDA antagonist, ketamine, in humans. Psychotomimetic, perceptual, cognitive, and neuroendocrine responses. *Arch Gen Psychiatry* 51:199-214.
- Latawiec D, Martin KA, Meskenaite V (2000) Termination of the geniculocortical projection in the striate cortex of macaque monkey: a quantitative immunoelectron microscopic study. *J Comp Neurol* 419:306-319.
- Lau CG, Murthy VN (2012) Activity-dependent regulation of inhibition via GAD67. *J Neurosci* 32:8521-8531.
- Law AJ, Kleinman JE, Weinberger DR, Weickert CS (2007) Disease-associated intronic variants in the ErbB4 gene are related to altered ErbB4 splice-variant expression in the brain in schizophrenia. *Hum Mol Genet* 16:129-141.
- Law AJ, Wang Y, Sei Y, O'Donnell P, Piantadosi P, Papaleo F, Straub RE, Huang W, Thomas CJ, Vakkalanka R, Besterman AD, Lipska BK, Hyde TM, Harrison PJ, Kleinman JE, Weinberger DR (2012) Neuregulin 1-ErbB4-PI3K signaling in schizophrenia and phosphoinositide 3-kinase-p110delta inhibition as a potential therapeutic strategy. *Proc Natl Acad Sci U S A* 109:12165-12170.

- Lazarus MS, Krishnan K, Huang ZJ (2015) GAD67 deficiency in parvalbumin interneurons produces deficits in inhibitory transmission and network disinhibition in mouse prefrontal cortex. *Cereb Cortex* 25:1290-1296.
- Lee HJ, Jung KM, Huang YZ, Bennett LB, Lee JS, Mei L, Kim TW (2002) Presenilin-dependent gamma-secretase-like intramembrane cleavage of ErbB4. *J Biol Chem* 277:6318-6323.
- Lee S, Kruglikov I, Huang ZJ, Fishell G, Rudy B (2013) A disinhibitory circuit mediates motor integration in the somatosensory cortex. *Nat Neurosci* 16:1662-1670.
- Lewis DA (1997) Development of the prefrontal cortex during adolescence: insights into vulnerable neural circuits in schizophrenia. *Neuropsychopharmacology* 16:385-398.
- Lewis DA (2002) The human brain revisited: opportunities and challenges in postmortem studies of psychiatric disorders. *Neuropsychopharmacology* 26:143-154.
- Lewis DA, Lieberman JA (2000) Catching up on schizophrenia: natural history and neurobiology. *Neuron* 28:325-334.
- Lewis DA, Sweet RA (2009) Schizophrenia from a neural circuitry perspective: advancing toward rational pharmacological therapies. *J Clin Invest* 119:706-716.
- Lewis DA, Hashimoto T, Volk DW (2005) Cortical inhibitory neurons and schizophrenia. *Nat Rev Neurosci* 6:312-324.
- Lewis DA, Cruz D, Eggen S, Erickson S (2004) Postnatal development of prefrontal inhibitory circuits and the pathophysiology of cognitive dysfunction in schizophrenia. *Ann N Y Acad Sci* 1021:64-76.
- Lewis DA, Curley AA, Glausier JR, Volk DW (2012) Cortical parvalbumin interneurons and cognitive dysfunction in schizophrenia. *Trends Neurosci* 35:57-67.
- Li KX, Lu YM, Xu ZH, Zhang J, Zhu JM, Zhang JM, Cao SX, Chen XJ, Chen Z, Luo JH, Duan S, Li XM (2012) Neuregulin 1 regulates excitability of fast-spiking neurons through Kv1.1 and acts in epilepsy. *Nat Neurosci* 15:267-273.
- Lichtman JW, Colman H (2000) Synapse elimination and indelible memory. *Neuron* 25:269-278.
- Liu X, Bates R, Yin DM, Shen C, Wang F, Su N, Kirov SA, Luo Y, Wang JZ, Xiong WC, Mei L (2011) Specific regulation of NRG1 isoform expression by neuronal activity. *J Neurosci* 31:8491-8501.
- Lopez AD, Disease Control Priorities Project. (2006) Global burden of disease and risk factors. New York, NY  
Washington, DC: Oxford University Press ;  
World Bank.
- Luna B, Padmanabhan A, O'Hearn K (2010) What has fMRI told us about the development of cognitive control through adolescence? *Brain Cogn* 72:101-113.
- Maatta JA, Sundvall M, Junttila TT, Peri L, Laine VJ, Isola J, Egeblad M, Elenius K (2006) Proteolytic cleavage and phosphorylation of a tumor-associated ErbB4 isoform promote ligand-independent survival and cancer cell growth. *Mol Biol Cell* 17:67-79.
- MacCabe JH, Lambe MP, Cnattingius S, Torrang A, Bjork C, Sham PC, David AS, Murray RM, Hultman CM (2008) Scholastic achievement at age 16 and risk of schizophrenia and other psychoses: a national cohort study. *Psychol Med* 38:1133-1140.
- Marin O, Rico B (2013) A new beginning for a broken mind: balancing neuregulin 1 reverses synaptic dysfunction. *Neuron* 78:577-579.
- Massi L, Lagler M, Hartwich K, Borhegyi Z, Somogyi P, Klausberger T (2012) Temporal dynamics of parvalbumin-expressing axo-axonic and basket cells in the rat medial prefrontal cortex in vivo. *J Neurosci* 32:16496-16502.

- Matta JA, Pelkey KA, Craig MT, Chittajallu R, Jeffries BW, McBain CJ (2013) Developmental origin dictates interneuron AMPA and NMDA receptor subunit composition and plasticity. *Nat Neurosci* 16:1032-1041.
- Mauney SA, Athanas KM, Pantazopoulos H, Shaskan N, Passeri E, Berretta S, Woo TU (2013) Developmental pattern of perineuronal nets in the human prefrontal cortex and their deficit in schizophrenia. *Biol Psychiatry* 74:427-435.
- Mei L, Xiong WC (2008) Neuregulin 1 in neural development, synaptic plasticity and schizophrenia. *Nat Rev Neurosci* 9:437-452.
- Mei L, Nave KA (2014) Neuregulin-ERBB signaling in the nervous system and neuropsychiatric diseases. *Neuron* 83:27-49.
- Melchitzky DS, Lewis DA (2003) Pyramidal neuron local axon terminals in monkey prefrontal cortex: differential targeting of subclasses of GABA neurons. *Cereb Cortex* 13:452-460.
- Melchitzky DS, Sesack SR, Lewis DA (1999) Parvalbumin-immunoreactive axon terminals in macaque monkey and human prefrontal cortex: laminar, regional, and target specificity of type I and type II synapses. *J Comp Neurol* 408:11-22.
- Mellios N, Huang HS, Baker SP, Galdzicka M, Ginns E, Akbarian S (2009) Molecular determinants of dysregulated GABAergic gene expression in the prefrontal cortex of subjects with schizophrenia. *Biol Psychiatry* 65:1006-1014.
- Melone M, Burette A, Weinberg RJ (2005) Light microscopic identification and immunocytochemical characterization of glutamatergic synapses in brain sections. *J Comp Neurol* 492:495-509.
- Mitchell RM, Janssen MJ, Karavanova I, Vullhorst D, Furth K, Makusky A, Markey SP, Buonanno A (2013) ErbB4 reduces synaptic GABA currents independent of its receptor tyrosine kinase activity. *Proc Natl Acad Sci U S A* 110:19603-19608.
- Moghaddam B, Krystal JH (2012) Capturing the angel in "angel dust": twenty years of translational neuroscience studies of NMDA receptor antagonists in animals and humans. *Schizophr Bull* 38:942-949.
- Mohamed S, Rosenheck R, Swartz M, Stroup S, Lieberman JA, Keefe RS (2008) Relationship of cognition and psychopathology to functional impairment in schizophrenia. *Am J Psychiatry* 165:978-987.
- Muraoka-Cook RS, Sandahl MA, Strunk KE, Miraglia LC, Husted C, Hunter DM, Elenius K, Chodosh LA, Earp HS, 3rd (2009) ErbB4 splice variants Cyt1 and Cyt2 differ by 16 amino acids and exert opposing effects on the mammary epithelium in vivo. *Mol Cell Biol* 29:4935-4948.
- Nakata K, Lipska BK, Hyde TM, Ye T, Newburn EN, Morita Y, Vakkalanka R, Barenboim M, Sei Y, Weinberger DR, Kleinman JE (2009) DISC1 splice variants are upregulated in schizophrenia and associated with risk polymorphisms. *Proc Natl Acad Sci U S A* 106:15873-15878.
- Neddens J, Fish KN, Tricoire L, Vullhorst D, Shamir A, Chung W, Lewis DA, McBain CJ, Buonanno A (2011) Conserved interneuron-specific ErbB4 expression in frontal cortex of rodents, monkeys, and humans: implications for schizophrenia. *Biol Psychiatry* 70:636-645.
- Ni CY, Murphy MP, Golde TE, Carpenter G (2001) gamma -Secretase cleavage and nuclear localization of ErbB-4 receptor tyrosine kinase. *Science* 294:2179-2181.

- Norenberg A, Hu H, Vida I, Bartos M, Jonas P (2010) Distinct nonuniform cable properties optimize rapid and efficient activation of fast-spiking GABAergic interneurons. *Proc Natl Acad Sci U S A* 107:894-899.
- Norris AD, Calarco JA (2012) Emerging Roles of Alternative Pre-mRNA Splicing Regulation in Neuronal Development and Function. *Front Neurosci* 6:122.
- Pelkey KA, Barksdale E, Craig MT, Yuan X, Sukumaran M, Vargish GA, Mitchell RM, Wyeth MS, Petralia RS, Chittajallu R, Karlsson RM, Cameron HA, Murata Y, Colonnese MT, Worley PF, McBain CJ (2015) Pentraxins coordinate excitatory synapse maturation and circuit integration of parvalbumin interneurons. *Neuron* 85:1257-1272.
- Petanjek Z, Judas M, Simic G, Rasin MR, Uylings HB, Rakic P, Kostovic I (2011) Extraordinary neoteny of synaptic spines in the human prefrontal cortex. *Proc Natl Acad Sci U S A* 108:13281-13286.
- Pfeffer CK, Xue M, He M, Huang ZJ, Scanziani M (2013) Inhibition of inhibition in visual cortex: the logic of connections between molecularly distinct interneurons. *Nat Neurosci* 16:1068-1076.
- Pi HJ, Hangya B, Kvitsiani D, Sanders JI, Huang ZJ, Kepecs A (2013) Cortical interneurons that specialize in disinhibitory control. *Nature* 503:521-524.
- Pierri JN, Chaudry AS, Woo TU, Lewis DA (1999) Alterations in chandelier neuron axon terminals in the prefrontal cortex of schizophrenic subjects. *Am J Psychiatry* 156:1709-1719.
- Porta EA (2002) Pigments in aging: an overview. *Ann N Y Acad Sci* 959:57-65.
- Rakic P, Bourgeois JP, Goldman-Rakic PS (1994) Synaptic development of the cerebral cortex: implications for learning, memory, and mental illness. *Prog Brain Res* 102:227-243.
- Rao SG, Williams GV, Goldman-Rakic PS (1999) Isodirectional tuning of adjacent interneurons and pyramidal cells during working memory: evidence for microcolumnar organization in PFC. *J Neurophysiol* 81:1903-1916.
- Rao SG, Williams GV, Goldman-Rakic PS (2000) Destruction and creation of spatial tuning by disinhibition: GABA(A) blockade of prefrontal cortical neurons engaged by working memory. *J Neurosci* 20:485-494.
- Reichenberg A, Weiser M, Rabinowitz J, Caspi A, Schmeidler J, Mark M, Kaplan Z, Davidson M (2002) A population-based cohort study of premorbid intellectual, language, and behavioral functioning in patients with schizophrenia, schizoaffective disorder, and nonpsychotic bipolar disorder. *Am J Psychiatry* 159:2027-2035.
- Rico B, Marin O (2011) Neuregulin signaling, cortical circuitry development and schizophrenia. *Curr Opin Genet Dev* 21:262-270.
- Rio C, Buxbaum JD, Peschon JJ, Corfas G (2000) Tumor necrosis factor-alpha-converting enzyme is required for cleavage of erbB4/HER4. *J Biol Chem* 275:10379-10387.
- Rocco BR, Lewis DA, Fish KN (2015) Markedly Lower Glutamic Acid Decarboxylase 67 Protein Levels in a Subset of Boutons in Schizophrenia. *Biol Psychiatry*:in press.
- Rotaru DC, Barrionuevo G, Sesack SR (2005) Mediodorsal thalamic afferents to layer III of the rat prefrontal cortex: synaptic relationships to subclasses of interneurons. *J Comp Neurol* 490:220-238.
- Rotaru DC, Yoshino H, Lewis DA, Ermentrout GB, Gonzalez-Burgos G (2011) Glutamate receptor subtypes mediating synaptic activation of prefrontal cortex neurons: relevance for schizophrenia. *J Neurosci* 31:142-156.

- Saha S, Chant D, McGrath J (2007) A systematic review of mortality in schizophrenia: is the differential mortality gap worsening over time? *Arch Gen Psychiatry* 64:1123-1131.
- Sardi SP, Murtie J, Koirala S, Patten BA, Corfas G (2006) Presenilin-dependent ErbB4 nuclear signaling regulates the timing of astrogenesis in the developing brain. *Cell* 127:185-197.
- Saunders JA, Tatar-Leitman VM, Suh J, Billingslea EN, Roberts TP, Siegel SJ (2013) Knockout of NMDA receptors in parvalbumin interneurons recreates autism-like phenotypes. *Autism Res* 6:69-77.
- Schiffmann SN, Cheron G, Lohof A, d'Alcantara P, Meyer M, Parmentier M, Schurmans S (1999) Impaired motor coordination and Purkinje cell excitability in mice lacking calretinin. *Proc Natl Acad Sci U S A* 96:5257-5262.
- Schizophrenia Working Group of the Psychiatric Genomics C (2014) Biological insights from 108 schizophrenia-associated genetic loci. *Nature* 511:421-427.
- Schwaller B, Dick J, Dhoot G, Carroll S, Vrbova G, Nicotera P, Pette D, Wyss A, Bluethmann H, Hunziker W, Celio MR (1999) Prolonged contraction-relaxation cycle of fast-twitch muscles in parvalbumin knockout mice. *Am J Physiol* 276:C395-403.
- Segal I, Korkotian I, Murphy DD (2000) Dendritic spine formation and pruning: common cellular mechanisms? *Trends Neurosci* 23:53-57.
- Senkowski D, Gallinat J (2015) Dysfunctional prefrontal gamma-band oscillations reflect working memory and other cognitive deficits in schizophrenia. *Biol Psychiatry* 77:1010-1019.
- Seshadri S, Faust T, Ishizuka K, Delevich K, Chung Y, Kim SH, Cowles M, Niwa M, Jaaro-Peled H, Tomoda T, Lai C, Anton ES, Li B, Sawa A (2015) Interneuronal DISC1 regulates NRG1-ErbB4 signalling and excitatory-inhibitory synapse formation in the mature cortex. *Nat Commun* 6:10118.
- Shah A, Lodge DJ (2013) A loss of hippocampal perineuronal nets produces deficits in dopamine system function: relevance to the positive symptoms of schizophrenia. *Transl Psychiatry* 3:e215.
- Silberberg G, Darvasi A, Pinkas-Kramarski R, Navon R (2006) The involvement of ErbB4 with schizophrenia: association and expression studies. *Am J Med Genet B Neuropsychiatr Genet* 141B:142-148.
- Sohal VS, Zhang F, Yizhar O, Deisseroth K (2009) Parvalbumin neurons and gamma rhythms enhance cortical circuit performance. *Nature* 459:698-702.
- Soiza-Reilly M, Commons KG (2011) Quantitative analysis of glutamatergic innervation of the mouse dorsal raphe nucleus using array tomography. *J Comp Neurol* 519:3802-3814.
- Steullet P, Cabungcal JH, Cuenod M, Do KQ (2014) Fast oscillatory activity in the anterior cingulate cortex: dopaminergic modulation and effect of perineuronal net loss. *Front Cell Neurosci* 8:244.
- Sundvall M, Veikkolainen V, Kurppa K, Salah Z, Tvorogov D, van Zoelen EJ, Aqeilan R, Elenius K (2010) Cell death or survival promoted by alternative isoforms of ErbB4. *Mol Biol Cell* 21:4275-4286.
- Sweet RA, Henteleff RA, Zhang W, Sampson AR, Lewis DA (2009) Reduced dendritic spine density in auditory cortex of subjects with schizophrenia. *Neuropsychopharmacology* 34:374-389.
- Tan W, Dean M, Law AJ (2010) Molecular cloning and characterization of the human ErbB4 gene: identification of novel splice isoforms in the developing and adult brain. *PLoS One* 5:e12924.

- Thomson AM, Lamy C (2007) Functional maps of neocortical local circuitry. *Front Neurosci* 1:19-42.
- Ting AK, Chen Y, Wen L, Yin DM, Shen C, Tao Y, Liu X, Xiong WC, Mei L (2011) Neuregulin 1 promotes excitatory synapse development and function in GABAergic interneurons. *J Neurosci* 31:15-25.
- Uemura T, Lee SJ, Yasumura M, Takeuchi T, Yoshida T, Ra M, Taguchi R, Sakimura K, Mishina M (2010) Trans-synaptic interaction of GluRdelta2 and Neurexin through Cbln1 mediates synapse formation in the cerebellum. *Cell* 141:1068-1079.
- Uhlhaas PJ, Singer W (2010) Abnormal neural oscillations and synchrony in schizophrenia. *Nat Rev Neurosci* 11:100-113.
- van Oel CJ, Sitskoorn MM, Cremer MP, Kahn RS (2002) School performance as a premorbid marker for schizophrenia: a twin study. *Schizophr Bull* 28:401-414.
- Veikkolainen V, Vaparanta K, Halkilahti K, Iljin K, Sundvall M, Elenius K (2011) Function of ERBB4 is determined by alternative splicing. *Cell Cycle* 10:2647-2657.
- Volk DW, Chitrapu A, Edelson JR, Lewis DA (2014) Chemokine receptors and cortical interneuron dysfunction in schizophrenia. *Schizophr Res*.
- Volk DW, Chitrapu A, Edelson JR, Lewis DA (2015) Chemokine receptors and cortical interneuron dysfunction in schizophrenia. *Schizophr Res* 167:12-17.
- Volk DW, Austin MC, Pierri JN, Sampson AR, Lewis DA (2000) Decreased glutamic acid decarboxylase67 messenger RNA expression in a subset of prefrontal cortical gamma-aminobutyric acid neurons in subjects with schizophrenia. *Arch Gen Psychiatry* 57:237-245.
- Volk DW, Radchenkova PV, Walker EM, Sengupta EJ, Lewis DA (2012a) Cortical opioid markers in schizophrenia and across postnatal development. *Cereb Cortex* 22:1215-1223.
- Volk DW, Matsubara T, Li S, Sengupta EJ, Georgiev D, Minabe Y, Sampson A, Hashimoto T, Lewis DA (2012b) Deficits in transcriptional regulators of cortical parvalbumin neurons in schizophrenia. *Am J Psychiatry* 169:1082-1091.
- Vullhorst D, Neddens J, Karavanova I, Tricoire L, Petralia RS, McBain CJ, Buonanno A (2009) Selective expression of ErbB4 in interneurons, but not pyramidal cells, of the rodent hippocampus. *J Neurosci* 29:12255-12264.
- Wang HX, Gao WJ (2009) Cell type-specific development of NMDA receptors in the interneurons of rat prefrontal cortex. *Neuropsychopharmacology* 34:2028-2040.
- Weinberger DR (1987) Implications of normal brain development for the pathogenesis of schizophrenia. *Arch Gen Psychiatry* 44:660-669.
- Whittington MA, Traub RD, Kopell N, Ermentrout B, Buhl EH (2000) Inhibition-based rhythms: experimental and mathematical observations on network dynamics. *Int J Psychophysiol* 38:315-336.
- Williams SM, Goldman-Rakic PS, Leranth C (1992) The synaptology of parvalbumin-immunoreactive neurons in the primate prefrontal cortex. *J Comp Neurol* 320:353-369.
- Wills ZP, Mandel-Brehm C, Mardinly AR, McCord AE, Giger RJ, Greenberg ME (2012) The nogo receptor family restricts synapse number in the developing hippocampus. *Neuron* 73:466-481.
- Wilson NR, Kang J, Hueske EV, Leung T, Varoqui H, Murnick JG, Erickson JD, Liu G (2005) Presynaptic regulation of quantal size by the vesicular glutamate transporter VGLUT1. *J Neurosci* 25:6221-6234.

- Woo RS, Li XM, Tao Y, Carpenter-Hyland E, Huang YZ, Weber J, Neiswender H, Dong XP, Wu J, Gassmann M, Lai C, Xiong WC, Gao TM, Mei L (2007) Neuregulin-1 enhances depolarization-induced GABA release. *Neuron* 54:599-610.
- Woo TU, Miller JL, Lewis DA (1997) Schizophrenia and the parvalbumin-containing class of cortical local circuit neurons. *Am J Psychiatry* 154:1013-1015.
- Yin DM, Sun XD, Bean JC, Lin TW, Sathyamurthy A, Xiong WC, Gao TM, Chen YJ, Mei L (2013a) Regulation of spine formation by ErbB4 in PV-positive interneurons. *J Neurosci* 33:19295-19303.
- Yin DM, Chen YJ, Lu YS, Bean JC, Sathyamurthy A, Shen C, Liu X, Lin TW, Smith CA, Xiong WC, Mei L (2013b) Reversal of behavioral deficits and synaptic dysfunction in mice overexpressing neuregulin 1. *Neuron* 78:644-657.
- Zaitsev AV, Gonzalez-Burgos G, Povysheva NV, Kroner S, Lewis DA, Krimer LS (2005) Localization of calcium-binding proteins in physiologically and morphologically characterized interneurons of monkey dorsolateral prefrontal cortex. *Cereb Cortex* 15:1178-1186.
- Zeng F, Xu J, Harris RC (2009) Nedd4 mediates ErbB4 JM-a/CYT-1 ICD ubiquitination and degradation in MDCK II cells. *FASEB J* 23:1935-1945.